Marker-Free Isolation and Enrichment of Rare Cell Types Including Tumor Initiating Cells through Contactless Dielectrophoresis

Hadi Shafiee

Dissertation submitted to the faculty of the Virginia Polytechnic Institute and State University in partial fulfillment of the requirements for the degree of
Doctor of Philosophy
In
Engineering Science and Mechanics

Rafael V. Davalos
Ishwar K. Puri
Raffaella De Vita
Mark A. Stremler
Shane D. Ross

October 25th, 2010
Blacksburg, Virginia

Keywords: Dielectrophoresis, Contactless Dielectrophoresis, Lab on a Chip, Rare Cell Enrichment, Tumor Initiating Cell

Marker-Free Isolation and Enrichment of Rare Cell Types Including Tumor Initiating Cells through Contactless Dielectrophoresis

Hadi Shafiee

Abstract: Microfluidics has found numerous applications ranging from the life sciences industries for pharmaceuticals and biomedicine (drug design, delivery and detection, diagnostic devices) to industrial applications of combinational synthesis (such as rapid analysis and high throughput screening). Among all these, one of the intriguing exploitation of microfluidics or micro total analysis systems (μTAS) is the separation of circulating tumor cells (CTCs) from body fluids. Cancer cells spread from the initial site of a tumor by first invading the surrounding tissue, then by entering the blood or lymph vessels, and finally by crossing the vessel wall to exit the vasculature into distal organs. The September 2006 issue of the Journal of the National Cancer Institute (NCI) states: *"The war on cancer was declared 40 years ago and cancer is still here," and "Technologies that capture enemy CTCs for further interrogation might prove useful in the war on cancer***.**" CTCs cannot only become a new marker for cancer prognosis, but their detection can also be a valid new parameter for diagnosing cancer early, for monitoring disease progression and relapse, and for optimizing therapy.

This research established a new method to manipulate rare cell types based on their electrical signatures using dielectrophoresis (DEP) without having direct contact between the electrodes and the sample, known as contactless dielectrophoresis (cDEP). DEP is the motion of a particle in a suspending medium due to its polarization in the presence of a non-uniform electric field. cDEP relies upon reservoirs filled with highly conductive fluid to act as electrodes and provide the necessary electric field. These reservoirs are placed adjacent to the main microfluidic channel and are separated from the sample by a thin barrier of a dielectric material as is shown in Figure 1h. The application of a high-frequency electric field to the electrode reservoirs causes their capacitive coupling to the main channel and an electric field is induced across the sample fluid. Similar to traditional DEP, cDEP exploits the varying geometry of the electrodes to create spatial non-uniformities in the electric field. However, by utilizing reservoirs filled with a highly conductive solution, rather than a separate thin film array, the electrode structures employed by cDEP can be fabricated in the same step as the rest of the device; hence the process is conducive to mass production.

We demonstrated the ability to isolate human leukemia cancer cells (THP-1) cells from a heterogeneous mixture of live and dead cells using cDEP with more than 99% selectivity and 95% removal efficiency. Through numerical and experimental investigations, new generation of cDEP devices have been designed and tested to detect and isolate THP-1 cells from spiked blood samples with high selectivity and cell capture efficiency. Our experimental observations, using prototype devices, indicate that breast cancer cell lines at their different stages (MCF-7, MCF-10, and MDA-MB231) have unique electrical. Furthermore, through collaborations at the Wake Forest Comprehensive Center, we demonstrated that prostate tumor initiating cells (TICs) exhibit unique electrical signatures and DEP responses and cDEP technology can be exploited to isolate and enrich TICs for further genetic pathways investigations.

Acknowledgment

I would like to first thank my great adviser, Dr. Rafael V. Davalos for his supervision, advice, support, and guidance through this exciting interdisciplinary cancer research from the very early stage. It is also a pleasure to thank all of the graduate and undergraduate students and faculties that assisted me in creating ideas, designing devices, and conducting experiments during my stay at the Bioelectromechanical systems laboratory. I have to specifically convey that this thesis would not have been possible without the collaborations and brainstorming with my dear friends Michael B. Sano, John L. Caldwell, and Erin B. Henslee. I am grateful in any possible way and hope to keep up our collaboration in the future.

To my beloved wife, Asal, who has made available her support in so many ways, thank you for your love and being patient during the time it took me to graduate. I certainly, owe my deepest gratitude to my dear parents for their never-ending love from the time I was not in this world. It is not easy and possible to put the feelings about you in words and I can just say thank you for everything you have done. I will never forget the love, prayer, and hard work of my parents which have been substantial to reach all of these achievements.

I would like to dedicate this research to Dr. Liviu Librescue, who encouraged me to pursue my graduate studies at Virginia Tech and died as he lived, people who died because of cancer including my cousin, Mahmoud Reza Shafiee, people who are still fighting with cancer including my own sister, Zahra Shafiee and Anne-Marie Bracken, and my father who passed away in peace and I was not able to even attend his ceremony.

Table of Contents

List of Figures

List of Tables

Chapter 1
Introduction

1.1. Motivation

Isolation and enrichment of cells/micro-particles from a biological sample is one of the first crucial processes in many biomedical and homeland security applications [1]. Water quality analysis to detect viable pathogenic bacterium [2-6] and the isolation of rare circulating tumor cells (CTCs) for early cancer detection [7-19] are important examples of the applications of this process**.** Current enrichment techniques for sample preparation include density gradient based centrifugation or membrane filtration [20], fluorescent and magnetic activated cell sorting (F/MACS) [21], cell surface markers [9], and laser tweezers [22].

Approximately 24.6 million people live with cancer worldwide. According to the World Health Organization (WHO), 7.9 million people died of cancer in 2007 and this rate will continue to rise up to an estimated 12 million people in 2030. In the United States, cancer is the second most common cause of death behind cardiovascular disease and accounts for one out of every four deaths. Based on the American Cancer Society (ACS) Facts and Figures, the overall cost of cancer to society in 2008 was estimated to be 228.1 billion dollars. An estimated one-third of all cancers could be cured, if detected and treated in a timely and effective manner.

Early detection is a critical event for the successful treatment of cancer that greatly impacts the survival of many patients. The majority of tumors originate from epithelial cells that can disseminate from the primary tumor into bodily fluids once they progress to advanced (metastatic) stages. The key to using circulating tumor cells (CTCs) as predictive clinical biomarkers is their separation and enrichment. Even more challenging is the detection of early stage cancer cells since their concentration in peripheral blood may be low. Furthermore, specific tumor cell surface markers required by some approaches may not be known for some cancers, or the individual degree and pattern of genetic alterations in multi-genetic cancers does not allow for the use of a single or even multiple-gene product(s) with a sufficient rate of identification. In

addition, the expression levels may not be comparable in all stages, which may cause cells with a different genotype to remain undetected, greatly impacting the detection and treatment decisions for various forms of cancers [1-6].

1.2. Current Technologies for the Detection of Circulating Cancer Cells

During progression, tumor cells acquire the capacity to disseminate into blood circulation until they either are detected and eliminated by the immune system or attach to the endothelial cells, extravasate and grow as secondary tumors (metastasis) at distant sites. The detection of these Circulating Tumor Cells (CTCs) in peripheral blood would allow for non-invasive cancer detection and thereby could improve the patient's prognosis. The idea of CTCs in bodily fluids is not new, but the ability to find these few cells among the many millions of cells present is a relatively recent development. The use of non-invasive methods to detect and enrich cancer cells independent of their genotype is also critical for diagnostic purposes. Although it is still debated if CTCs in body fluids rather than in lymph nodes and bone marrow have prognostic potential[23]. The most reliable method currently available for CTC detection is automated digital microscopy (ADM), which uses image analysis to recognize immunochemically or immunomagnetically labeled tumor cells. The CellSearch System™ (Veridex LLC, Warren, NJ), as an example, was approved by the FDA in December 2006 as an aid to monitor breast, prostate and colon cancer patients. This system involves mixing a blood sample with iron particles coated with an antibody that targets the epithelial cell adhesion molecule (EpCAM). Using this test, Daniel Hayes, M.D., and his colleagues at the University of Michigan Comprehensive Cancer Center reported that the overall survival of patients with breast cancers harboring fewer than five CTCs in about 7mL blood after 3-5 weeks of starting their therapy was a relatively long 18.5 months. Women who had five CTCs or more had much shorter median survival times, ranging from 1.3 to 3.6 months [24, 25]. The existing technology provides proof-of-principle that CTCs are valuable diagnostic and prognostic cancer markers. However, the disadvantage of this principle is the dependence on cancer cell surface markers that may not be expressed in all patients and limit the number of diagnosed patients. Furthermore, the surface marker may not be constitutively expressed throughout all stages of the disease and, thus, detection may be limited to late stage disease.

Detection techniques such as quantitative polymerase chain reaction (qRT-PCR), immunochemistry and flow cytometry are effective means of verifying the presence of these exfoliated cancer cells under specific conditions. The majority of recent investigations have utilized qRT-PCR for the confirmation and genotyping of CTCs. This technique has been reported in scientific literature as a valid method to confirm various CTCs derived from bladder [26], breast [27], lung [28], prostate [29, 30], and esophagus [31]. Immunocytochemistry methods, using antibody-antigen detection are typically based on detection of specific tumor or epithelial cell markers present in CTCs. While these are reliable methods, the specificity of CTC separation and their enrichment determines the quality of the results (see above). The major drawback to this approach is that other cells, such as hematopoietic or fibroblasts cells, can express several epithelial markers such as keratins as well [32, 33], causing an incomplete separation.

These examples demonstrate the most common problem encountered with current detection techniques: the typical inverse relationship between specificity and sensitivity. If a technology could be developed to overcome the specificity challenge, one would then be free to concentrate solely on sensitivity using protocols and routines already available such as qRT-PCR, nucleic acid sequence based amplification (NASBA) or immunocytochemistry. One of the critical issues that must be addressed, therefore, is the presence of a sufficient number of physically isolated exfoliated neoplastic cells for this detection methodology to be effective.

1.3. Dielectrophoresis

One alternative to these methods is dielectrophoresis (DEP) which is the motion of a particle due to its polarization in the presence of a non-uniform electric field [34, 35]. Currently, typical dielectrophoretic devices employ an array of thin-film interdigitated electrodes placed within the flow of a channel to generate a non-uniform electric field that interacts with particles near the surface of the electrode array [36]. Such platforms have shown that DEP is an effective means to concentrate and differentiate cells rapidly and reversibly based on their size, shape, and intrinsic electrical properties such as conductivity and polarizability. These intrinsic properties arise due to the membrane compositional and electrostatic characteristics, internal cellular structure, and the type of nucleus [37] associated with each type of cell.

The application of dielectrophoresis to separate target cells from a solution has been studied extensively in the last two decades. Examples of the successful use of dielectrophoresis include the separation of human leukemia cells from red blood cells in an isotonic solution [7], entrapment of human breast cancer cells from blood [8], and separation of U937 human monocytic from peripheral blood mononuclear cells (PBMC) [9]. DEP has also been used to separate neuroblastoma cells from HTB glioma cells [2], isolate cervical carcinoma cells [10], isolate K562 human CML cells [11], separate live yeast cells from dead [12], and segregate different human tumor cells [13]. Unfortunately, the microelectrode-based devices used in these experiments are susceptible to electrode fouling and require complicated fabrication procedures [38, 39].

One unique advantage of DEP over existing methods for cell separation is that the DEP force is strongly dependent on cell viability. The cell membrane, which is normally impermeable and highly insulating, typically becomes permeable after cell death [40]. This results in the release of ions from the cytoplasm through the structural defects in the dead cell membrane and the cell conductivity will increase dramatically [41]. This alteration in electrical properties after cell death, make DEP live/dead cell separation and isolation possible.

The utilization of DEP to manipulate live and dead cells has previously been demonstrated through several approaches. To start, Suehiro *et al.* were able to utilize dielectrophoretic impedance measurements to selectively detect viable bacteria [42]. Conventional interdigitated electrode DEP micro devices have also been used to separate live and heat-treated Listeria cells [43]. Huang *et al.* investigated the difference in the AC electrodynamics of viable and non-viable yeast cells through DEP and electrorotation experiments [44] and a DEP-based microfluidic device for the selective retention of viable cells in culture media with high conductivity was proposed by Docoslis et al.[45].

1.4. Insulator-based DEP (iDEP)

Insulator-based dielectrophoresis (iDEP) is a practical method to obtain the selectivity of dielectrophoresis while overcoming the robustness and throughput issues associated with traditional dielectrophoresis platforms. iDEP uses insulating obstacles instead of electrodes within the device to produce spatial nonuniformities in the electric field. The basic concept of the iDEP technique was first presented by Masuda *et al.* [46]. Chou *et al.* have previously

demonstrated with glass insulating structures and AC electric fields that iDEP can separate DNA molecules, *Escherichia coli* cells, and hematapoietic cells [47]. Others have reported the trapping and separation of latex particles [48], the differentiation of live and dead bacteria [2], the separation of species of different viable prokaryotic cells [49], and the trapping and concentration of viruses [50]. It has been shown that polymer-based iDEP devices are effective for selective trapping of a range of biological particles in an aqueous sample [51]. The patterned electrodes at the bottom of the channel in DEP create the gradient of the electric field near the electrodes such that the cells close enough to the bottom of the channel can be manipulated. However, the insulator structures in iDEP that usually transverse the entire depth of the channel provide non uniform electric field over the entire depth of the channel. iDEP technology has also shown the potential for water quality monitoring [52], separating and concentrating prokaryotic cells and viruses [53], concentration and separation of live and dead bacteria [2], sample concentration followed by impedance detection [11], and manipulation of protein particles [54].

The targeted particles are released from the dielectrophoretic traps when the voltage is lowered. iDEP technology has proven to be an effective means of separating and concentrating prokaryotic cells and viruses [50]. Cancer cells have unique electrokinetic and dielectrophoretic properties when compared to non-neoplastic cells found in peripheral blood or body fluids. Since iDEP screens biological particles in fluids based on both size and intrinsic properties, the abnormal size of cancer cells makes them prime candidates for dielectrophoretic manipulation. iDEP has a number of major advantages over currently available enrichment techniques:

1. An iDEP device can be scaled to meet sample throughput requirements (1-500µL/min).
2. An iDEP device can achieve 10^3 concentration factors without fouling.
3. iDEP devices can be placed in series to attain higher levels of selectivity and concentration or placed in parallel for higher throughput.
4. The iDEP device is extremely portable.
5. iDEP can be fully automated, and the iDEP chip can be produced inexpensively using common manufacturing techniques.

It has been shown that iDEP is effective for selective trapping of a range of biological particles such as separating and concentrating prokaryotic cells and viruses [55, 56], and sample concentration followed by impedance detection [57]. This technology has shown concentration

factors on the order of 6000x and removal efficiencies greater than 98%[56]. So far, iDEP devices have been demonstrated on glass and polymer substrates [49, 55, 56, 58-66] allowing large electric fields (~10kV/m) to generate eletrokinetic flow and to trap particles. Unfortunately, when used with a highly conductive physiological fluid (such as blood), the relatively high electrical current flow causes dramatic temperature increases due to joule heating and hydrolysis (bubble generation) effects. Additionally, the sample is susceptible to contamination due to direct contact between the electrodes and the sample.

1.5. Drawbacks associated with DEP and iDEP

While many have had success designing and fabricating different DEP and iDEP microdevices to manipulate particles in biological fluids, there are some potential drawbacks of these techniques. The traditional DEP technique suffers from fouling, contamination, bubble formation near integrated electrodes, low throughput, and an expensive and complicated fabrication process [38, 39]. The insulating obstacles employed by iDEP are meant to address these shortcomings and are less susceptible to fouling than integrated electrodes [67]. iDEP's fabrication process is also much less complicated; the insulating obstacles can be patterned while etching the microchannel in one step. This technique has the added benefit of making the process more economical in that mass fabrication can be facilitated through the use of injection molding. Unfortunately, one of the primary drawbacks of an iDEP system is the presence of a high electric field intensity within the highly conductive biological fluid inside the microchannel [38, 68]. The relatively high electrical current flow in this situation causes joule heating and a dramatic temperature increase. The ideal technique would combine iDEP's simple fabrication process and resistance to fouling with DEP's reduced susceptibility to joule heating all-the-while preserving the cell manipulation abilities of both methods.

1.6. Contactless Dielectrophoresis (cDEP)

A third manifestation of DEP, contactless dielectrophoresis (cDEP), employs the simplified fabrication processes of iDEP yet lacks the problems associated with the electrode-

sample contact [69]. cDEP relies upon reservoirs filled with highly conductive fluid to act as electrodes and provide the necessary electric field. These reservoirs are placed adjacent to the main microfluidic channel and are separated from the sample by a thin barrier of a dielectric material. The application of a high-frequency electric field to the electrode reservoirs causes their capacitive coupling to the main channel and an electric field is induced across the sample fluid. Similar to traditional DEP, cDEP exploits the varying geometry of the electrodes to create spatial non-uniformities in the electric field. However, by utilizing reservoirs filled with a highly conductive solution, rather than a separate thin film array, the electrode structures employed by cDEP can be fabricated in the same step as the rest of the device; hence the process is conducive to mass production [69].

In order to demonstrate this new method for cell separation and manipulation, we have designed and fabricated a microfluidic device to observe the DEP response of cells to a non-uniform electric field created without direct contact from electrodes. Modeling of the non-uniform electric field distribution in the device was accomplished through an equivalent electronic circuit and finite element analysis of the microfluidic device. The effects of different parameters such as total applied voltage, applied frequency, and the electrical conductivity of the fluid inside and outside of the main channel on the resulting DEP response were simulated and then observed through experimentation. A DEP response was observed primarily as a change in cell trajectory or velocity as it traveled through the device. Further evidence of this DEP response to the non-uniform electric field is provided by the electrorotation of cells, and their aggregation in “pearl chain” formations.

The abilities of cDEP to selectively isolate and enrich a cell population was also investigated. This was demonstrated through the separation of viable cells from a heterogeneous population also containing dead cells. Two cDEP microfluidic devices were designed and fabricated out of polydemethilsiloxane (PDMS) and glass using standard photolitography. The DEP response of the cells was investigated under various electrical experimental conditions in the range of our power supply limitations. Human leukemia THP-1 viable cells were successfully isolated from dead (heat treated) cells without lysing.

The separation of viable and nonviable cells is a critical starting point for this new technology to move towards more advanced applications. Optimization of these devices would allow for selective separation of cells from biological fluids for purposes such as: the diagnosis

of early stages of diseases, drug screening, sample preparation for downstream analysis, enrichment of tumor cells to evaluate tumor lineage via PCR, as well as treatment planning[70-75]. By using viable/nonviable separation as a model for these applications, a new generation of cDEP devices can be tailored around the results reported in this study.

1.7. cDEP to detect tumor initiating cells (TICs)

For many, many years scientists have thought of the cancer cells as all behaving the same. One tumor cell is just like the cell next one to it. Each has the same ability to form a tumor, or worse, to spread. But now we know that this is not the case. Some cells within the tumor are the parents of the other cells [76, 77]. The parents divide in two to make one cell that is an offspring (a son if you will in the case of a prostate tumor) and one cell that can continue to divide. Occasionally the parent will divide and make two copies of itself, increasing the number of parents. But mostly it makes one copy and one son. The son can also divide, but not as many times as the parent, maybe three or four times. The parent, however, can keep dividing and making a copy of itself and new sons. By this process, the parent population doesn't really grow that much, but the number of offspring grows and grows and grows.

If you were to take a single son and ask, will this make a new tumor? The answer would be no, because it can only divide 3 or 4 times. But the parent can make a new tumor because it will divide indefinitely. The parent we call the "tumor initiating cell." Because the parent only occasionally makes a copy of itself it is relatively rare in the tumor compared to the sons. It is just like the grandfather with 35 grandchildren, each generation grows bigger by expansion.

Because the tumor initiating cell is the parent of the tumor, it is the most important target for therapeutic targeting. Kill the tumor initiating cell and you kill the tumor. Our aim for the next generation of cDEP devices is to isolate the tumor initiating cells from a prostate tumor and identify the genetic programming that preserves its tumor initiating properties.

Tumor initiating cells (TICs) are cells within a tumor possessing the ability to generate a new tumor from an existing one that exhibits a similar histopathology as the tumor from which it was derived [76]. There is evidence from a number of tumor types, including prostate tumors [77], that not all cells within the tumor have TIC properties. Some people refer to TICs as tumor or cancer stem cells. The TIC is the most relevant therapeutic target. Kill the TIC and you kill

the tumor. Identification of the specific gene expression patterns and genetic alterations in TICs will likely lead to an increased understanding of the most appropriate therapeutic strategies to ablate this cell population. Current efforts in this direction are hampered by the lack of a suitable high throughput and rapid method to isolate these cells.

Most methods currently rely on time-consuming labeling of surface marker expression followed by cell sorting via flow cytometry [78-80]. This delay may compromise gene expression. These efforts in this direction are hampered by the lack of a suitable high throughput and rapid method to isolate these cells. Most methods currently rely on time-consuming labeling of surface marker expression followed by cell sorting via flow cytometry [78-80]. This delay may compromise gene expression.

Normal stem cells and cancer cells possess similar attributes that suggest a common origin (reviewed in [76]). Like normal stem cells, tumor cells possess self-renewal capabilities. Additionally, some data suggest that the bulk of a tumor is generated from a finite number of cells that possess extended replicative capacity. It is hypothesized that after asymmetric division, daughter tumor cells can undergo some degree of differentiation. Several pathways associated with tumorigenesis have also been implicated in stem cell self-renewal and differentiation. Mutations and alterations in the Wnt, TGF-□/BMP, Notch, and Integrin signaling pathways have been identified in several tumor systems including hematopoietic, gastrointestinal, breast and prostate cancers. These pathways have also been implicated in stem cell self-renewal and differentiation in numerous systems. The common phenotypic attributes of normal stem cells and tumor cells, and the presence of mutations in signaling pathways important for normal stem cell self-renewal in tumor cells have led to the hypothesis that normal stem cells are the target of mutagenesis leading to tumor formation. An alternative model is that intermediate progenitor cells are the cellular targets of mutations that promote a more stem cell-like phenotype.

We demonstrated that prostate TICs possess unique electrical fingerprints compared to non-TICs which make their differentiation and enrichment possible utilizing cDEP technology for further genetic characterization to investigate the targeted therapies.

Chapter 2
Theory

2.1. Net Force on a Dipole

A polarized small neutral particle exposed in electric field $\vec{E}(\vec{r})$ is shown in the following figure. Charges +q and –q are separated with a distance $\vec{d}$. The net force applying on the dipole is:

$$\vec{F} = q\vec{E}(\vec{r} + \vec{d}) - \vec{q}\vec{E} \tag{1}$$

Using the Taylor series $\vec{E}(\vec{r} + \vec{d})$ can be expanded for infinitesimal $\vec{d}$ as follow:

$$\vec{E}(\vec{r} + \vec{d}) = \sum_{j=0}^{\infty} [\frac{1}{j!}(\vec{d} \cdot \vec{\nabla})^{j} \vec{E}(\vec{r})] \tag{2}$$

The zero and first order terms are $\vec{E}(\vec{r})$ and $(\vec{d} \cdot \vec{\nabla})\vec{E}(\vec{r})$. Considering these terms in the first equation, the infinitesimal dipole force will be:

$$F_{dipole} = q\vec{d} \cdot \vec{\nabla}\vec{E}(\vec{r}) \equiv \vec{P} \cdot \vec{\nabla}\vec{E}(\vec{r}) \tag{3}$$

Where $\vec{P}$is defined as dipole moment [35, 81, 82].

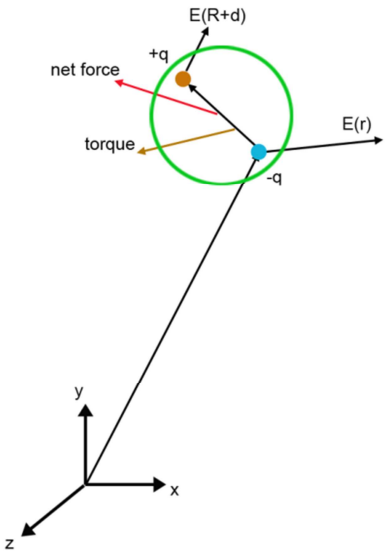

Fig.2.1. A dipole in a Cartesian coordinate system.

2.2. Torque on a Dipole

As described in Holmes' thesis [82], a same dipole shown in the previous figure can experience a net torque

$$\vec{T} = \frac{\vec{d}}{2} \times q\vec{E} + \frac{-\vec{d}}{2} \times (-q\vec{E}) \tag{4}$$

$$\vec{T} = q\vec{d} \times \vec{E} \equiv \vec{p} \times \vec{E} \tag{5}$$

Dielectric materials are characterized by their relative permittivity or dielectric constant, which changes from 1 (for vacuum) to 78 (for water). Absolute permittivity is $\varepsilon_0 = 8.85 \times 10^{-12}$F/m, which is the permittivity of free space.

The electrostatic potential for a dipole of magnitude p in a medium of permittivity $\varepsilon_1$can be written as

$$\Phi_{dipole} = \frac{p \cos\theta}{4\pi\varepsilon_1 r^2} \tag{6}$$

where r and θ are the spherical coordinates.

2.3. Effective Dipole Moments of Lossless Dielectric Particles

2.3.1. Lossless Dielectric Sphere in an Electric Field

As represented in Holmes' thesis [82], by solving the Laplace's equation($\nabla \cdot (\nabla E) = 0$) for a non-charged spherical particle of radius R and permittivity ε_2 suspended in a medium of permittivity ε_1 and a uniform external electric field of magnitude E, one can derive the electrostatic potential distribution outside and inside the particle as follows:

Outside $$\Phi_1(r,\theta) = -Er\cos\theta + \frac{A\cos\theta}{r^2}, r > R \quad (7)$$

Inside $$\Phi_2(r,\theta) = -Br\cos\theta\,, r < R \quad (8)$$

Considering the boundaries for the problem, the constants A and B can be evaluated.

Boundary 1: $\varepsilon_1\left(-\frac{\partial\Phi_1}{\partial r}\right) = \varepsilon_2\left(-\frac{\partial\Phi_2}{\partial r}\right)$

Boundary 2: $\Phi_1 = \Phi_2$

Constants A and B are

$$A = \frac{\varepsilon_2 - \varepsilon_1}{\varepsilon_2 + 2\varepsilon_1}R^3E \qquad \text{B}= \frac{3\varepsilon_1}{\varepsilon_2+2\varepsilon_1}E \quad (7)$$

Comparing equations (6) and (7) and neglecting the small terms, the effective dipole moment can be written as

$$p_{eff} = 4\pi\varepsilon_1 A = 4\pi\varepsilon_1\left(\frac{\varepsilon_2 - \varepsilon_1}{\varepsilon_2 + 2\varepsilon_1}\right)R^3E = 4\pi\varepsilon_1 K(\varepsilon_1,\varepsilon_2)R^3E \quad (8)$$

The $K(\varepsilon_1,\varepsilon_2)$is known as clausius-Mossotti function, which varies between -0.5 and +1.0.

2.3.2 Lossless Dielectric Shells in an Electric Field

Using the same approach presented above and in Holmes' thesis [82], the electrostatic functions are reported as follows:

outside $$\Phi_1(r,\theta) = -Er\cos\theta + \frac{A\cos\theta}{r^2}, \qquad r > R = R_2 \quad (7)$$

shell $$\Phi_2(r,\theta) = -Br\cos\theta\,\frac{C\cos\theta}{r^2}, \qquad R_2 < r < R_3 \quad (8)$$

inside $$\Phi_3(r,\theta) = -Dr\cos\theta\,, \qquad r < R_3 \quad (9)$$

Radial displacement flux and the electric potential are continuous at the boundaries.

$$A = \frac{\varepsilon_2^{eff} - \varepsilon_1}{\varepsilon_2^{eff} + 2\varepsilon_1} R^3 E \tag{10}$$

Shells can be considered as homogeneous spheres in calculations such as Clausius-Mossotti factor by just considering the effective permittivity of the shell seen from outside.

$$\varepsilon_2^{eff} = \varepsilon_2 \left\{ \frac{\left(\frac{R_2}{R_3}\right)^3 + 2\left(\frac{\varepsilon_3 - \varepsilon_2}{\varepsilon_3 + 2\varepsilon_2}\right)}{\left(\frac{R_2}{R_3}\right)^3 - \left(\frac{\varepsilon_3 - \varepsilon_2}{\varepsilon_3 + \varepsilon_2}\right)} \right\} \tag{11}$$

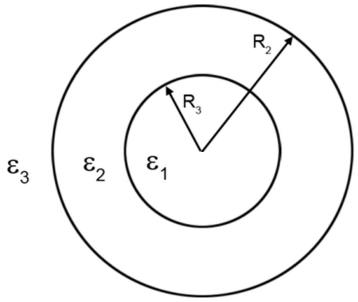

Fig. 2.2. A shell with a core permittivity ε_1 and membrane permittivity $\varepsilon_2$suspended in a medium with permittivity ε_3.

2.4. Clausius-Mossotti Factors of Dielectric Particles with Loss

2.4.1. Lossy Dielectric Particle in an AC Electric Field

Particles that are not perfectly insulating in an AC electric field have a different behavior. The permittivity of these particles is a function of the applied frequency and is defined as a complex function [82]

$$\varepsilon^* = \varepsilon - j\frac{\sigma}{\omega} \tag{12}$$

And the Clausius-Mossotti function is rewritten as a complex function as well

$$K(\varepsilon_1^*, \varepsilon_2^*) = \left(\frac{\varepsilon_2^* - \varepsilon_1^*}{\varepsilon_2^* + 2\varepsilon_1^*}\right) \tag{13}$$

2.4.2. Lossy Dielectric Sphere in an AC Electric Field, Charge Relaxation

There is a delay for dipole moment of an imperfect insulating particle in an instantaneous field. On the other hand, the dipole moment exhibits a phase lag in an AC field. The ratio

between polarizability and depolarization ability are two important factors affect the delay lag which is defined as follows (adopted from Holmes' thesis [82]):

$$charge\ relaxation\ time\ \tau = \frac{\epsilon}{\sigma}$$

Thus the complex form of the Clausius-Mossotti factor can be rewritten as

$$K(\varepsilon_1^*, \varepsilon_2^*) = \left(\frac{\sigma_2 - \sigma_1}{\sigma_2 + 2\sigma_1}\right)\left[\frac{j\omega\tau_0 + 1}{j\omega\tau_{MW} + 1}\right] \quad (12)$$

Where τ_{MW} is the Maxwell-Wagner relaxation time corresponding to the free charge at the particle-medium interface and $\tau_0$is a constant [83].

$$\tau_{MW} = \left(\frac{\varepsilon_2 + 2\varepsilon_1}{\sigma_2 + 2\sigma_1}\right) \text{ and } \qquad \tau_0 = \left(\frac{\varepsilon_2 - \varepsilon_1}{\sigma_2 - \sigma_1}\right) \quad (13)$$

2.4.3. Lossy Dielectric Shell in an AC Electric Field

The same functions that have been used for lossless dielectric shell, can be used for lossy ones, utilizing the effective permittivity of the shell [82]

$$\varepsilon^{*}{}_2^{eff} = \varepsilon_2 \left\{ \frac{\left(\frac{R_2}{R_3}\right)^3 + 2\left(\frac{\varepsilon_3^* - \varepsilon_2^*}{\varepsilon_3^* + 2\varepsilon_2^*}\right)}{\left(\frac{R_2}{R_3}\right)^3 - \left(\frac{\varepsilon_3^* - \varepsilon_2^*}{\varepsilon_3^* + \varepsilon_2^*}\right)} \right\} \quad (14)$$

It should be noted that the scalar values of the effective permittivity $\varepsilon_2^{eff}$and conductivity σ_2^{eff} can be calculated using the definition of the complex permittivity.

$$\varepsilon_2^{eff} = Re\{\varepsilon^{*}{}_2^{eff}\} \quad \text{and} \quad \sigma_2^{eff} = -\omega Im\{\varepsilon^{*}{}_2^{eff}\} \quad (15)$$

where Re{} and Im{} are the real part and the imaginary part of the complex function, respectively[82, 83].

2.4.4. Lossy Dielectric Thin Shell in an AC Electric Field

As described in Holmes' thesis [82], the same set of equations used for homogenous spherical particles can be used, but with different boundary conditions representing the potential drop across the thin shell ($\Delta = (R_2 - R_3)) \ll (R_3 = R)$. Boundary conditions in this case are:

$$\varepsilon_1\left(-\frac{\partial\Phi_1}{\partial r}\right) = \varepsilon_2\left(-\frac{\partial\Phi_2}{\partial r}\right) \quad (16)$$

$$(\Phi_1^* - \Phi_2^*)(j\omega c_m + g_m) = -j\omega\varepsilon_1^* E_{radial}^* \quad (17)$$

where $c_m = \frac{\varepsilon_m}{\Delta}$ and $g_m = \frac{\sigma_m}{\Delta}$ are the capacitance and conductance of the thin shell (membrane).

The resulting effective permittivity of the thin shell particle is

$$\varepsilon^{*}{}_{2}^{eff} = \frac{c_m^* R \varepsilon_2^*}{c_m^* R + \varepsilon_2^*} \tag{18}$$

where c_m^* is defined as $c_m^* = c_m - j\frac{g_m}{\omega}$

2.5. Clausius-Mossotti Factors of Biological Cells

Biological particles or cells can be modeled as thin shell particles. The effective permittivity of a cell is given by [82, 84]

$$\varepsilon^{*}{}_{p}^{eff} \approx c_m R \frac{j\omega R\tau_c + 1}{j\omega(\tau_m + \tau_c) + 1} \tag{19}$$

where $\tau_m = \frac{c_m R}{\sigma_c}$ and $\tau_c = \frac{\varepsilon_c}{\sigma_c}$, c_m is the membrane capacitance per unit are, R is the radius of the cell, $\tau_m$and $\tau_c$are the relaxation times of the membrane and cytoplasm, respectively, and σ_c and ε_c are the conductivity and permittivity of the cytoplasm, respectively. The Clausius-Mossotti factor for such a cell is also given

$$K^*(\omega) = -\frac{\omega^2(\tau_1\tau_m - \tau_c\acute{\tau_m}) + j\omega(\acute{\tau_m} - \tau_1 - \tau_m) - 1}{\omega^2(\tau_c\acute{\tau_m} + 2\tau_1\tau_m) - j\omega(\acute{\tau_m} + 2\tau_1 + \tau_m) - 2} \tag{20}$$

where $\tau_1 = \frac{\varepsilon_1}{\sigma_1}$ and $\tau_m = \acute{} = \frac{c_m R}{\sigma_1}$

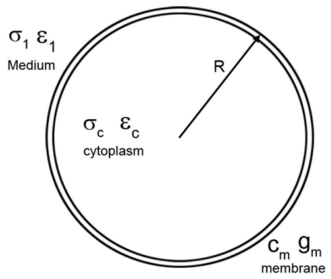

Fig. 2.3. Schematic of a biological cell.

2.6. Dielectrophoretic Force

Substituting the effective dipole moment function (equation 8) in the net dipole force (equation 3) and applying a simple math rule ($\nabla(a.b) = \nabla a \cdot b + b \cdot \nabla a$)), the dielectrophoretic force on a lossless dielectric sphere is given by:

$$\vec{F}_{dipole} = \vec{P} \cdot \vec{\nabla}\vec{E} = 4\pi\varepsilon_1 \left(\frac{\varepsilon_2-\varepsilon_1}{\varepsilon_2+2\varepsilon_1}\right) R^3 \vec{E} \cdot \vec{\nabla}\vec{E} = 4\pi\varepsilon_1 \left(\frac{\varepsilon_2-\varepsilon_1}{\varepsilon_2+2\varepsilon_1}\right) R^3 \frac{1}{2} \nabla(\vec{E} \cdot \vec{E})$$

$$\vec{F}_{dipole} = 2\pi\varepsilon_1 R^3 \left(\frac{\varepsilon_2 - \varepsilon_1}{\varepsilon_2 + 2\varepsilon_1}\right) \nabla(\vec{E} \cdot \vec{E}) \tag{21}$$

The general formula for the a net dipole force on a particle is given based on the Clausius-Mossotti factor

$$\vec{F}_{dipole} = 2\pi\varepsilon_1 R^3 Re\{K(\varepsilon_1^*, \varepsilon_2^*)\} \nabla(\vec{E} \cdot \vec{E}) \tag{22}$$

where the CM factor has been given for different particles with different electrical and geometrical conditions [81-83, 85].

2.7. DEP Cross-over Frequency

The DEP force on a particle may be positive or negative depending on the relationship of the applied frequency to the particles DEP crossover frequency. DEP crossover frequency is the frequency in which the real part of the Clausius-Mossotti (C.M.) factor is equal to zero and is given by [1, 86]

$$f_c = \frac{1}{2\pi} \sqrt{\frac{(\sigma_1 - \sigma_2)(\sigma_2 + 2\sigma_1)}{(\varepsilon_2 - \varepsilon_1)(\varepsilon_2 + 2\varepsilon_1)}} \tag{23}$$

where f_c is the crossover frequency and σ_1 and σ_2 are the conductivity of the particle and medium, respectively. This shows that DEP can be used to differentiate micro-particles based on their difference in C.M. factor by adjusting the frequency.

2.8. Dimensionless Navier-Stokes Equation

The Navier-Stokes equation is given

$$St \frac{\partial V^*}{\partial t^*} + V^* \cdot \nabla^* V^* = -Eu \nabla^* p^* + \frac{1}{Re} \nabla^{*2} V^* + \frac{1}{Fr^2} g^* \tag{24}$$

where $St = \frac{L}{T\|V\|}$ is the Strouhal number, $Re = \rho \| V \| L/\eta$ is the Reynolds number, $Eu = \frac{p_0 - p_\infty}{\rho V^2}$ and $Fr^2 = \frac{\|V\|^2}{gL}$is the Froude number. L, T, and $\| V \|$ are the characteristic length, time,

and velocity, respectively. $V^*$is the dimensionless velocity, p^* is the dimensionless pressure, and g^* is the dimensionless gravity and η is the dynamic viscosity of the fluid.
Froude number is important when we have free surfaces in the flow and we can neglect the term with the Froude number in physiological fluids.

2.9. Low Reynolds number Flow around a Sphere

In Fluid flows with low Reynolds number, the viscous forces are much more important than the inertial forces. The pressure is scaled down by $p_0 - p_\infty = \eta \parallel V \parallel / L$. On the other hand $Eu = \frac{p_0 - p_\infty}{\rho V^2} = \frac{1}{Re}$. In this study, the frequency of the applied signal is on the order of hundreds of kHz, the width of the channel is on the order of hundreds of mirco-meters, and the velocity of the fluid is on the order of hundreds of micro-meters per second. Thus the Strouhal number is very small ($St \ll 1$) and we can neglect the time dependent term of the Navier Stokes equation. The dimensionless Navier-Stokes equation is rewritten as

$$\nabla^* p^* = \nabla^{*2} V^* \tag{25}$$

And by just substituting the definitions for dimensionless parameters and the Reynolds number, the dimensional Navier Stokes equation will be written as

$$\nabla p = \eta \nabla^2 V \tag{26}$$

In order to study the moving of a biological particle or cell in a physiological fluid such as blood, we assume a rigid sphere exposed to a very low Reynolds number fluid flow.

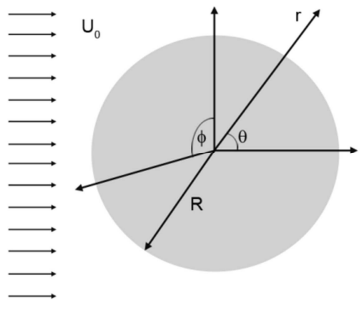

Fig. 2.4. A sphere suspended in a uniform flow with a radius R.
The boundary conditions for such a problem with a spherical coordinate with an origin placed at the center of the sphere are given

$r \to \infty$ $$v_r = u_0 \cos\theta \tag{27}$$

$r \to \infty$ $$v_\theta = -u_0 \sin\theta \tag{28}$$

$r \to \infty$ $$p = p_0 \tag{29}$$

$r = R$ $$v_r = v_\theta = 0 \tag{30}$$

The goal is to determine the velocity profile, calculate the shear stress, and then to determine the force on the sphere.

The continuity equation for a steady and incompressible fluid is

$$\nabla \cdot V = 0 \tag{31}$$

This can be rewritten in the spherical coordinates

$$\frac{1}{r^2}\frac{\partial(r^2 V_r)}{\partial r} + \frac{1}{r\sin\theta}\frac{\partial(V_\theta \sin\theta)}{\partial\theta} = 0 \tag{32}$$

And the Navier Stokes equations are

$$-\frac{\partial p}{\partial r} + \eta\left(\frac{1}{r^2}\frac{\partial^2\left(\left(r^2\frac{\partial V_r}{\partial r}\right)\right)}{\partial r^2}\right) + \frac{1}{r^2\sin\theta}\frac{\partial(\sin\theta\frac{\partial V_r}{\partial\theta})}{\partial\theta} - 2\frac{V_r}{r^2} - \frac{2}{r^2}\frac{\partial V_\theta}{\partial\theta} - \frac{2}{r^2}V_\theta\cot\theta = 0 \tag{33}$$

and

$$-\frac{1}{r}\frac{\partial p}{\partial\theta} + \eta\left(\frac{1}{r^2}\frac{\partial\left(r^2\frac{\partial V_\theta}{\partial r}\right)}{\partial r} + \frac{1}{r^2}\frac{\partial\left(\frac{1}{\sin\theta}\frac{\partial(V_\theta\sin\theta)}{\partial\theta}\right)}{\partial\theta} + \frac{2}{r^2}\frac{\partial V_r}{\partial\theta} - \frac{V_\theta}{r^2\sin^2\theta}\right) = 0 \tag{34}$$

Considering the fluid behavior far from the sphere, the velocity profile can be assumed such a way that satisfy these boundary conditions

$$v_r = u_0\,\mathrm{f(r)}\cos\theta \tag{35}$$

$$v_\theta = -u_0\,\mathrm{g(r)}\sin\theta \tag{36}$$

$$v_\emptyset = 0 \tag{37}$$

Applying the continuity equation, the first relation for the functions f and g is

$$\frac{d(r^2 f)}{dr} = 2rg \tag{38}$$

Other boundary conditions at the surface (no slip) and far from the surface of the sphere are

$r = R$ $$f = 0 \quad g = 0 \quad \frac{df}{dr} = 0 \tag{39}$$

$r \to \infty$ $$f = 1 \quad g = 1 \quad \frac{df}{dr} = 0 \tag{40}$$

The final expression for the velocity profile and the pressure of the fluid around the sphere are

$$V_r = u_0[1 - \frac{3}{2}\frac{R}{r} + \frac{1}{2}\frac{R^3}{r^3}]\cos\theta \tag{41}$$

$$V_\theta = -u_0[1 - \frac{3}{4}\frac{R}{r} - \frac{1}{4}\frac{R^3}{r^3}]\sin\theta \tag{42}$$

$$p = p_\infty - \frac{3\eta u_0}{2R}(\frac{R}{r})^2\cos\theta \tag{43}$$

The drag force on the sphere due to a low Reynolds number flow can be calculated as follows

$$F_z = F \cdot e_z = -e_z \cdot \int n \cdot \sigma dS \tag{44}$$

The pressure and shear stress are the main causes for the net force on the surface of the sphere.

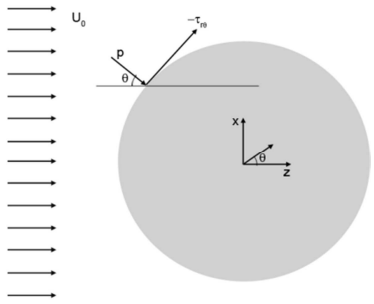

Fig. 2.5. Pressure and shear stress acting on the surface of a sphere

The differential surface area on the sphere is $R^2 \sin\theta\, d\theta d\emptyset$.The force in the direction of the fluid flow can be evaluated as

$$F_z = \iint p(r=R)\cos\theta d\theta d\emptyset + \iint -\tau_{r\theta}(r=R)\sin\theta\, R^2 d\theta d\emptyset \tag{45}$$

After integration over the surface, the resulting expression for the surface force become

$$F_z = \frac{4}{3}\pi R^3 \rho g\cos\alpha + 2\pi\eta u_0 R + 4\pi\mu u_0 R \tag{46}$$

where α is the angle between the gravity vector and the fluid flow direction. The first term is the buoyant force. The second term is because of the pressure, and the third term is due to the shear stress on the surface. Most of the times, we have 90 degree relative angle between the gravity vector and the flow direction. So the first term in the drag force equation becomes zero. The sum of the forces due to pressure and shear stress is known as drag force and is given by

$$F_z = 6\pi\eta u_0 R \tag{47}$$

2.10. Electrorotation (ROT)

Electrorotation is the rotation of polarized particles suspended in a liquid due to an induced torque in a rotating electric field [87]. The maximum magnitude of the torque is given by

$$\Gamma = -4\pi\varepsilon_m \boldsymbol{r}^3 \,\mathrm{Im}\{\boldsymbol{K}(\omega)\}(\boldsymbol{E}_{rms} \cdot \boldsymbol{E}_{rms}) \tag{48}$$

where $\mathrm{Im}\{\boldsymbol{K}(\omega)\}$ is the imaginary part of the Clausius-Mossotti factor $\boldsymbol{K}(\omega)$.

ROT is a powerful technique to characterize the electrical properties of the cell membrane. The dipole creation and decay in a particle has a characteristic time, which is dependent on the electrical signatures of the particle. Due to this delay in response, a torque resulting from the interaction between the rotating electric field and the dipole, cell spins at a unique specific rate at each frequency. It should be noted that, however the field rotates at rates greater than $10^7 S^{-1}$, the dipole spins at a rate distinguishable with eye. Rotation rates vary between -3 and +1.5 rotations per second[88]. Traditional ROT devices with four independent electrodes with 90^o phase difference have been used to measure the rotation rate of cells for a wide range of frequencies [87, 89-92]. ROT has been used to study the electrical properties of acellular prokaryotes like virus [93]and bacteria [94, 95], eukaryotes like protozoa [90, 96], yeast [92], algae [94], plant cells [87], and insect cell line [91], mammalian cells, like cell lines [96], lymphocyte [95], and erythrocyte [96].

2.11. Velocity of the Particle

Assuming the cells are spherical particles in the medium, the hydrodynamic frictional force, $\boldsymbol{f}_{Drag}$, due to translation and hydrodynamic frictional torque, R, due to rotation are given by:

$$f_{Drag} = 6\eta r\pi(u_p - u_f) \tag{49}$$

$$R = 8\eta\pi r^3\Omega \tag{50}$$

where r is the particle radius, μ is the medium viscosity, u_p is the velocity of the particle, u_f is the medium velocity, R is induced torque, and Ω is electrorotation rate (rad.S^{-1}).

The magnitude of the translational velocity is determined by Newton's second law with the dielectrophoretic force and Stoke's drag force as the applied forces on a cell. Assuming the

particle is at rest at time t=0, the exact solution for the Newton's second law can be evaluated as follow [1, 97]

$$\sum F = m_p a \tag{51}$$

$$F_{ext} - f_{Drag}(u_p - u_f) = m_p \frac{du_p}{dt} = m_p \dot{u_p} \tag{52}$$

$$m_p \dot{u_p} + f_{Drag} u_p = F_{ext} + f_{Drag} u_f \tag{53}$$

$$\dot{u_p} + \frac{f_{Drag}}{m_p} u_p = \frac{F_{ext} + f_{Drag} u_f}{m_p} \tag{54}$$

$$\mu(t) = e^{\int \frac{f_{Drag}}{m_p} dt} = e^{\frac{f_{Drag}}{m_p} t} \tag{55}$$

$$e^{\frac{f_{Drag}}{m_p} t} \dot{u_p} + e^{\frac{f_{Drag}}{m_p} t} \frac{f_{Drag}}{m_p} u_p = e^{\frac{f_{Drag}}{m_p} t} \left(\frac{F_{ext} + f_{Drag} u_f}{m_p}\right) \tag{56}$$

$$\frac{d\left(e^{\frac{f_{Drag}}{m_p} t} \frac{f_{Drag}}{m_p} u_p\right)}{dt} = e^{\frac{f_{Drag}}{m_p} t} \left(\frac{F_{ext} + f_{Drag} u_f}{m_p}\right) \tag{57}$$

$$d\left(e^{\frac{f_{Drag}}{m_p} t} \frac{f_{Drag}}{m_p} u_p\right) = e^{\frac{f_{Drag}}{m_p} t} \left(\frac{F_{ext} + f_{Drag} u_f}{m_p}\right) dt \tag{58}$$

$$\int d\left(e^{\frac{f_{Drag}}{m_p} t} \frac{f_{Drag}}{m_p} u_p\right) = \int e^{\frac{f_{Drag}}{m_p} t} \left(\frac{F_{ext} + f_{Drag} u_f}{m_p}\right) dt \tag{59}$$

$$e^{\frac{f_{Drag}}{m_p} t} \frac{f_{Drag}}{m_p} u_p = \left(\frac{F_{ext} + f_{Drag} u_f}{m_p}\right) \frac{m_p}{f_{Drag}} e^{\frac{f_{Drag}}{m_p} t} + c \tag{60}$$

$$\frac{f_{Drag}}{m_p} u_p = \left(\frac{F_{ext}}{f_{Drag}} + u_f\right) + c e^{-\frac{f_{Drag}}{m_p} t} \tag{61}$$

At t=0, the cell is at rest ($u_p = 0$), so

$$c = -\left(\frac{F_{ext}}{f_{Drag}} + u_f\right) \tag{62}$$

$$u_p = \left(u_f + \frac{F_{ext}}{f_{Drag}}\right)\left[1 - e^{-\left(f_{Drag}/m_p\right) t}\right] \tag{63}$$

where $F_{ext}$is the external forces on the particle other than drag force, and m_p is the mass of the particle. The term $\frac{m_p}{f_{Drag}} = (\frac{2\rho r^2}{9\eta})$ that appears in the exponential term is known as the characteristic term. Where ρ is the density of the particle that can be estimated as the density of the medium for the cells. r is the radius of the particle, and η is the viscosity of the medium.
For cells with with ~15μm diameter this characteristic time is ~12μs, which is orders of magnitude smaller than the time scale of the external forces and our experimental observations.
Thus by substituting the formula for the dielectrophoretic force as the only external force F_{ext}, the translational velocity of the cell would be

$$u_p = u_f - \mu_{DEP}\nabla(E \cdot E) \tag{64}$$

where μ_{DEP} is the dielectrophoretic mobility of the particle and is defined as:

$$\mu_{DEP} = \frac{\varepsilon_m r^2}{3\eta} Re\{K(\varepsilon_1^*, \varepsilon_2^*)\} \tag{65}$$

Using the same approach, the steady state rotational velocity of the particle is given by

$$\Omega = \frac{\varepsilon_m}{2\eta} Im\{K(\varepsilon_1^*, \varepsilon_2^*)\}\mathrm{E} \cdot \mathrm{E} \tag{66}$$

2.12. Trapping prediction in iDEP through theory

The movement of the particle obeys the same formula presented in equation (63). However, the external force is the summation of dielectrophoretic and electro-kinetic force. Hence, the velocity of the particle can be expressed as

$$u_p = u_f + \frac{f_{EP} + f_{DEP}}{6\pi\eta r} \tag{67}$$

The dielectrophoretic mobility, μ_{DEP}, (equation 65) can be rewritten considering the fact that the applied signal is DC

$$\mu_{DEP} = \frac{\varepsilon_m r^2}{3\eta} \frac{\sigma_p - \sigma_f}{\sigma_p + 2\sigma_f} \tag{68}$$

In this analysis, the velocity of the fluid is due to electroosmotic flow. Electroosmotic flow and electrophoresis are both linearly proportional to the local electric field. Therefore, the electrokinetic induced particle velocity is related linearly to the electric field and can be expressed using a proportionality constant, electrokinetic mobility, $\mu_{EK} = \mu_{EO} - \mu_{Ep}$ where μ_{EP}

and μ_{EO} are the electrophoretic and electroosmotic mobilities, respectively, and $u_f = \mu_{EO}E$ and $u_{EP} = -\mu_{EP}E$. Substituting these terms into equation (3) and expressing the dielectrophoretic particle velocity in terms of its mobility, gives us the following expression for the total velocity of the particle:

$$u_p = \mu_{EK}E + \mu_{DEP}\nabla(E \cdot E) \tag{69}$$

In other words, the velocity of the particle is the sum of the local liquid velocity due to electroosmosis and the velocities induced by the particle forces (i.e. dielectrophoresis and electrophoresis).

A particle traps when the dielectrophoretic force is greater than the electrokinetic force. For a particle to become trapped in our device, the dielectrophoretic force on the particle must overcome the electrokinetic force on the particle. This can be represented mathematically as

$$\frac{u_{DEP}u_{EK}}{u_{EK}u_{EK}} = \frac{\mu_{DEP}}{\mu_{EK}} \frac{\nabla(E \cdot E)}{E \cdot E} \tag{70}$$

where $u_{DEP} = \mu_{DEP}\nabla(E \cdot E)$ and μ_{DEP} are the dielectrophoretic velocity and mobility of the particle, respectively, and $u_{EK} = \mu_{EK}E \cdot E$ and μ_{EK} are the electrokinetic velocity and mobility of the particle. As the field strength is increased, dielectrophoresis increases as the square of the field and electrokinetic flow only increases linearly with the field. Eventually, the dielectrophoretic velocity will overcome the electrokinetic velocity and the particles will trap [51].

2.13. Electroporation

Intense but short electrical fields can increase the permeability of the cell membrane in a process referred to as electroporation. Reversible electroporation has become an important tool in biotechnology and medicine. The various applications of reversible electroporation require cells to survive the procedure and, therefore, the occurrence of irreversible electroporation (IRE), following which cells die, is obviously undesirable.

The cell membrane is essentially a non-conductive barrier that protects the inside of the cell from the outside, controlling transport into and out of the cell through ion channels and the membrane's resting potential. Electroporation is a molecular tool and an electromechanical method used to introduce polar molecules into a cell through the cell membrane via intense and

short electrical fields [98]. The natural transmembrane potential is on the order of 70 mV in healthy cells. If the potential drop across the membrane is made to exceed approximately 1 V by the action of an applied electric field, structural rearrangement of the lipid bilayer occurs, creating permanent aqueous pathways or pores for ions and macromolecules to pass through, i.e. irreversible electroporation (IRE) [99].

The typical formula to approximate the induced transmembrane potential (V_m) resulting from an applied electric field for a cell in suspension is:

$$V_m = \lambda r E_a \cos\theta \left[1 + \left({}^{f}/_{f_s}\right)^2\right]^{-0.5} \tag{71}$$

where λ is the shape factor of the cell (1.5 for spherical cells), r is the radius of the cell, E_a is the applied electric field, θ is the angle between electric field and the vector from the cell center to any point on its surface, fs is approximately equal to the frequency where the beta dielectric dispersion occurs (below which the cell membrane charge is in step with the electric field) and f is the frequency of the assumed sinusoidal E_a [100]. This results from the simplifying model of a cell as a resistor (intra- and extra-cellular path-resistance) in series with a capacitor (membrane capacitance). For most cases, the transient terms can be neglected because the electroporation pulse (100 µs - 50 ms) is much larger than the membrane charging time (about 1 µs for spherical cells about 10 µm in diameter) [101].

During the last three decades, when the field of electroporation has become dominated by reversible electroporation applications, irreversible electroporation (IRE) was viewed as an undesirable side effect. However, during the last few years IRE has begun to emerge as an important minimally invasive non-thermal ablation technique in its own right for tumors and arrhythmogenic regions in the heart [102-109]. IRE's ability to create complete and predictable cell ablation with sharp transition between normal and necrotic tissue, while sparing neighboring blood vessels, connective tissue, and nerves, is of great advantage in numerous medical applications.

IRE had been studied primarily only to define the upper limit of electrical parameters that induces reversible electroporation. Thus, the line which delineates IRE from conventional thermal damage is poorly defined. There have been experimental studies on viability of cells following electric pulses. Some of these proposed empirical relationships connect probability of cell death to pulse strength, duration, or number of pulses [110-112]. There is a great degree of

disagreement: some studies find correlation between cell death and the total energy delivered by the pulse, [111, 113], while other do not [114, 115], and yet others correlate cell death with the total charge [112]. The mechanism of cell death is still not well-understood but it has been postulated that it is via necrosis in IRE presumably due to loss of homeostasis as opposed to supraporation, which is via apoptosis [116]. R.C. Lee et al. and Martin et al. have extensively investigated the thermal effects that may be induced by high voltage electroporation pulses as a mechanism of cell death during electroporation [117, 118]. Lee has investigated tissue damage in high-voltage electrical trauma and estimated the extent of heat mediated cellular injury using the Arrhenius equation [118]. Three possible mechanisms for tissue damage in skin have been proposed by Martin et al. [117]. The damage results from long exposure time to temperatures exceeding a threshold or a phase change in the stratum corneum (SC) lipids or water [117].

In order to aid planning IRE treatments, several theoretical studies have focused on computing electrical and thermal conditions in the treated tissue [119-122]. Given the electrode configuration and tissue properties, the models predict the electric field in the tissue, pulse-induced transmembrane potential and rise in temperature. Typically, a threshold value of E or V_m has to be assumed based on experimental measurements to estimate the extent of tissue destroyed by the pulse [102].

Chapter 3
Literature Review

3.1. History of Dielectrophoresis

Efficient biological particle separation and manipulation is a crucial issue in the development of integrated microfluidic systems. Current enrichment techniques for sample preparation include density gradient based centrifugation or membrane filtration [20], fluorescent and magnetic activated cell sorting (F/MACS) [21], cell surface markers [9], and laser tweezers [22]. Each of these techniques relies on different cell properties for separation and has intrinsic advantages and disadvantages. Typically more sensitive techniques may require prior knowledge of cell-specific markers and antibodies to prepare target cells for analysis.

One alternative to these methods is dielectrophoresis (DEP) which is the motion of a particle due to its polarization in the presence of a non-uniform electric field [123, 124]. Many device architectures and configurations have been developed to efficiently sort biological particles by DEP. Early DEP experiments, carried out by Pohl et al., utilized pin-plate and pin-pin electrodes to differentiate live and dead yeast cells, and then collected the yeast cells at the surface of the electrode [125]. The challenge for these early large scale devices was overcoming unwanted thermal effects (heating in excess of 30oC) and hydrolysis (bubble generation) effects due to the large voltages that needed to be applied [126]. Currently, typical dielectrophoretic devices employ an array of thin-film interdigitated electrodes placed within a flow channel to generate a nonuniform electric field that interacts with particles near the surface of the electrode array [127]. Such platforms have shown that DEP is an effective means to concentrate and differentiate cells rapidly and reversibly based on their size, shape, internal structure, and intrinsic properties such as conductivity and polarizability. These intrinsic properties arise due to the membrane compositional and electrostatic characteristics, internal cellular structure, and the type of nucleus [37] associated with each type of cell. A few pertinent examples of DEP technology include the concentration of human leukemia cells in an isotonic solution [7], the

separation of human breast cancer cells from blood [8], the concentration and separation of live yeast cells from dead [12], and the segregation of different human tumor cells [128]. The selectivity of dielectrophoresis has been further demonstrated through the differentiation of cells of the same type based on their activation state [126, 129]. Unfortunately, microelectrode-based devices are susceptible to electrode fouling and are not suitable for high-throughput applications since the electric field gradient rapidly dissipates above the surface of the electrode array. Typical sample volumes that are processed within these devices are on the order of nano- to microliters, far below that of typical clinical diagnostic sample volumes (mL).

Currently, typical dielectrophoretic devices employ an array of thin-film interdigitated electrodes placed within the flow of a channel to generate a non-uniform electric field that interacts with particles near the surface of the electrode array [127]. Such platforms have shown that DEP is an effective means to concentrate and differentiate cells rapidly and reversibly based on their size, shape, and intrinsic electrical properties such as conductivity and polarizability. These intrinsic properties arise due to the membrane compositional and electrostatic characteristics, internal cellular structure, and the type of nucleus [37] associated with each type of cell.

The application of dielectrophoresis to separate target cells from a solution has been studied extensively in the last two decades. Examples of the successful use of dielectrophoresis include the separation of human leukemia cells from red blood cells in an isotonic solution [7], entrapment of human breast cancer cells from blood [8], and separation of U937 human monocytic from peripheral blood mononuclear cells (PBMC) [9]. DEP has also been used to separate neuroblastoma cells from HTB glioma cells [2], isolate cervical carcinoma cells [10], isolate K562 human CML cells [11], separate live yeast cells from dead [12], and segregate different human tumor cells [128]. Unfortunately, the microelectrode-based devices used in these experiments are susceptible to electrode fouling and require complicated fabrication procedures [38, 39].

Insulator-based dielectrophoresis (iDEP) is a practical method to obtain the selectivity of dielectrophoresis while overcoming the robustness issues associated with traditional dielectrophoresis platforms. iDEP relies on insulating obstacles rather than the geometry of the electrodes to produce spatial non-uniformities in the electric field. The basic concept of the iDEP technique was first presented by Masuda et al. [46]. Others have previously demonstrated with

glass insulating structures and AC electric fields that iDEP can separate DNA molecules, bacteria, and hematapoietic cells [47]. It has been showed that polymer-based iDEP devices are effective for selective trapping of a range of biological particles in an aqueous sample [51]. iDEP technology has also shown the potential for water quality monitoring [52], separating and concentrating prokaryotic cells and viruses [53], concentration and separation of live and dead bacteria [2], sample concentration followed by impedance detection [11], and manipulation of protein particles [54].

While many have had success designing and fabricating different DEP and iDEP microdevices to manipulate particles in biological fluids, there are some potential drawbacks of these techniques. The traditional DEP technique suffers from fouling, contamination, bubble formation near integrated electrodes, low throughput, and an expensive and complicated fabrication process [38, 39]. The insulating obstacles employed by iDEP are meant to address these shortcomings and are less susceptible to fouling than integrated electrodes[67]. iDEP's fabrication process is also much less complicated; the insulating obstacles can be patterned while etching the microchannel in one step. This technique has the added benefit of making the process more economical in that mass fabrication can be facilitated through the use of injection molding. Unfortunately, one of the primary drawbacks of an iDEP system is the presence of a high electric field intensity within the highly conductive biological fluid inside the microchannel[38, 68]. The relatively high electrical current flow in this situation causes joule heating and a dramatic temperature increase. The ideal technique would combine iDEP's simple fabrication process and resistance to fouling with DEP's reduced susceptibility to joule heating all-the-while preserving the cell manipulation abilities of both methods.

We have developed an alternative method to provide the spatially non-uniform electric field required for DEP in which electrodes are not in direct contact with the biological sample. The absence of contact between electrodes and the sample fluid inside the channel prevents bubble formation and mitigates fouling. It is also important to note that without direct contact between the electrodes and the sample fluid, any contaminating effects of this interaction can be avoided. In fact, the only material in contact with the sample fluid is the substrate material the device is patterned on. In our method, an electric field is created in the microchannel using electrodes inserted in a highly conductive solution which is isolated from the main channel by thin insulating barriers. These insulating barriers exhibit a capacitive behavior and therefore an

electric field can be produced in the main channel by applying an AC electric field across them. Furthermore, non-uniformity of the electric field distribution inside the main channel is provided by the geometry of insulating structures both outside and inside the channel.

3.2. Circulating Tumor Cells

The critical and vital information regarding the function of different organs are saved and transported in the blood through delivering oxygen, nutrients, and immune cells. So blood sampling and analysis is playing a crucial role in many biological, medical, and science applications. Flow cytometry is one of the most important advanced techniques with a relatively high throughput that provides detail wealthy information about a blood sample. However, only trained professionals can use the not portable and complicated equipment. Furthermore, previous knowledge of specific cell surface markers with respect to a target cell type is required and target cell labeling is time consuming [130]. Microfluidic technology is one of the most interesting methods among the advanced technologies for blood analysis. The portable lab-on-a-chip devices can be utilized by potential non-professional users for diagnostic purposes through a rapid and accurate measurement of different parameters such as the concentration of red blood cells, white blood cells, neuthrophils, cancer cells, etc. However, there are technical challenges with respect to blood sample analysis. Plasma and cells are the components of blood. 45% of the blood volume is due to blood cells. Therefore, depending on the diagnostic requirements, only some of the target cells are supposed to be isolated from other non-target cells for further analytical and genetic investigations. Approximately, there are more than 5×10^{9} cells per one milliliter of blood. A general classification for different types of cell lines in blood and their concentration is given in Table 3.1 which has been adapted from [130, 131].

It is of course a huge technical challenge to identify and isolate a specific cell type among this diverse cell types in blood to investigate their function and/or concentration for diagnosis or treatment purposes. The handling and separation procedures are extremely important as some of the cells in blood such as leukocytes are designed to respond quickly to the changes in their environments. Thus their function can be changed due to using improper chemicals or microenvironments which can consequently affect their further studies [130, 132, 133]. Lab-on-a-chip technologies are representing new promising methods to not only miniaturize the macro

systems, but also more importantly to demonstrate delegate technologies for gentle separation methods.

Table 3.1. Cell Populations and Subpopulations in normal blood. Adapted from [130, 131].

Cell Type	**Cell Population/ mL**
Erythrocytes (RBC)	5×10^{9}
Reticulocytes	$30\times10^{6} – 70\times10^{6}$
Platelets	$200\times10^{6} – 500\times10^{6}$
All leukocytes (total)	$5\times10^{6} – 10\times10^{6}$
Neutrophils	$4\times10^{6} – 8\times10^{6}$
Eosinophils	$0.05\times10^{6} – 0.3\times10^{6}$
Basophils	$0 – 0.1\times10^{6}$
Lymphocytes (total)	$1\times10^{6} – 4\times10^{6}$
CD4 + T Cell	$0.4\times10^{6} – 1.6\times10^{6}$
CD8 + T Cell	$0.2\times10^{6} – 0.8\times10^{6}$
B-Cell	$0.2\times10^{6} – 0.8\times10^{6}$
NK	$0.1\times10^{6} – 0.5\times10^{6}$

There are different methods to identify and isolate cells from a background. The characteristic property of the target cell that distinguishes the cell type, the sample size available for analysis, purity of the isolated sample, process time, the viability of the target isolated cells, the physical stress on the cell during the process, and the process cost are some of the crucial criteria to select an appropriate separation method. Density, size, cell surface marker morphology, and dielectric and electrical properties of the cell types are the physical and surface properties of the cells that can be used in separation methods. However, there are challenges and drawbacks associated with each method. Prior knowledge of the density of the target cell type, high maintenance costs, and protein denaturation are some of the potential pitfalls with respect to centrifugation methods. Device clogging and difficult cell recovery after process are also the drawbacks regarding to the size methods. The large number of cells for analysis, the time needed to process the signal data, and prior knowledge of the target cell surface proteins are the disadvantages of the flow cytometry method [134].

Approximately 24.6 million people live with cancer worldwide. According to the World Health Organization (WHO), 7.9 million people died of cancer in 2007. Based on projections, cancer deaths will continue to rise with an estimated 12 million people dying from cancer in 2030. Lung, stomach, liver, colon, and breast cancers are the main types, leading to overall cancer mortality. In the United States, cancer is the second most common cause of death behind cardiovascular disease and accounts for one out of every four deaths. Based on the American Cancer Society (ACS) Facts and Figures, the overall cost of cancer to society in 2008 was estimated to be 228.1 billion dollars. If cancer is detected early and if treatment is delivered in a timely, effective manner, survival rates increase significantly. An estimated one-third of all cancers could be cured if detected and treated early.

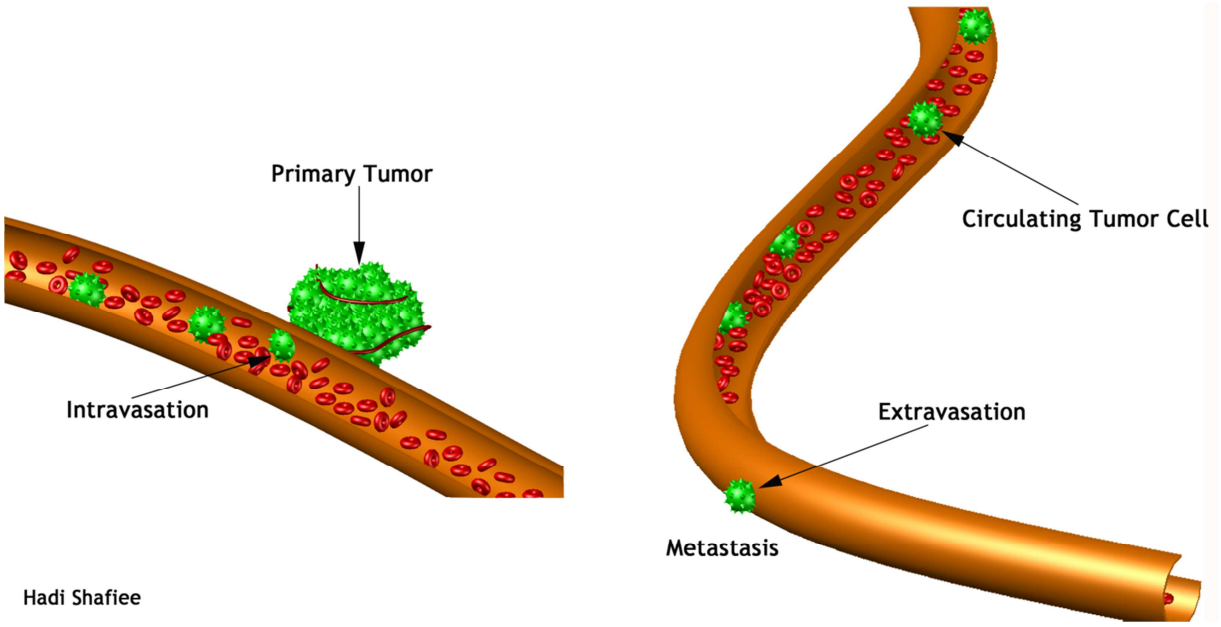

Fig. 3.1. Cancer cells get off from the primary tumor and enter the blood vessels to circulate through the blood stream in order to find a new micro-environment to regenerate a new tumor.

Microfluidics has found numerous applications ranging from the life sciences industries for pharmaceuticals and biomedicine (drug design, delivery and detection, diagnostic devices) to industrial applications of combinational synthesis (such as rapid analysis and high throughput screening) [135]. Among all these, one of the intriguing exploitation of microfluidics or micro total analysis systems (μTAS) is the separation of circulating tumor cells (CTCs) from body fluids. In different human tumor types, the dissemination of cancer cells throughout the body has

already occurred by the time a primary tumor is typically detected. Cancer cells spread from the initial site of a tumor by first invading the surrounding tissue, then by entering the blood or lymph vessels, and finally by crossing the vessel wall to exit the vasculature into distal organs. Cancer cells then colonize the new site and proliferate to form a second tumor mass. CTCs in the blood stream can be used to detect cancer cells before the primary tumor is large enough to be detected by standard screening examinations. The September 2006 issue of the Journal of the National Cancer Institute (NCI) states: "The war on cancer was declared 40 years ago and cancer is still here," and "Technologies that capture enemy CTCs for further interrogation might prove useful in the war on cancer." CTCs cannot only become a new marker for cancer prognosis, but their detection can also be a valid new parameter for diagnosing cancer early, for monitoring disease progression and relapse, and for optimizing therapy [25, 136-139]. "The thing I find really exciting about CTCs is that they likely represent the state of your cancer right now" said Jeff Smerage, M.D., Ph.D., of the University of Michigan in Ann Arbor. " It's like having access to tumor tissue that you might not be able to get to. "[140]

There are accumulating reports of the detection, isolation, enrichment, and characterization of CTCs [141-150]. The previous findings indicate that CTCs can be found in patients before the primary tumor is detected and in a significant percentage of patients after carcinoma reoccurrence. There has been evidence that CTCs derived from the primary tumor exist in the blood of patients even after removal of the primary tumor and they may reflect the tumor burden at all stages of tumor progression [151]. Therefore, CTCs can be considered as tools for early diagnosis as well as genetic characterization and immunophenotypic changes studies, thus helping to conduct targeted therapies [152]. It should be noted that blood tests are safe and can be performed frequently, whereas invasive methods such as bone marrow aspiration are difficult and inconvenient.

However, some cancers do not disseminate cells easily into systemic distribution. For example, currently breast cancer CTCs can only be detected when the disease is spreading and even then less than 10 cancer cells in 7.5ml of blood can be found in most patients [153].Thus, for these cancers, other bodily fluids such as nipple aspirates or ascites fluid need to be considered to detect early stages of the disease. The idea that disseminated tumor cells slip into body fluids is not new, but the ability to find these few cells among the many millions of cells present is a relatively recent development.

3.3. Current Methods to Detect CTCs

The most reliable method currently available for CTC detection is automated digital microscopy (ADM) which uses image analysis to recognize immunochemically or immunomagnetically labeled tumor cells. The CellSearch System™ (Veridex, LLC; Warren, NJ), as an example, was approved by the FDA in December 2006 as an aid for monitoring patients with metastatic breast cancer. This system involves mixing a blood sample with iron particles coated with an antibody that targets the epithelial cell adhesion molecule (EpCAM). Using this test, Daniel Hayes, M.D. and his colleagues at the University of Michigan Comprehensive Cancer Center reported that the overall survival of patients with breast cancers harboring fewer than five CTCs in about 7mL blood after 3-5 weeks of starting their therapy was a relatively long 18.5 months. Women who had five CTCs or more had much shorter median survival times ranging from 1.3 to 3.6 months [24, 25]. Their study tested 177 metastatic breast cancer patients and found patients with fewer than 5 CTCs/7.5ml of blood demonstrated a mean progression free survival time of 7 months. The patients with greater than 5 CTCs/7.5ml of blood had a mean progression free survival time of only 2.7 months. This result was also reflected in the patients' overall survival time of 18 months and 8.2 months respectively[153]. Kurusu et al. assayed for carcinoembryonic antigen (CEA) in peripheral blood from 103 lung cancer patients through reverse transcriptase-polymerase chain reaction. No CEA was detected in control samples. Sixty-two of the 103 patients were positive for CEA in the peripheral blood. Of these 62, 27 remained positive after surgical intervention showing high correlation with pathologic TNM stage of the disease[154]. These results provide proof-of-principle that CTCs are valuable early diagnostic and prognostic cancer markers. The accuracy, precesion, and linearity of CellSearch system as well as the number of CTCs per 7.5 mL of blood in healthy subjects, patients with non-malignant disease, and patients with a variety of metastatic carcinomas has been investigated by Allard *et al.*[150]. Blood samples spiked with tumor cell lines were used to investigate accuracy, reproducibility, and linearity of the system. The result of their studies represented that the enumeration of spiked tumor cells was linear over the range of 5 to 1,142 cells, with an average recovery of >85% at each spike level. 0.3% of the healthy and nonmalignant disease subjects had >2 CTCs per 7.5 mL of blood. They have reported the average of 60 – 693 CTCs per 7.5mL blood for 964 metastatic carcinoma patients (2183 blood

samples). CTCs ranged from 0 to 23,618 per 7.5mL and and 36% (781 of 2,183) of the specimens had ≥2 CTCs. Detection of ≥2 CTCs occurred at the following rates: 57% (107 of 188) of prostate cancers, 37% (489 of 1,316) of breast cancers, 37% (20 of 53) of ovarian cancers, 30% (99 of 333) of colorectal cancers, 20% (34 of 168) of lung cancers, and 26% (32 of 125) of other cancers [150].

The majority of recent investigations have utilized RNA-amplification RT-PCR as a sensitive technique for detecting circulating tumor cells. This technique has been reported in scientific literature as a valid method to detect various circulating tumor cells derived from the bladder [26], breast [27], lung [28], prostate [29], and esophagus [31]. RT-PCR is a versatile technique, yet may not be implemented in a clinical setting due to problems associated with reproducibility, high reagent cost, and no clear path to full automation [155].

Immunocytochemistry methods, using antibody-antigen detection, are typically based on detection of cytokeratin present in some types of exfoliated cells, such as squamous cell carcinoma. The major drawback to this approach is that other cells such as hematopoietic cells, can express cytokeratins as well [32]. One of the critical issues that must be addressed, therefore, is the presence of a sufficient number of physically-isolated exfoliated neoplastic cells for this detection methodology to be effective.

These two examples demonstrate the most common problem encountered with current detection techniques: the typical inverse relationship between specificity and sensitivity. If a technology could be developed to overcome the specificity challenge, one would then be free to concentrate solely on sensitivity using protocols and routines already available such as RT-PCR, nucleic acid sequence based amplification (NASBA) or immunocytochemistry. If high-throughput methods to selectively concentrate and isolate the exfoliated malignant cells in bodily fluids can be developed, it would allow for the detection of precancerous lesions, the early onset of cancer, and/or the detection of micro-metastatic tumors. Early detection of cancer cells, coupled with effective treatment of the disease, would reduce morbidity and mortality associated with the progressive growth of malignancies.

Chapter 4
Methods

4.1 Microfabrication Process

4.1.1. Deep Reactive Ion Etching (DRIE)

A silicon master stamp was fabricated on a <100> silicon substrate. AZ 9260 (AZ Electronic Materials) photoresist was spun onto a clean silicon wafer and softbaked at 114C for 45 seconds (Fig. 4.1.a). The wafer was then exposed to UV light for 45 seconds with an intensity of 12 W/m through a chrome plated glass mask. The exposed photoresist was then removed using Potassium based buffered developer AZ400K followed by another hard baking at 115C for 45 seconds (Fig. 4.1.b). Deep Reactive Ion Etching (DRIE) was used to etch the silicon master stamp to depths ranging from 50-100 microns (Fig. 4.1.c). The silicon master stamp was then cleaned with acetone to remove any remaining photoresist (Fig. 4.1.d). The scalloping effect, a typical effect of the DRIE etching method, creates a surface roughness which is detrimental to the stamping process. In order to reduce the surface roughness, silicon oxide was grown on the silicon master using thermal oxidation and then was removed (Fig. 4.1.g-i). Another way to remove the scalloping effect and make the surface of the silicon replica hydrophobic to help PDMS peeling off process is wet chemical etching using TMAH at 70 °C for 5 minutes followed by Teflon deposition in DRIE machine for 3 minutes.

4.1.2. PDMS

The liquid phase PDMS was made by mixing the PDMS monomers and the curing agent in a 10:1 ratio (Sylgrad 184, Dow Corning, USA). The bubbles in the liquid PDMS were removed by exposing the mixture to vacuum for an hour. A enclosure was created around the wafer using aluminum foil in order to contain the PDMS on the wafer as well as to ensure the proper depth for the PDMS portion of the device. The clean PDMS liquid was then poured onto the silicon master and 15 minutes was allowed for degassing. The PDMS was then cured for 45

min at 100 C (Fig. 4.1.e) and then removed from the mold. Finally, fluidic connections to the channels were punched with 15 gauge blunt needles (Howard Electronic Instruments, USA).

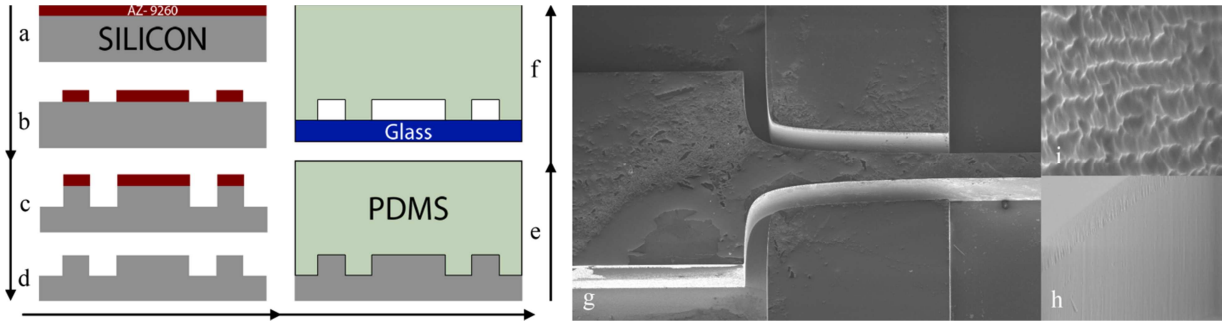

Fig. 4.1. (a-i) Schematic of the fabrication process used to create the microfluidic chambers and the SEM image of the Scalloping effect on the silicon master. Steps a through d are followed only once to create a master stamp. Steps e and f are repeated to produce an indefinite number of experimental devices. (g) SEM image of the silicon wafer mold at the intersection between the side and the main channel of the microfluidic device (h) Scalloping effect after DRIE (i) surface roughness of the wafer after growing and removing the oxide layer. With kind permission from Springer Science+Business Media: Contactless Dielectrophoresis: A New Technic for Cell Manipulation, Volume 11 Number 5, 2009, p997-1006, Hadi Shafiee, John L. Caldwell, Michael B. Sano, and Rafael V. Davalos, Fig. 1.

4.1.3. Bonding

Microscope glass slides (3” X 2” X 1.2mm, Fisher Scientific, USA) were cleaned with soap and water and rinsed with distilled water and isopropyl alcohol then dried with a nitrogen gun. The PDMS replica was bonded with the clean glass slides after treating with oxygen plasma for 40 s at 50 W RF power (Fig. 4.1f).

4.2. Schematic of the first cDEP device

A schematic with dimensions and equivalent circuit model of our device is presented in Figure 4.2a. The side channels are separated from the sample channel with 20 µm PDMS barriers.

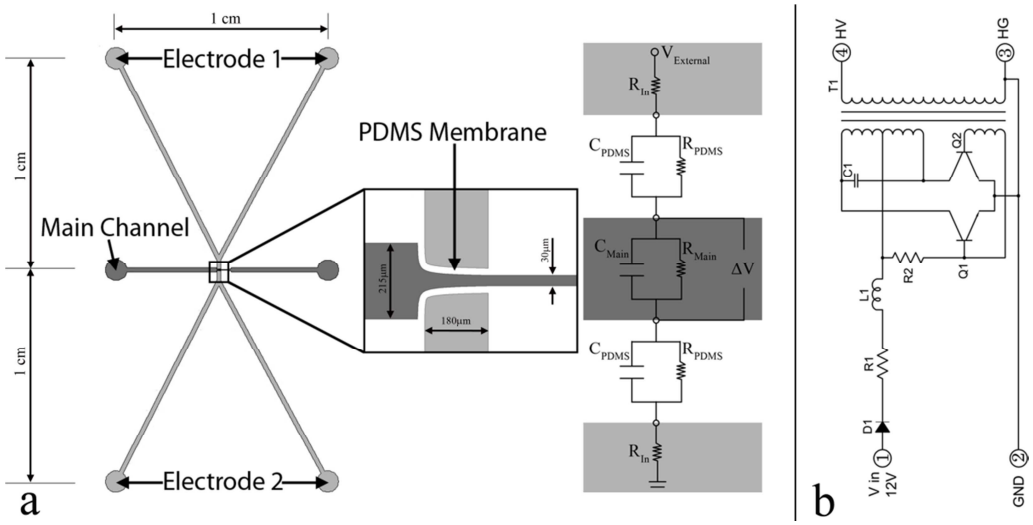

Fig. 4.2. (a) Schematic of the microfluidic device and the equivalent circuit model. (b) Schematic of the two transistor inverter circuit provided by JKL Components Corp. With kind permission from Springer Science+Business Media: Contactless Dielectrophoresis: A New Technic for Cell Manipulation, Volume 11 Number 5, 2009, p997-1006, Hadi Shafiee, John L. Caldwell, Michael B. Sano, and Rafael V. Davalos, Fig. 2.

4.3. Schematic of the second cDEP device

A schematic with dimensions is presented in Figure 4.3. The thickness of the PDMS barrier between the side channels and the main channel is 20 μm.

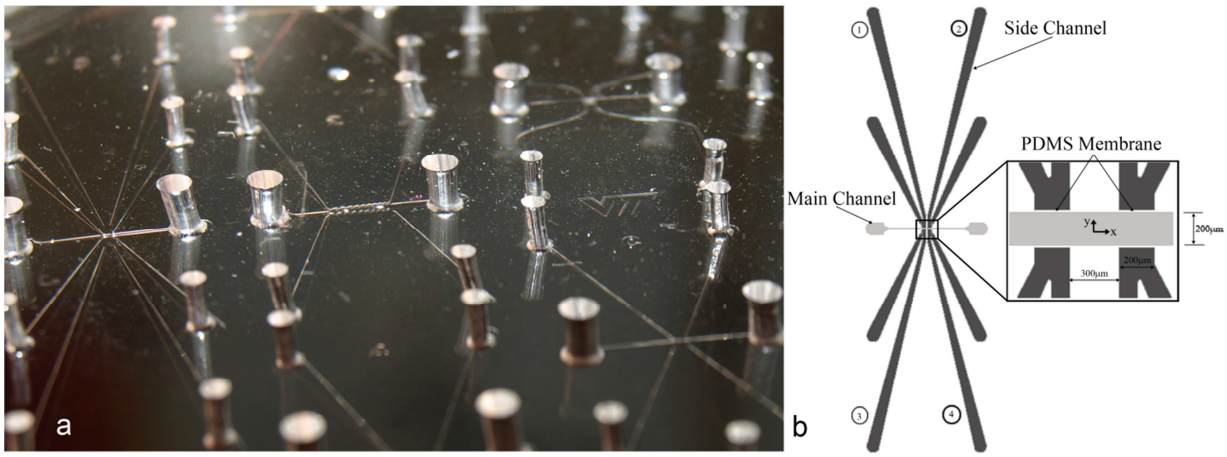

Fig. 4.3. (a) A PDMS mold from a silicon master stamp containing multiple microfluidic devices. 2D Schematic of the device with straight main channel used in this study. The channel depth is 50μm. Reprinted from Journal of the Association and Laboratory Automation, Volume 15 Issue 3, Hadi Shafiee, John L. Caldwell, and Rafael V. Davalos, A Microfluidic System for Biological Particle Enrichment Using Contactless Dielectrophoresis, p224-232, Copyright (2010), with permission from Elsevier.

4.4. Experimental Setup

4.4.1 First generation of cDEP devices

Pipette tips, inserted in the punched holes in the PDMS portion of the device, were used as reservoirs for fluidic connections to the channels. Pressure driven flow (10 to 15μl/hr was provided by an imbalance in the amount of the sample in these reservoirs of the main channel.An inverted light microscope (Leica DMI 6000B, Leica Microsystems, Bannockburn, IL) equipped with a digital camera (Hamamatsu EM-CCD C9100, Hamamatsu Photonics K.K. Hamamatsu City, Shizuoka Pref., 430-8587, Japan) was used to monitor cells in the main channel. Microfluidic devices were placed in a vacuum jar for at least half an hour before running the experiments to reduce priming issues and then the side and main microchannels were filled with PBS and DEP buffer respectively.

4.4.2 Second generation of cDEP devices

The 3D schematic of the experimental set up and device 1 is shown in Figure 4.4. The microfluidic devices were placed in a vacuum jar for 30 minutes prior to experiments to reduce problems associated with priming. Pipette tips were used to fill the side channels with Phosphate Buffered Saline (PBS) and acted as reservoirs.

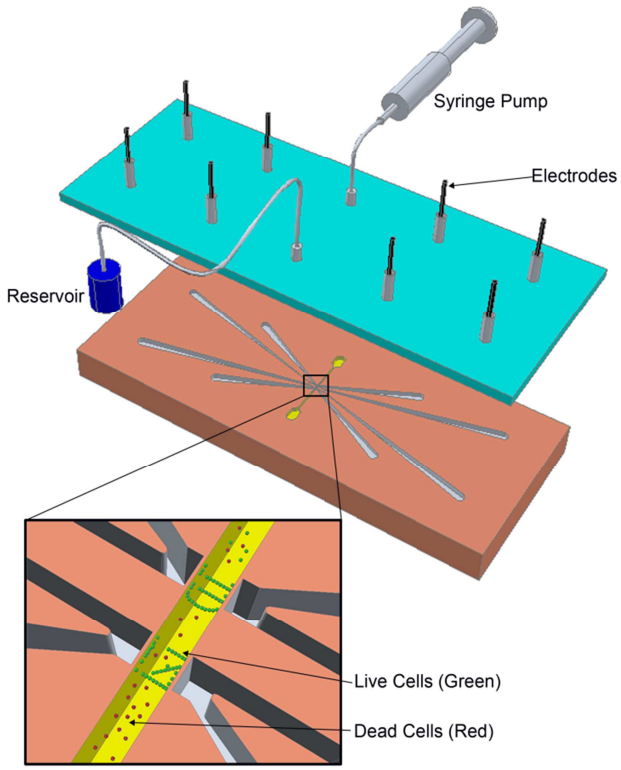

Fig. 4.4. 3D schematic of the experimental set up. Reproduced by permission of the Royal Society of Chemistry

Aluminum electrodes were placed in the side channel reservoirs. The electrodes inserted in side channels 1 and 2 of device 1 (Figure 6.1a) were used for excitation while the electrodes inserted in side channels 3 and 4 were grounded. Thin walled Teflon tubing (Cole-Parmer Instrument Co., Vernon Hills, IL) was inserted into the inlet and outlet of the main channel. A 1ml syringe containing the cell suspension was fastened to a micro-syringe pump (Cole Parmer, Vernon Hills, IL) and connected to the inlet tubing. Once the main channel was primed with the cell suspension, the syringe pump was set to 0.02mL/hr; equivalent to a velocity of 556μm/sec for device 1 and 222 μm/sec for device 2. This flow rate was maintained for 5 minutes prior to experiments.

An inverted light microscope (Leica DMI 6000B, Leica Microsystems, Bannockburn, IL) equipped with color camera (Leica DFC420, Leica Microsystems, Bannockburn, IL) was used to monitor the cells flowing through the main channel. Once the flow rate of 0.02ml/hr was maintained for 5 minutes an AC electric field was applied to the electrodes.

4.5. Electronics

4.5.1. First generation of the cDEP devices

A commercially available two-transistor inverter circuit (BXA-12576, JKL Components Corp., USA) was modified to provide a high-frequency and high-voltage AC signal for the device (Fig. 4.2b). The circuit relies on the oscillation created by the two-transistors and passive components to create an AC voltage on the primary side of a transformer. This voltage is then stepped-up by the transformer to give a high-output voltage on the secondary side to which the microfluidic device was connected.

The resonant frequency at which the circuit operates is highly dependant on the load impedance connected to the secondary side of the transformer. Two high-voltage power supplies were fabricated with resonant frequencies of 85kHz and 126kHz. A DC input voltage was provided by a programmable DC power supply (PSP-405, Instek America Corp., USA) which allowed adjustment of the output voltage by varying the input voltage. This technique allowed the output voltage of the power supplies to be varied from approximately 100Vrms to 500Vrms. A three-resistor voltage divider network, with a total impedance of one megaohm, was added to the output of the inverter circuit in order to provide a scaled (100:1) output voltage to an oscilloscope (TDS-1002B,Tektronix, USA) which facilitated monitoring the frequency and magnitude of the signal applied to the microfluidic device. All circuitry was housed in a plastic enclosure with proper high-voltage warnings on its exterior and connections were made to the microfluidic device using high-voltage test leads.

4.5.2. Second generation of the cDEP devices

AC electric fields were applied to the microfluidic devices using a combination of waveform generation and amplification equipment. Waveform generation was performed by a function generator (GFG-3015, GW Instek, Taipei, Taiwan) whose output was then fed to a

wideband power amplifier (AL-50HF-A, Amp-Line Corp., Oakland Gardens, NY). The wideband power amplifier performed the initial voltage amplification of the signal and provided the necessary output current to drive a custom-wound high-voltage transformer (Amp-Line Corp., Oakland Gardens, NY). This transformer was placed inside a grounded cage and attached to the devices using high-voltage wiring. Frequency and voltage measurements were accomplished using an oscilloscope (TDS-1002B, Tektronics Inc. Beaverton, OR) connected to a 100:1 voltage divider at the output of the transformer.

4.6. Numerical Modeling

The electric field distribution and its gradient $\nabla E = \nabla(\nabla\emptyset)$ were modeled numerically in Comsol multi-physics 3.5 using the AC/DC module (Comsol Inc., Burlington, MA, USA). This is done by solving for the potential distribution, ϕ, using the governing equation, $\nabla \cdot (\sigma^* \nabla\emptyset) = 0$, where σ^* is the complex conductivity ($\sigma^* = \sigma + j\omega\varepsilon$) of the sub-domains in the microfluidic devices. The boundary conditions used are prescribed uniform potentials at the inlet or outlet of the side channels. The values for the electrical conductivity and permittivity of the PDMS, PBS, and DEP buffer that we used in this numerical modeling are given in table 4.1. PBS and DEP buffer electrical properties are used for the side and main microfluidic channels, respectively.

Table 4.1. Electrical properties of the materials and fluids. With kind permission from Springer Science+Business Media: Contactless Dielectrophoresis: A New Technic for Cell Manipulation, Volume 11 Number 5, 2009, p997-1006, Hadi Shafiee, John L. Caldwell, Michael B. Sano, and Rafael V. Davalos, Table 1.

Electrical Properties / Materials	Electrical Conductivity (S/m)	Relative Electrical Permittivity
PDMS	0.83 × e-12	2.65
PBS	1.4	80
DEP Buffer	0.01	80

All of the boundaries of the devices were defined as insulator except the inlets and outlets of the main channel which were defined as ground and electric potential. The boundary setting module can be found in Physics/Boundary Settings. The frequency of the ac signal was entered in application scalar variables module of the program which can be found in Physics/Scalar

Variables. The material properties of different subdomains in the model were defined in Subdomain Setting (Physics/Subdomain Setting). In order to be able to create the surface and line plot of the gradient of the electric field, we used the following definitions in the Scalar Expression module that can be reached in Options/Expressions/Scalar Expression as follows:

EdotE = Ex_emqvw*Ex_emqvw+Ey_emqvw*Ey_emqvw

DEPx = d(EdotE, x)

DEPy = d(EdotE, y)

DEP = (DEPx^2+DEPy^2)^0.5

The model can be drawn in Comsol via Draw module or can be imported from Autocad as a dxf file. If the model is imported from Autocad, it must be first converted to solid through “coerce to solid” module (Draw/Coerce to solid) and the scaled down by 10^{-6} scale factor (Draw/Modify/Scale). The model is then exploded to subdomains via Split module (Draw/Split Object). The initialized mesh can be refined in general (Mesh/Refine Mesh) or can be refined in just specific areas of interest (Mesh/Refine Selection). The numerical results can be viewed in the postprocessing section of the software. Surface, contour, boundary, arrow, and particle tracing are some of the important results that one can observe for a model via Plot parameters module (Postprocessing/Plot Parameters). In order to generate the surface plot of the gradient f the electric field, the expression DEP is typed in the Postprocessing/Plot Parameters/Surface/Expression. The Surface Plot module must be checked marked as well.

Chapter 5
First cDEP Microfluidic Device as a Proof of Concept

Dielectrophoresis (DEP) has become a promising technique to separate and identify cells and microparticles suspended in a medium based on their size or electrical properties. Presented herein this chapter is a new technique to provide the non-uniform electric field required for DEP that does not require electrodes to contact the sample fluid. In our method, electrodes are capacitively-coupled to a fluidic channel through dielectric barriers; the application of a high-frequency electric field to these electrodes then induces an electric field in the channel. This technique combines the cell manipulation abilities of traditional DEP with the ease of fabrication found in insulator-based technologies. A microfluidic device was fabricated based on this principle to determine the feasibility of cell manipulations through contactless DEP. We were able to demonstrate cell responses unique to the DEP effect in three separate cell lines indicating the potential for this technique to identify cells through their electrical properties without fear of contamination from electrodes.

5.1. Numerical Results

Figure 5.1. shows the surface and line plot of the gradient of the electric field inside the main microfluidic channel at the intersection between the main and the side channels. There is a high gradient of the electric field at the corners (points 1 and 2) as well as point 3, which can provide a strong DEP force. These results indicate that changes in the thickness of the PDMS barrier have a more significant effect on the gradient of the induced electric field inside the main channel than changes in the channel's geometry which is in agreement with our analytical results.

In Figure 5.1b the gradient of the electric field along the line a-b is plotted for different applied frequencies (40, 85, 125, and 200KHz) at 250Vrms. The effect of the total external

voltage across the microfluidic device on the gradient of the electric field (along the line a-b) is also investigated in Figure 5.1c. DEP response of the system is plotted for four different voltages (100, 200, 350, and 500V) at 85 kHz.

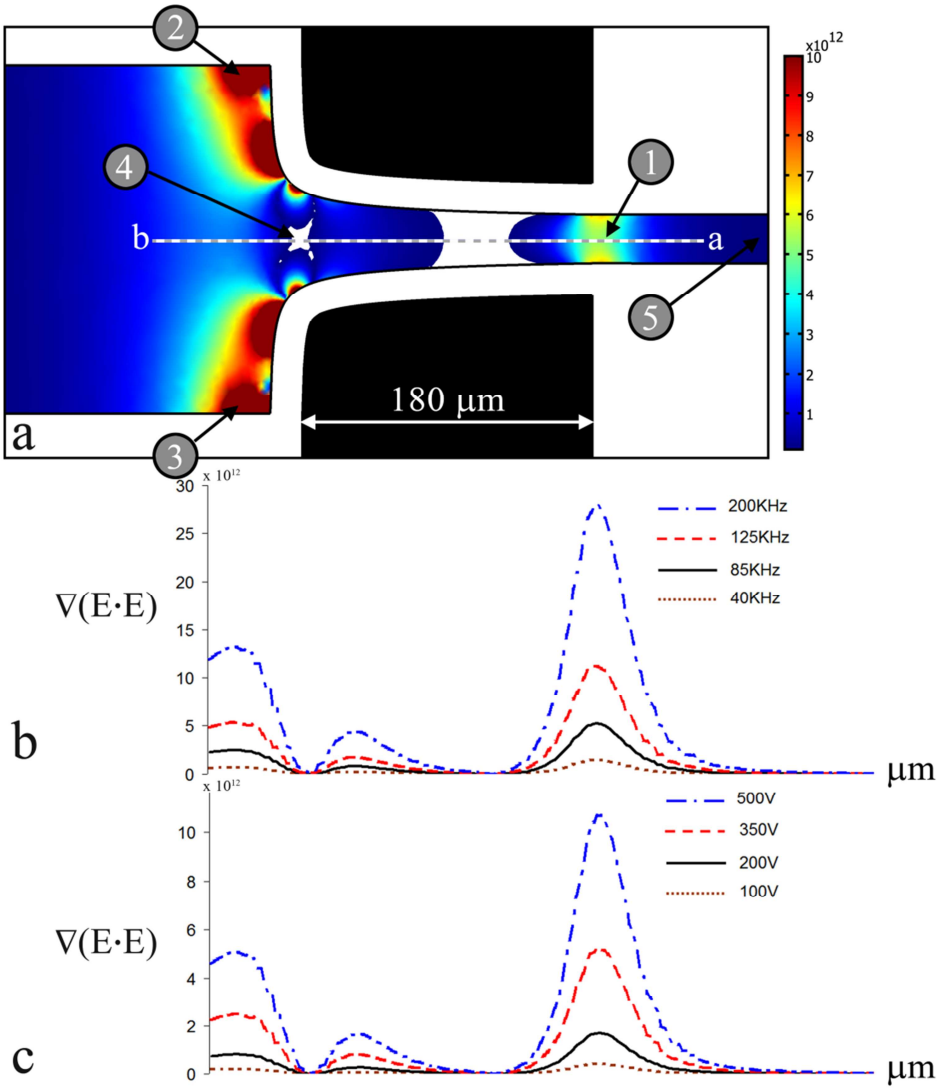

Fig. 5.1. Numerical results of the electric field gradient within the sample channel (a) Surface plot of the gradient of the field ($kg^2mC^{-2}S^{-4}$)within the main microchannel (b) Line plot of the gradient ($kg^2mC^{-2}S^{-4}$) along the line a-b (mm)for four different frequencies (40, 85, 125, and 200kHz) at 250Vrms (c) The line plot of the gradient of the electric field along the line a-a for four different applied voltages (100, 200, 350, and 500V) at 85 kHz. With kind permission from Springer Science+Business Media: Contactless Dielectrophoresis: A New Technic for Cell Manipulation, Volume 11 Number 5, 2009, p997-1006, Hadi Shafiee, John L. Caldwell, Michael B. Sano, and Rafael V. Davalos, Fig. 3.

An increased gradient of the electric field can be obtained by increasing the applied frequency or increasing the total applied voltage although it should be noted that adjusting the

frequency will also affect the Clasius-Mossotti factor of the microparticles and needs to be considered. Also the induced gradient of the electric field in the main microfluidic channel is on the order of 10^{12} ($kg^2.m.C^{-2}.S^{-4}$) which is strong enough for particle manipulations. Based on this numerical modeling, the voltage drop across the 20μm PDMS barrier was 250V for an applied total voltage of 500V across the microfluidic electrode channels. This voltage drop is lower than the 400V break down voltage for a 20μm PDMS channel wall. Thus, the DEP force can be amplified by adjusting the input voltage with some tolerance.

Electric Field Surface Plot

Figure 5.2a-c shows the induced electric field intensity distribution inside the main microfluidic channel filled with the DEP buffer with a conductivity of 100μS/cm. The highest electric field is induced at the zone of intersection between the main and the side channels and between the PDMS barriers. Figure 5.2c also shows that with an applied AC electric field of 250Vrms and 85 kHz the electric field does not significantly exceed 0.2 kV/cm in the main microfluidic channel.

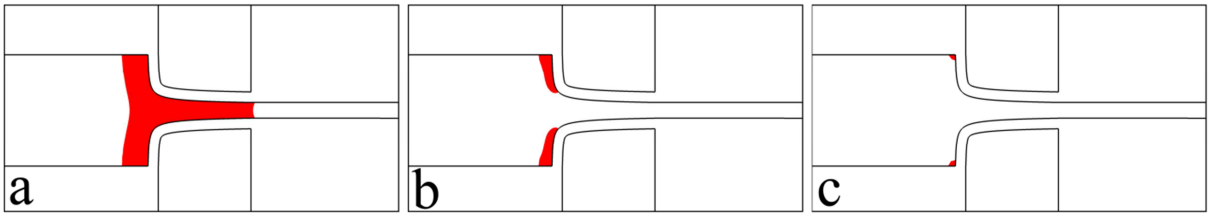

Fig. 5.2. Electric field surface plot for an applied AC field at 85kHz and 250V_{rms}. Areas with the induced electric field intensity higher than (a) 0.1kV/cm, (b) 0.15kV/cm, (c) 0.2kV/cm. With kind permission from Springer Science+Business Media: Contactless Dielectrophoresis: A New Technic for Cell Manipulation, Volume 11 Number 5, 2009, p997-1006, Hadi Shafiee, John L. Caldwell, Michael B. Sano, and Rafael V. Davalos, Fig. 4.

5.2. Cells and buffer

The THP-1 human Leukemia monocytes, MCF-7 breast cancer cells, and MCF-10A breast cells were washed twice and resuspended in our prepared DEP buffer (8.5% sucrose [wt/vol], 0.3% glucose [wt/vol], and 0.725% [vol/vol] RPMI)[156]. The electrical conductivity of the buffer was measured with a Mettler Toledo SevenGo pro conductivity meter (Mettler-Toledo, Inc., Columbus, OH) to ensure that its conductivity was 100μS/cm. These cells were

observed to be spherical while they are in suspension. The measured cell diameters of with the corresponding standard deviations (n=30) of these cell are given in Table 5.1.

5.3. Translational and Rotational Velocity Measurement

We measured the average velocity of the THP-1, MCF-7 and MCF-10A cells in our microfluidic device along the centerline a-b in Figure 5.1. from point 1 to point 4. Time-lapse videos were recorded of the cells motion before and after applying an ac electric field through the platinum electrodes inserted in the side channels. These recorded videos then were converted to JPEG files using the Leica software, (Leica DMI 6000B, LAS AF 1.6.3Leica Microsystems, Bannockburn, IL), in order to measure the traveling time of the target cells, for a known specific distance in the microchannel, before and after inducing the electric field in the main microfluidic channel.

5.4. Experimental Results

5.4.1. Cell trapping-Contactless DEP Evidence

Figure 5.3 shows the experimental results we attained using MCF-7 breast cancer cells and THP-1 leukemia cells in our device. The behavior of cells traveling through the device under static conditions was observed to be significantly different than when an electric field was applied to the device. Three induced DEP responses were studied, rotation, velocity changes, and chaining.

Under a pressure driven flow, without an applied electric field, it was observed that THP-1 leukemia and MCF-7 breast cancer cells flow through the main microfluidic channel from right to left without any disruption or trapping. The cells were observed to be trapped, experiencing a positive DEP force, once an AC electric field at 85KHz and 250Vrms was applied.These results indicate that these cells have positive Clausius-Mossotti factor at 85kHz frequency. Their velocity decreased at the intersection between the main and the side channels where the thin PDMS barriers are located. With the same electrical boundary conditions we didn't observe any trapping or cell movement disruption for MCF-10A normal breast cells. However, these cells were trapped once an electric field at 125kHz and 250Vrms was applied.

Since the positive DEP force in the main microchannel depends on the electrical properties of the cells, different cell lines experience different forces at the same electrical boundary conditions (external voltage and frequency) in the same buffer. Cell bursting or lysis was not observed during contactless DEP trapping.

5.4.2. Translational Velocity

The cells were observed to move faster along the centerline of the sample channel in Figure 5.1a from point 5 to point 1 when the electric field was applied as compared to their velocity due to pressure driven flow. As shown in Figure 5.1., the magnitude of the DEP force is high at point 1. Because the DEP force is positive at 85 kHz, the cells are attracted to this point. Therefore, as the cells approach point 1 from the right, the positive DEP force is in the direction of the pressure driven flow, causing the cells to move faster down the channel. Conversely, the average velocity of the cells in the area between the thin PDMS barriers (from 1 to 4) decreases when the voltage is applied because the positive DEP force now acts in the opposite direction of the pressure driven flow.

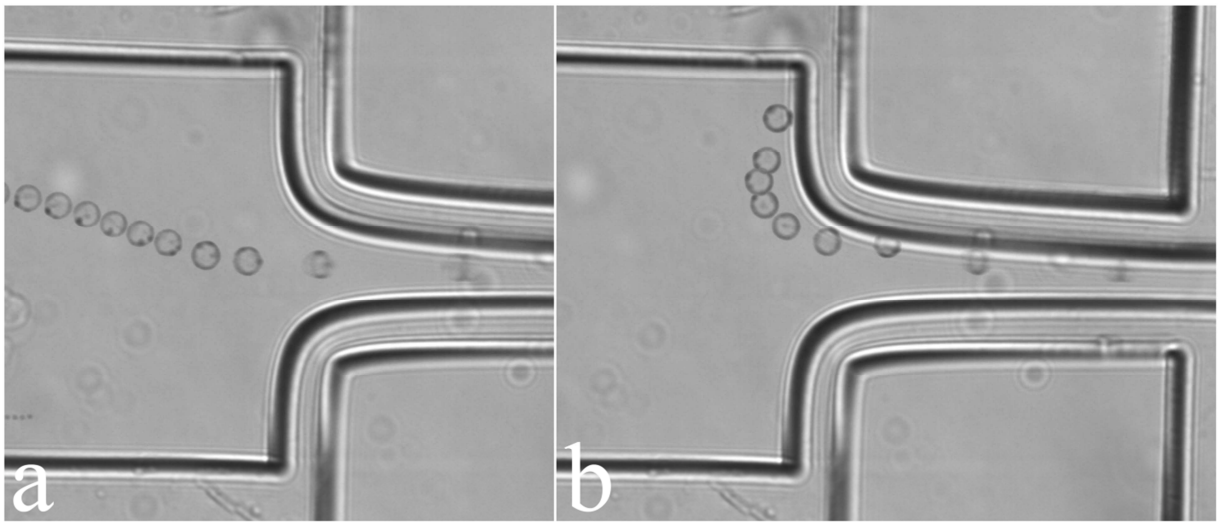

Fig.5.3. Superimposed images showing the trajectory of one cell through the device. (a) The cell is moving from right to left under an applied pressure (b) with an applied voltage of $250V_{rms}$ at 85kHz. The superimposed images were approximately 250 ms apart. With kind permission from Springer Science+Business Media: Contactless Dielectrophoresis: A New Technic for Cell Manipulation, Volume 11 Number 5, 2009, p997-1006, Hadi Shafiee, John L. Caldwell, Michael B. Sano, and Rafael V. Davalos, Fig. 5.

Table 5.1. compares the induced velocities of the cells with respect to their velocity under pressure driven flow. The normalized velocity (Uon /Uoff) for the three cell lines under the same electrical boundary conditions ($250V_{rms}$ at 85 kHz) are also reported in Figure 5.4. The results show that there is a statistically significant difference in the cells velocity when the field is applied. Furthermore, when the experiments are normalized for comparison, the results suggest that this technique can be used to differentiate cells based on their electrical properties.

The same experiments with the same buffers and electrical boundary conditions were performed on MCF-10A breast cells without noticeable trapping or disruption, which shows that the electrical properties of the normal breast cells are different compared to the MCF-7 breast cancer cells. It also shows the sensitivity of the contactless DEP technique to isolate cells with close electrical properties.

There was a great tendency for cells to move towards the corners in the main channel. This agrees with our numerical results, which show there is a high gradient of the induced electric filed at the corners, which causes a strong positive DEP force and pulls cells towards these zones of the main microfluidic channel.

Table 5.1 The measured average velocity from 1 to 4 (Fig. 5.1.) of five different cells before and after applying the electric field at the zone of trapping. With kind permission from Springer Science+Business Media: Contactless Dielectrophoresis: A New Technic for Cell Manipulation, Volume 11 Number 5, 2009, p997-1006, Hadi Shafiee, John L. Caldwell, Michael B. Sano, and Rafael V. Davalos, Table 2.

Cell Velocity / Cell line	**Diameter (µm)**	**Uon (µm/s)**	**Uoff (µm/s)**	**Uoff-Uon(µm/s)**	**Uon/Uoff**	**Ω (rad/s)**
THP-1	15.4±2	240±13	392±21	152±19	0.61	8.1±0.66
MCF-7	18.5±2.5	387±7	476±17	89±17	0.81	19.4±2.9
MCF-10A	18.2±2.1	310±17	313±16	3±24	0.99	N.A.

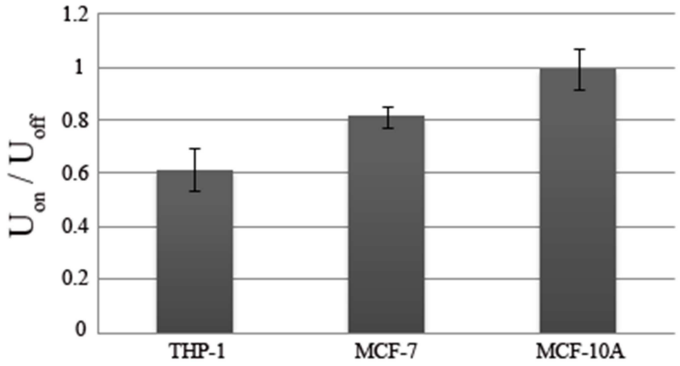

Fig. 5.4. The normalized velocity of THP-1, MCF-7, and MCF-10A cells. Uon is the velocity of the cells while applying e-field and Uoff is the velocity of the cells while the power is off. With kind permission from Springer Science+Business Media: Contactless Dielectrophoresis: A New Technic for Cell Manipulation, Volume 11 Number 5, 2009, p997-1006, Hadi Shafiee, John L. Caldwell, Michael B. Sano, and Rafael V. Davalos, Fig. 6.

5.4.3. Rotational Velocity

Cell rotation in the main channel at the zone of trapping and between the thin PDMS barriers was present with an applied electric field. The rotational velocity of the cell is a function of its electrical properties, the medium permittivity, the medium dynamic viscosity as well as the properties of the electric field. We measured the rotational velocity of the trapped THP-1, and MCF-7 cancer cells in different experiments at one spot of the main microfluidic channel. No cell rotation was observed without an applied electric field. The reported rotational velocities in Table 5.1 are the average rotational velocities of five different cells of each of the cancer lines. These results imply that the average rotation velocities of the THP-1 and MCF-7 cancer cell lines are significantly different. Cell rotation for the MCF-10A cells with the same electrical boundary conditions in the same buffer solution was not observed.

5.4.4. Pearl-chain

Cell aggregation and chain formation in DEP experiments with an AC field have been frequently observed and can be attributed to dipole-dipole interactions as well as local distortions of the electric field due to the cells' presence [20, 21, 34, 35].

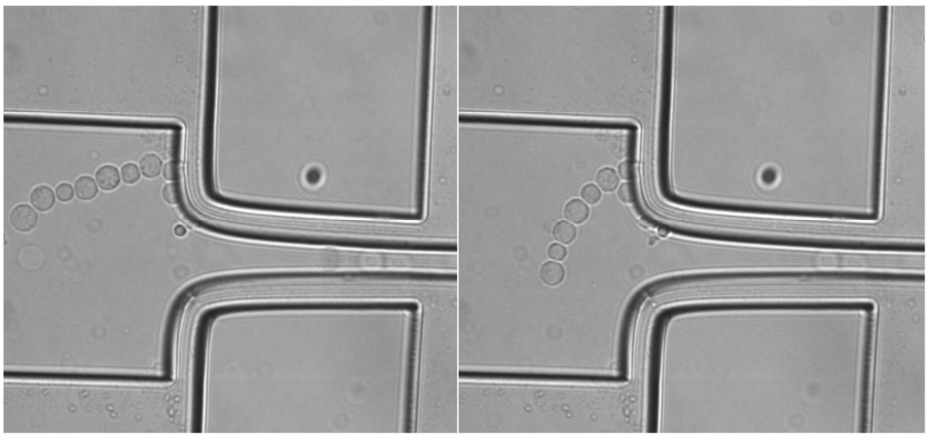

Fig. 5.5. Trapping due to DEP. These images show the 'pearl-chain' phenomena often encountered in DEP. With kind permission from Springer Science+Business Media: Contactless Dielectrophoresis: A New Technic for Cell Manipulation, Volume 11 Number 5, 2009, p997-1006, Hadi Shafiee, John L. Caldwell, Michael B. Sano, and Rafael V. Davalos, Fig. 7.

Particles parallel to the electric field attract each other because of this dipole-dipole force, resulting in pearl-chaining of the trapped cells in the direction of the electric field in the microfluidic channel. The cell chain formation was observed for the MCF-7 and THP-1 cancer cell lines in our experiments with an applied AC electric filed at 85KHz and 250Vrms (Fig. 5.5.).

5.5. Conclusion

Particles parallel to the electric field attract each other because of this dipole-dipole force, resulting in pearl-chaining of the trapped cells in the direction of the electric field in the microfluidic channel. The cell chain formation was observed for the MCF-7 and THP-1 cancer cell lines in our experiments with an applied AC electric filed at 85KHz and 250Vrms (Fig. 5.5.).

We have demonstrated a new technique for inducing electric fields in microfluidic channels in order to create a dielectrophoretic force. Our method relies on the application of a high-frequency AC electric signal to electrodes that are capacitively coupled to a microfluidic channel. In our device, the geometry of the electrodes and channels create the spatial non-uniformities in the electric field required for DEP. Three separate DEP responses were observed in our device, namely, translational velocity, rotational velocity, and chaining. In order to observe the devices effects in these three categories, three different cell lines were inserted into the devices and their individual responses recorded. Each cell line exhibited a response unique to

its type due to the cell's specific electrical properties. This result highlights the ability of our technique to differentiate cells by their intrinsic electrical properties.

We believe this technique may help overcome many of the challenges faced with traditional iDEP and DEP. Because the induced electric field is not as intense as comparable methods and is focused just at the trapping zone, we theorize the Joule heating within the main microfluidic channel is negligible. This could mitigate the stability and robustness issues encountered with conventional iDEP [68], due the conductivity distribution's strong dependence on temperature. Furthermore, challenges associated with cell lysing due to high temperatures [53] or irreversible electroporation due to high field strengths [157, 158] are overcome with our new design approach under these conditions.

Chapter 6
Second Generation of cDEP Devices to Isolate Live/Dead

Contactless dielectrophoresis (cDEP) is a recently developed method of cell manipulation in which the electrodes are physically isolated from the sample. In this chapter we present two microfluidic devices capable of selectively isolating live human leukemia cells from dead cells utilizing their electrical signatures. The effect of different voltages and frequencies on the gradient of the electric field and device performance was investigated numerically and validated experimentally. With these prototype devices we were able to achieve greater than 95% removal efficiency at 0.2-0.5mm/s with 100% selectivity between live and dead cells. In conjunction with enrichment, cDEP could be integrated with other technologies to yield fully automated lab-on-a-chip systems capable of sensing, sorting, and identifying rare cells.

6.1. Cells and buffer

The live samples of THP-1 human leukemia monocytes were washed twice and resuspended in a buffer used for DEP experiments (8.5%sucrose [wt/vol], 0.3% glucose [wt/vol], and 0.725% [wt/vol] RPMI [156]) to 10^6 cells/mL. The cell samples to be killed were first pipetted into a conical tube and heated in a 60°C water bath for twelve minutes; an adequate time determined to kill a majority of the cell sample.

To enable simultaneous observation under fluorescent microscope, cells were stained using a LIVE/DEAD® Viability/Cytotoxicity Kit for mammalian cells (Molecular Probes Inc.). Calcein AM, which is enzymatically converted to green fluorescent calcein, was added to the live cell sample at 2μL per ml of cell suspension. Ethidium homodimer-1 (EthD-1) was added to the dead cell sample at 6μL per ml of cell suspension. This can only pass through damaged cell membranes and upon nucleic acid-binding produces a red fluorescence.

The two samples were then vortexed for 5 minutes, washed once and resuspended in DEP buffer. The live and dead suspensions were then mixed together in one conical tube with a final concentration of 10^6 cells/mL and final conductivity of 110-115μS/cm measured with a SevenGo Pro conductivity meter (Mettler-Toledo, Inc., Columbus, OH). Live and dead cells were indistinguishable under bright field evaluation.

6.2. Results and Discussion

Device 1: Experiments were conducted at 50Vrms, 75Vrms, 100Vrms, 125Vrms and 150Vrms. Trapping boundary conditions for this device were determined through visual inspection of the cells passing through the main channel. At each voltage, frequency was recorded for 80% trapping and the beginning of cell lyses. Significant lysing was considered to be when at least 10% of the cell population became lysed. The electric field was maintained for 30 seconds during each experiment. Eight trials were conducted at each voltage and corresponding frequencies were recorded where 80% trapping was observed.

The geometry of device 1 allowed for the rapid simulation of DEP effects within the sample microchannel which could then be verified through an efficient fabrication and experimentation procedure. The gradient of the electric field along the center line of the main channel of device 1 was numerically modeled and the results are plotted in Figure 6.1b. Figure 6.1b also shows that the maximum gradient of the electric field occurs at the terminations of the side channels. The dependance of the gradient of the electric field in the main channel on distance from the channel wall is shown in Figure 6.1c. These numerical results indicate that the gradient of the electric field and thus the DEP effect is strongly related to the channel geometry.

Conclusions drawn from the numerical modeling of device 1 were verified through direct experimentation. Live cell concentration and trapping was observed for the electrical boundary conditions that were previously simulated (V_1=V_2=50V_{rms} at 220kHz, 100Vrms at 152kHz, and 150Vrms at 142kHz and V_3=V_4=Ground). A large DEP response was achieved with an applied voltage of 150Vrms at 142kHz, mirroring the numerical modeling shown in Figure 3.2.2b. The majority of cell trapping within the device occurred at the edges of the electrodes as predicted by numerical results found in Figure 6.1b.

When 80% trapping was observed, cells closest to the channel wall were trapped while those closer to the center of the channel were not; a result predicted by the numerical modeling presented in Figure 6.1c. These simulations further indicated that at low frequencies (≤100kHz) the gradient of the electric field inside the main channel would not be sufficient for DEP cell manipulation and this was confirmed in our experiments. The minimum frequency necessary to achieve an 80% trapping efficiency is given in Figure 6.3a as a function of applied voltage. Cell lysing was observed for 75Vrms, 100Vrms, 125Vrms, and 150Vrms at 296kHz, 243kHz, 197kHz, and 173kHz, respectively. No lysing was observed at 50Vrms within the frequency limits of the power supply. The concentration of live THP-1 cells using a 150kHz voltage signal at 100Vrms in device 1 is shown in Figure 6.4.

Device 2: Trapping efficiency for this device was determined for voltages of 20Vrms, 30Vrms, 40Vrms, 50Vrms and frequencies of 200kHz, 300kHz, 400kHz, 500kHz at a constant flow rate of 0.02mL/hr. Experimental parameters were tested at random to mitigate any variation in cell concentration, flow rate, device functionality and other experimental variables. Additionally, trapping efficiency was calculated at 0.02mL/hr, 0.04mL/hr, 0.06mL/hr, and 0.08mL/hr,with electrical parameters held constant at 500kHz and 30Vrms. Electrical parameters were selected randomly for each experiment for a total of five trials at each combination. The electric field was maintained for 30 seconds during each experiment. During the 30 second interval, all cells entering the trapping region of the device (the region containing pillars in the main channel) were counted, representing the total number of cells.

Numerical modeling proven valid for device 1 was used to predict the performance of device 2. The gradient of the electric field along the x-axis (y=0) of the main channel of device 2 is plotted in Figure 6.2b. Again, for these electrical boundary conditions (V1= 30Vrms at 200kHz, 300kHz, 400kHz, and 500kHz and V2=Ground) cell trapping was observed. Local maximums in the gradient of the electric field occurred in line with the edges of the insulating pillars while the minimum gradient was experienced as cells passed through the region between two pillars. The highest electric field gradient was observed to occur at the two insulating pillars which had edges in the center of the device. The electric field gradients in the center of device 2 along the y-axis (x=0) are shown in Figure 6.2c and the highest gradient was observed in line with the edges of the insulating pillars.

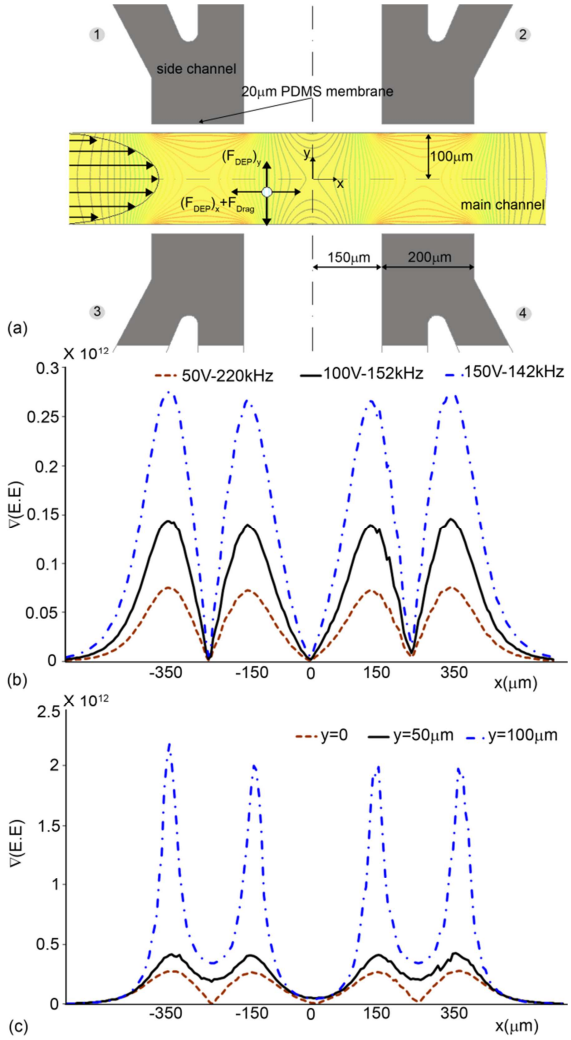

Fig.6.1. (a) 2D top view schematic of device 1 showing the dominated acting forces on the particle. The contours represent the electric fields modelled in Comsol multiphysics. **(b)** Line plot of the gradient of the electric field squared ($kg^2mC^{-2}S^{-4}$) for three different electrical boundary conditions with efficient numerical cell trapping ($V_1=V_2=50V_{rms}$ at 220 kHz, $100V_{rms}$ at 152kHz, and $150V_{rms}$ at 142kHz and $V_3=V_4$=Ground). **(c)** Line plot of the gradient of the electric field squared ($kg^2mC^{-2}S^{-4}$) along the lines parallel to the center line of the main channel and at different distances from the channel wall for $V_1=V_2=150V_{rms}$ at 140kHz boundary condition (y=0, 50, and 100μm). Reproduced by permission of the Royal Society of Chemistry

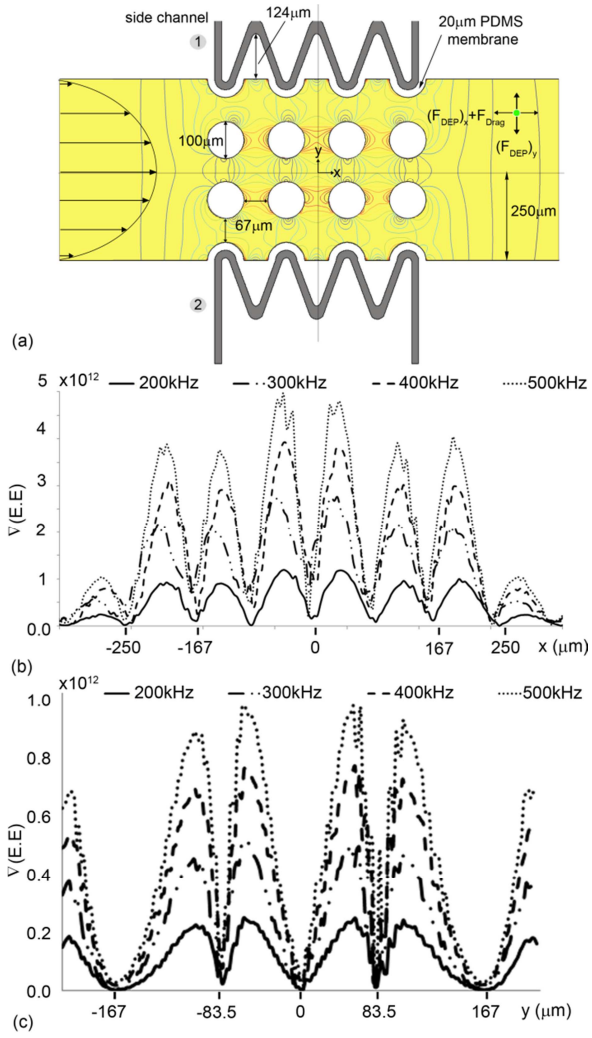

Fig.6.2. (a) 2D top view schematic of device 2, showing the dominated acting forces on the particle. The contours represent the electric fields modeled in Comsol multiphysics. **(b)** Line plot of the gradient of the electric field squared ($kg^2mC^{-2}S^{-4}$) for four different electrical boundary conditions with efficient numerical cell trapping ($V_1=30V_{rms}$ at 200kHz, 300kHz, 400kHz, and 500kHzV_2= Ground) along the x axis (y=0). **(c)** Line plot of the gradient of the electric field squared ($kg^2mC^{-2}S^{-4}$) for four different electrical boundary conditions with efficient numerical cell trapping ($V_1=30V_{rms}$ at 200kHz, 300kHz, 400kHz, and 500kHz, and V_2= Ground) along the y axis (x=0). Reproduced by permission of the Royal Society of Chemistry

It should be noted that the maximum gradient is observed at y=+/- 83.5µm and cells traveling through the exact center of the device (along the x-axis) experience a lower DEP force than those just off-center. The electric field gradient within the channel increased with applied signal frequency from 200kHz to 500kHz. This increase in gradient is not linear and these parameters represent the limitations of our current electrical setup.

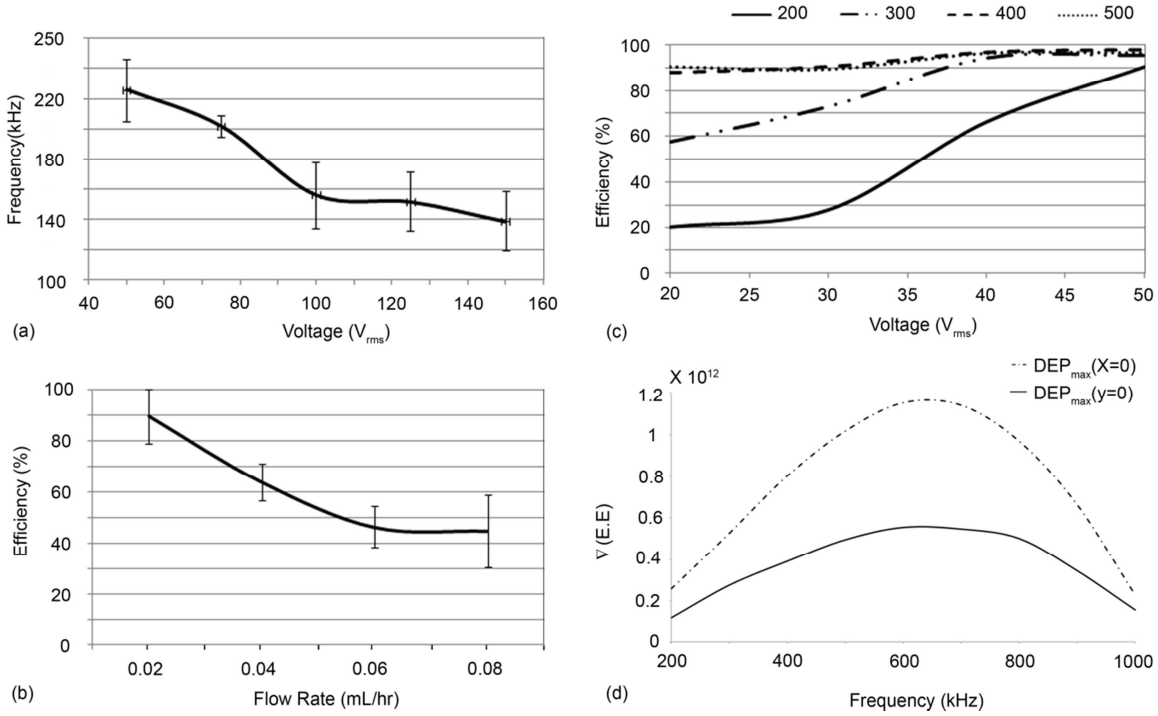

Fig.6.3. (a) Voltage-frequency pairs to achieve 80% trapping efficiency for device 1. **(b)** Trapping efficiency of device 2 at 500kHz and 30V_{rms} for flow rates of 0.02, 0.04, 0.06, and 0.08mL/hr. **(c)** Trapping efficiency at 0.02mL/hr of device 2 at 200, 300, 400, and 500kHz as voltages increase from 20V_{rms} to 50V_{rms}. **(d)** Maximum gradient of the electric field along the x (y=0) and y (x=0) axis of device 2 for frequencies between 200kHz and 1000kHz. Reproduced by permission of the Royal Society of Chemistry

Theoretically, device 2 has a maximum gradient of electric field within the channel occuring between 600kHz and 700kHz as seen in Figure 6.3d. Above this frequency, leakages in the system begin to dominate the response and the electric field within the channel drops off.

Live THP-1 cells were observed to experience positive DEP force at the reported frequencies and the DEP force applied on dead cells appeared to be negligible. In device 2, the majority of cell trapping was observed in the region between the first two columns of insulating barriers at 0.02mL/hour. However, the distribution of trapped cells became more uniform at higher flow rates.

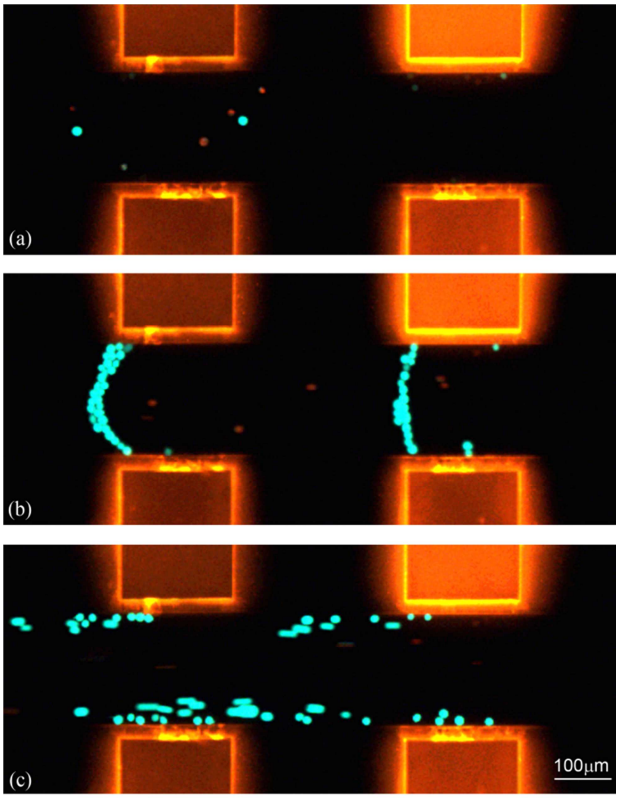

Fig. 6.4. Experimental results for device 1: (a) Dead (red) and live (green) THP-1 cells are moving from right to left due to pressure driven flow without applying electric field. (b) 30 seconds after applying the electric field (V1=V2=100Vrms at 152kHz and V3=V4=Ground). The live (green) cells were trapped due to positive DEP, but the dead (red) cells pass by the trapping area. (c) Releasing the trapped live cells by turning off the power supply. Side channels are fluorescent due to Rhodamine B dye suspended in PBS. Reproduced by permission of the Royal Society of Chemistry.

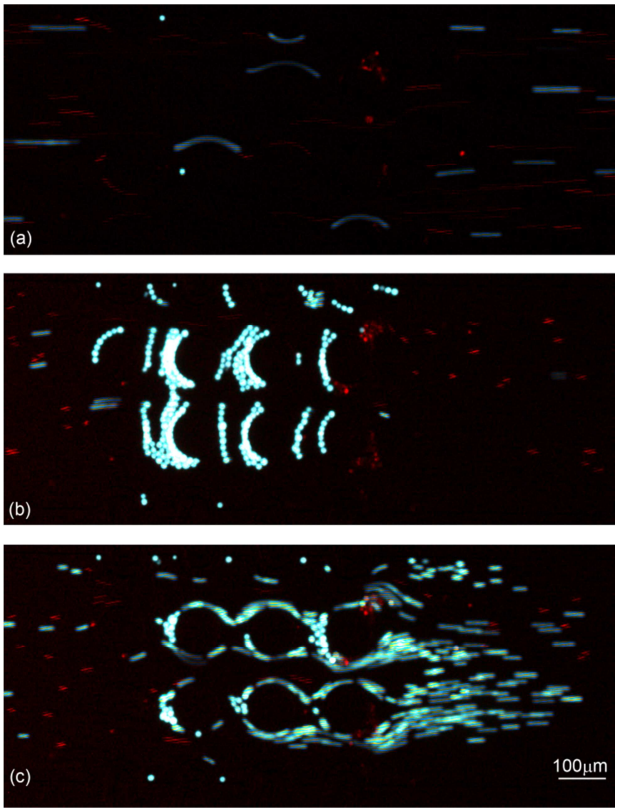

Fig. 6.5. Experimental results for device 2: (a) Dead (red and live (green) THP-1 cells are moving left to right due to pressure driven flow. (b) 30 seconds after applying the electric field (V1=40Vrms at 500 kHz and V2=Ground) live cells were trapped due to positive DEP but dead cells pass by. (c) Releasing the trapped live cells by turning off the power supply. Reproduced by permission of the Royal Society of Chemistry.

At 0.02 mL/hour, we observed trapping efficiencies greater than 90% at all tested frequencies (200kHz, 300kHz, 400kHz, and 500kHz). However, lysing was seen at all frequencies when a voltage of 50Vrms was applied. At the highest two frequencies, lysing was seen at 40Vrms and over 10% of the cells lysed at 50Vrms (Figure 6.3c). Aside from lysing, the maximum voltage we are able to apply to these devices is determined by the electrical breakdown voltage of the PDMS composing the barriers. Our results suggest that the

performance of our cDEP devices is comparable to and maybe able to exceed what is currently attainable and has been reported with DEP or iDEP [159-162].

In device 2, a maximum of 50Vrms was applied to the inlets of the electrode channels. In device 2, a maximum of 50Vrms at 500kHz signal was applied to the inlets of the electrode channels. Because the sample channel is non-uniform, it was found through our numerical results that the actual electric field experienced by cells within the channel was between 20V/cm and 200V/cm. However, there are minute regions at the sharp corners inside the main channel with a high electric field intensity (~350V/cm) that induces electroporation (IRE) [163, 164], which is what we have observed during the experiments. This was caused by the dramatic change in the thickness of the PDMS barrier in those locations. It was in these small regions which cell lysing was most commonly seen and we neglected to mention that the cells lysed only in these areas in device 2.

Trapping efficiency experiments for higher flow rates were conducted at 500kHz and $30V_{rms}$ because these parameters yielded a high trapping efficiency of 89.6% at 0.02mL/hour. Trapping efficiency was reduced by an increase in flow rate and reached a minimum of 44.8% (+/- 14.2) at 0.08 mL/hour (Figure 6.3b). Flow rates greater than 0.1mL/hour were not reported due to limitations of our recording software that resulted in the inability to accurately count the number of cells entering and exiting the trapping region of the device.

Due to the capacitance effect of the PDMS barriers in cDEP devices, the corresponding gradient of the electric field for voltage-frequency pairs are different for each design. These devices were designed to provide a sufficient gradient of the electric field for DEP cell manipulation within the limitations of our power supply and the PDMS breakdown voltage. The high trapping efficiency makes device 2 an optimal design for selective entrapment and enrichment of cell samples. This process is depicted in Figure 6.5; initially live cells (green) and dead cells (red) passed through the trapping region due to pressure driven flow (Figure 6.5a). Live cells were selectively concentrated in the trapping region under the application of a 500kHz, 40Vrms signal (Figure 6.5b). Under these parameters, the DEP force on the dead cells was not sufficient to influence their motion and they passed through the trapping region. The enriched sample of live cells can be controllably released for later analysis once the electric field is turned off (Figure 6.5c).

6.3. Conclusion

This work has demonstrated the ability of cDEP to selectively concentrate specific cells from diverse populations through the separation of viable cells from a sample containing both viable and non-viable human leukemia cells. Repeatability, high efficiency, sterility, and an inexpensive fabrication process are benefits inherent to cDEP over more conventional methods of cell separation. This method is also unique in that direct evaluation is possible with little or no sample preparation. The resulting time and material savings are invaluable in homeland security and biomedical applications. Given cDEP's numerous advantages, the technique has tremendous potential for sample isolation and enrichment for drug screening, disease detection and treatment, and other lab-on-a-chip applications.

Chapter 7
cDEP to Selectively Isolate Live THP-1 Cells from 10μm Beads

A microfluidic system for the enrichment of biological particles, operating on the principle of dielectrophoresis (DEP) is presented in this chapter. Through the use of a unique manifestation of dielectrophoresis, contactless dielectrophoresis (cDEP), this system illustrates the potential to sidestep the common tradeoff between sample throughput and selectivity without the need for a complicated fabrication process. The ability to concentrate particles from a sample fluid is validated experimentally through the concentration of 2 μm polystyrene beads and live THP-1 human leukemia cells from media heterogeneous solution. Finite element analysis of the electric field within the microfluidic channel of the device allows for the determination of effective experimental parameters and accurate predictions of a particle's trajectory through the device. The concentration of particles, combined with a fabrication procedure conducive to mass production makes cDEP an attractive alternative to current sample enrichment technologies.

7.1. Cells and buffer

Live samples of THP-1 human Leukemia monocytes were washed twice and resuspended in our prepared buffer (8.5%sucrose [wt/vol], 0.3% glucose [wt/vol], and 0.725% [wt/vol] RPMI) [156] to achieve 10^6 cells/ml cell concentration. The electrical conductivity of the buffer was measured with a Mettler Toledo SevenGo pro conductivity meter (Mettler-Toledo, Inc., Columbus, OH) to ensure that its conductivity was 130μS/cm. These cells were observed to be spherical with a diameter of ~13 μm when in suspension.

Carboxylate-modified polystyrene microspheres (Molecular Probes, Eugene, OR) having a density of 1.05 mg/mm3 and diameters of 2 μm and 10 μm were utilized at a dilution of 2:1000 from a 2% by wt. stock suspension. Bead suspensions were sonicated between steps of serial dilution and before use. The background solution was deionized water with a conductivity of 86

μS/cm. Live THP-1 cells were stained using cell trace calcein red-orange dye (Invitrogen, Eugene, Oregon, USA). The stained cell sample and the 10um beads sample were mixed in a ratio of 1:1.

7.2. Numerical results

7.2.1. Electric field and gradient of the electric field surface plots

Numerical modeling was used to determine relevant experimental conditions such as applied voltage and frequency. Experimental values for the voltage and frequency must be chosen to provide sufficient DEP force on the target particles without exceeding the dielectric breakdown voltage of the PDMS barriers (280V for a 20 μm barrier). Due to the capacitive properties of the thin PDMS barrier between the side channels and the main channel, the induced electric field inside the main channel is strongly dependent on the frequency and the applied voltage. Hence, a minimum frequency is required to provide strong gradient of the electric field with respect to a specific voltage for micro-particle manipulation. A 70 Vrms sinusoid at 300 kHz was found to provide significant DEP force in the microfluidic channel without damaging the device. This excitation signal was applied to the top two electrodes (electrodes 1 and 2) and the bottom two electrodes were grounded (electrodes 3 and 4). The electric field intensity surface plot in the main channel of the device at the experimental parameters is shown in Figure 7.1a. It is important to note that the electric field intensity did not reach 0.1 kV/cm, the necessary field strength to kill cells through irreversible electroporation. Electroporation is a phenomenon that increases the permeabilization of the cell membrane by exposing the cell to an electric field [163, 165, 166]. In irreversible electroporation, permanent pores open in the cell membrane which leads to cell death [165, 167].

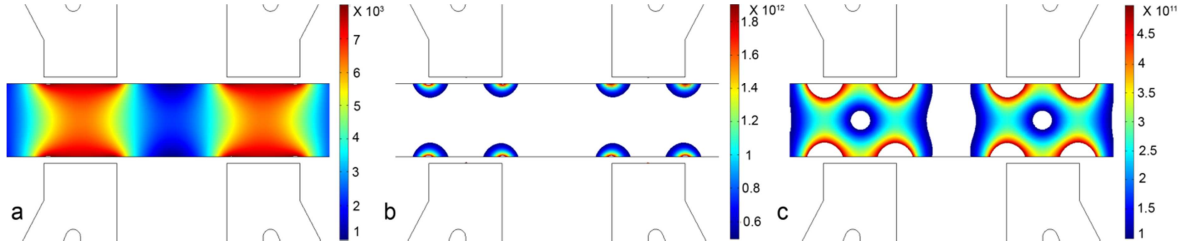

Fig. 7.1. (a) Electric field intensity (V/m) surface plot. **(b)** The gradient of the electric field squared ($\nabla(E \cdot E)$) ($kg^2mC^{-2}S^{-4}$) surface plot. V_1 = V_2 = 70 V_{rms} at 300 kHz and V_3 = V_4 = Ground (For side channel numbers see Fig. 6.1a). In this figure the scale bar is set such that $6\times10^{11} \leq (\nabla(E \cdot E) \leq 18\times10^{11}$. **(c)** The same results described in Figure (b), but with a different scale bar $1\times10^{11} \leq (\nabla(E \cdot E) \leq 5\times10^{11}$. Reprinted from Journal of the Association and Laboratory Automation, Volume 15 Issue 3, Hadi Shafiee, John L. Caldwell, and Rafael V. Davalos, A Microfluidic System for Biological Particle Enrichment Using Contactless Dielectrophoresis, p224-232, Copyright (2010), with permission from Elsevier.

The trapping regions and cell's trajectory through the microfluidic device can be predicted using the numerical modeling as DEP cell manipulation is strongly dependent on the gradient of the electric field. The highest gradient of the electric field is estimated to appear at the edges of the side channels as shown by numerical results found in Figure 7.1b. However, there is still a sufficient gradient of the electric field at the middle of the channel to manipulate the micro-particles. To clarify this, the same numerical results for the gradient of the electric field surface plot, but with a different representing range were shown in Figure 7.1c.

7.2.2. cDEP effect as a function of distance from the main channel wall

The DEP force is acting on the cell/micro-particle in both x and y directions. The gradient of the x-component of the electric field, which causes DEP force in the x-direction, is shown in Figure 7.2a for an applied signal of 70 Vrms and300 kHz at three different distances from the channel wall. In order to trap target cells, the x-component of the DEP force should overcome the hydrodynamic drag force. The x-component of the DEP force along the centerline of the main channel is negligible compared to the DEP force along the channel wall. Furthermore, this force is the strongest along the edges of the side channel walls (x = - 350, - 150, 150, 350 μm). The y-component of the gradient of the electric field at different distances from the origin (Figure 4.3., x = 0, 150, 250, 350, and 450 μm) is also shown in Figure 7.2b. These results show that the y-component of the DEP force is negligible for the particles along the lines x = 0 and x = 250 compared to the other positions and also indicate that y-component of the DEP force is the

strongest along the edges of the side channels (x = - 350, - 150, 150, 350 μm). While the x-component of the DEP force along the centerline of the main channel is almost negligible (Fig.7.2a), the y-component of the DEP force will pull particles off the centerline of the main channel and towards the channel walls in the case of positive DEP.

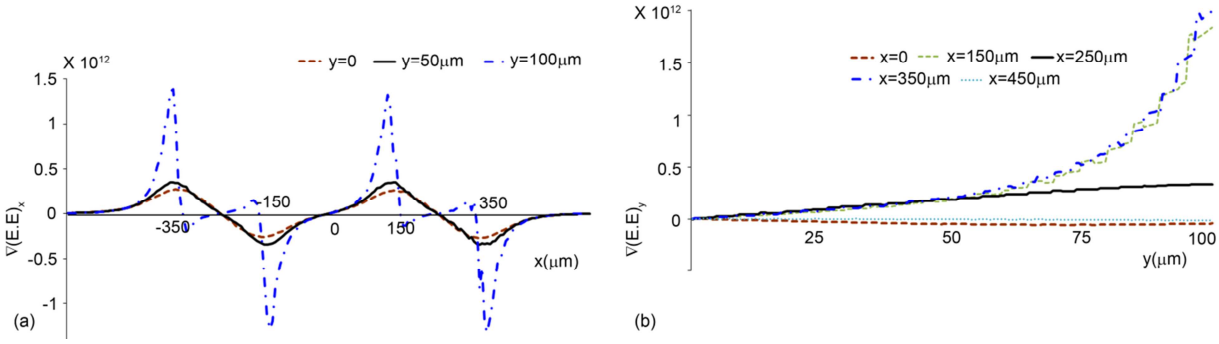

Fig.7.2. Numerical results: (a) Line plot of the x component of the gradient of the electric field squared ($kg^2mC^{-2}S^{-4}$) along the lines parallel to the center line of the main channel and at different distances from the channel wall for $V_1 = V_2 = 70\ V_{rms}$ at 300 kHz and $V_3 = V_4 =$ Ground boundary condition (y = 0, 50, and 100 μm). (b) Line plot of the y component of the gradient of the electric field squared ($kg^2mC^{-2}S^{-4}$) along the lines perpendicular to the center line of the main channel and at different distances from the origin for $V_1 = V_2 = 70\ V_{rms}$ at 300 kHz and $V_3 = V_4 =$ Ground boundary condition (x = 0, 150, 250, 350, and 450 μm). For side channel numbers see Fig. 6.1a. Reprinted from Journal of the Association and Laboratory Automation, Volume 15 Issue 3, Hadi Shafiee, John L. Caldwell, and Rafael V. Davalos, A Microfluidic System for Biological Particle Enrichment Using Contactless Dielectrophoresis, p224-232, Copyright (2010), with permission from Elsevier.

7.2.3. Electrode configuration effect on the gradient of the electric field

The effect of varying the electrode configuration on the gradient of the electric field along the centerline of the main channel was also investigated. Four different configurations with the same applied voltage and frequency were studied and the results shown in Figure 7.3. The DEP effects caused by having electrodes 1 and 2 charged and electrodes 3 and 4 grounded (case 1) are similar to the configuration with electrodes 1 and 4 charged and electrodes 2 and 3 grounded (case 3). The same can be said for the cases with electrodes 1, 2, and 4 charged (case 2) and electrode 3 grounded or electrode 1 charged and electrode 2 grounded (case 4). The surface plot of the gradient of the electric field with respect to these four cases of the electrode configurations were shown in Figure 7.3b.

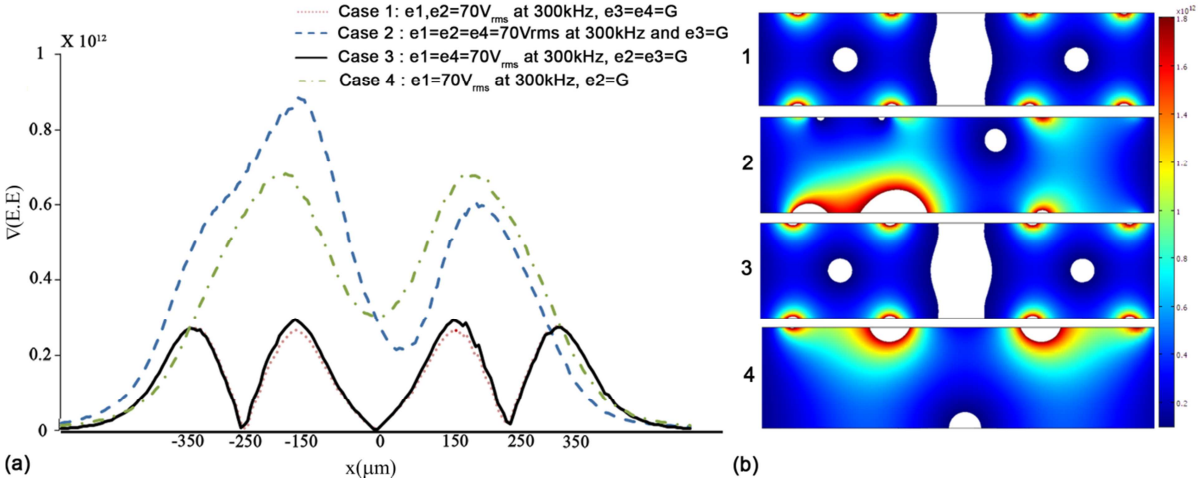

Fig. 7.3. The gradient of the electric field intensity along the centerline of the main channel for different electrode configurations. The electrodes are charged with 70V_{rms} and 300 kHz in the side channels in all cases. Case1: charged electrodes are in channels 1 & 2 and ground electrodes are in channels 3 & 4, Case 2: charged electrodes are in channels 1, 2 & 4 and ground electrodes are in channels 3, Case 3: charged electrodes are in channels 1 & 4 and ground electrodes are in channels 2 & 3, Case 4: charged electrodes are in channel 1 and ground electrodes are in channel 2. Reprinted from Journal of the Association and Laboratory Automation, Volume 15 Issue 3, Hadi Shafiee, John L. Caldwell, and Rafael V. Davalos, A Microfluidic System for Biological Particle Enrichment Using Contactless Dielectrophoresis, p224-232, Copyright (2010), with permission from Elsevier.

These numerical results indicate that the electrode configuration has a substantial effect on the gradient of the electric field and the resulting DEP cell manipulation. A benefit of this analysis is that one may change the cell/particle manipulation strategy by changing the electrode configurations. For example, the configuration used in case 4 (electrodes on just one side of the main channel) can deflect the target cell/particle trajectory in the main channel such that it leads to a specific reservoir.

7.3. Experimental results

7.3.1 THP-1 cell concentration

The validity of the numerical modeling was confirmed by demonstrating the system's ability to concentrate particles through both positive and negative DEP. Live THP-1 cells were observed to be trapped efficiently due to positive DEP force at $V_1 = V_2 = 70$ Vrms at 300 kHz, $V_3 = V_4$ = Ground (Fig.7.4) (For side channel numbers see Fig. 6.1a). Particles parallel to the electric field attract each other due to dipole-dipole interaction, resulting in pearl-chain

formations of the trapped cells in the direction of the electric field [21, 35, 81]. Referring to Figure 7.1b, particles concentrated through positive DEP should show a predisposition to group at locations with a high gradient of the electric field, in this case at the edges of the electrode reservoirs. As can be seen in Figure 7.4, this is indeed the case. The pearl chain formations attach to the side wall at locations with a high gradient of the electric field and then spread towards the center of the channel.

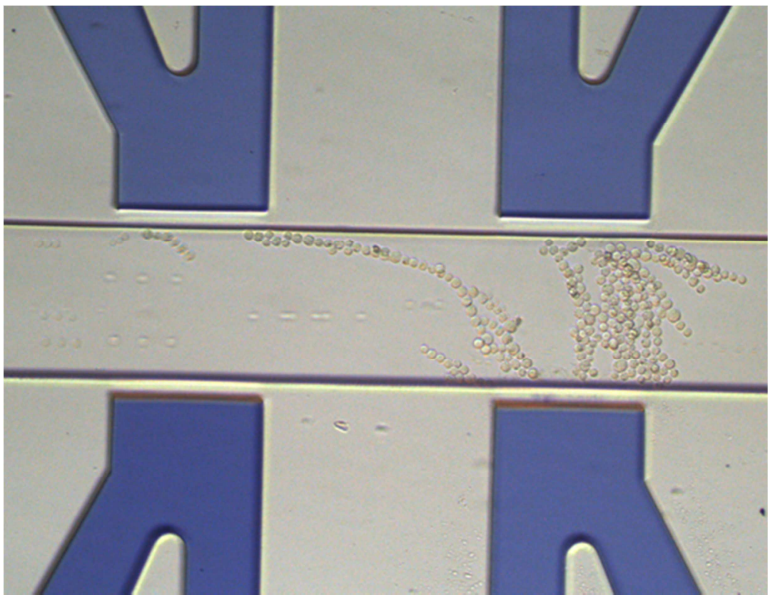

Fig. 7.4. Experimental results: Bright field image of live THP-1cells, shown here 30 seconds after applying the electric field ($V_1 = V_2 = 70\ V_{rms}$ at 300 kHz and $V_3 = V_4$ = Ground). The cells were trapped due to positive DEP. Reprinted from Journal of the Association and Laboratory Automation, Volume 15 Issue 3, Hadi Shafiee, John L. Caldwell, and Rafael V. Davalos, A Microfluidic System for Biological Particle Enrichment Using Contactless Dielectrophoresis, p224-232, Copyright (2010), with permission from Elsevier.

7.3.2. Selective trapping of THP-1 cells from 10μm beads

The selectivity of the device to differentiate two different particles with almost the same size was also examined via separation of THP-1 cells from 10μm beads. The THP-1 cells were observed to be trapped at 70Vrms and 300kHz and the 10μm beads went through the main channel without significant DEP disturbance (Figure 7.5). However, in order to increase the trapping efficiency, the voltage and/or frequency of the applied signal should be increased such that the particles passing through the middle of the channel experience strong DEP effect. At these higher voltage/frequencies we observed that both cells and beads close to the channel walls

were trapped, reducing the device's selectivity. We attribute this effect to the non-uniform gradient of the electric field across the main channel and between the side channels.

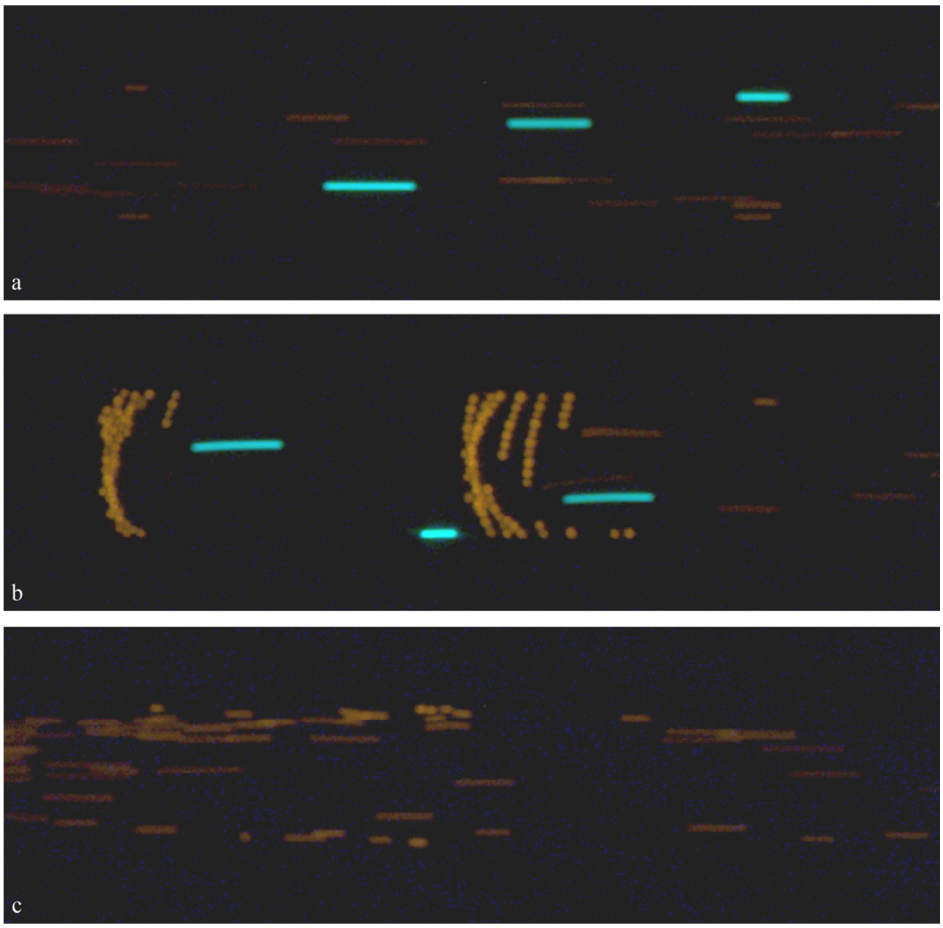

Fig. 7.5. Experimental Results: Selective trapping of live THP-1 cells (red) from a mixture also containing 10μm polystyrene beads (blue). THP-1 live cells were stained using cell trace calcein red-orange dye (a) Cells and beads are moving from right to left due to pressure driven flow. (b) THP-1 cells are trapped via dielectrophoresis and beads are passing through the trapping zone. Charged electrodes are in channels 1 & 2 (V_1=V_2=70V_{rms}) at 300kHz and ground electrodes are in channels 3 & 4 (V_3=V_4=Ground). (c) Releasing the trapped cells. For side channel numbers see Fig. 6.1a. Reprinted from Journal of the Association and Laboratory Automation, Volume 15 Issue 3, Hadi Shafiee, John L. Caldwell, and Rafael V. Davalos, A Microfluidic System for Biological Particle Enrichment Using Contactless Dielectrophoresis, p224-232, Copyright (2010), with permission from Elsevier.

7.3.3. Negative DEP trapping of 2μm beads

Particle concentration through negative DEP was displayed using 2 μm beads suspended in DI water at V_1 = V_2 = 190 V_{rms} at 300 kHz and V_3 = V_4 = Ground (For side channel numbers see Fig. 6.1a). These experimental results are shown in Figure 7.6. As is consistent with a

negative DEP response, the beads grouped in regions away from high gradients of the electric fields which, in this case, is in the centerline of the channel (Figures 7.6b and c). The inability to focus the microscope on all of the trapped beads simultaneously indicates that the beads were trapped at multiple heights in the main channel.

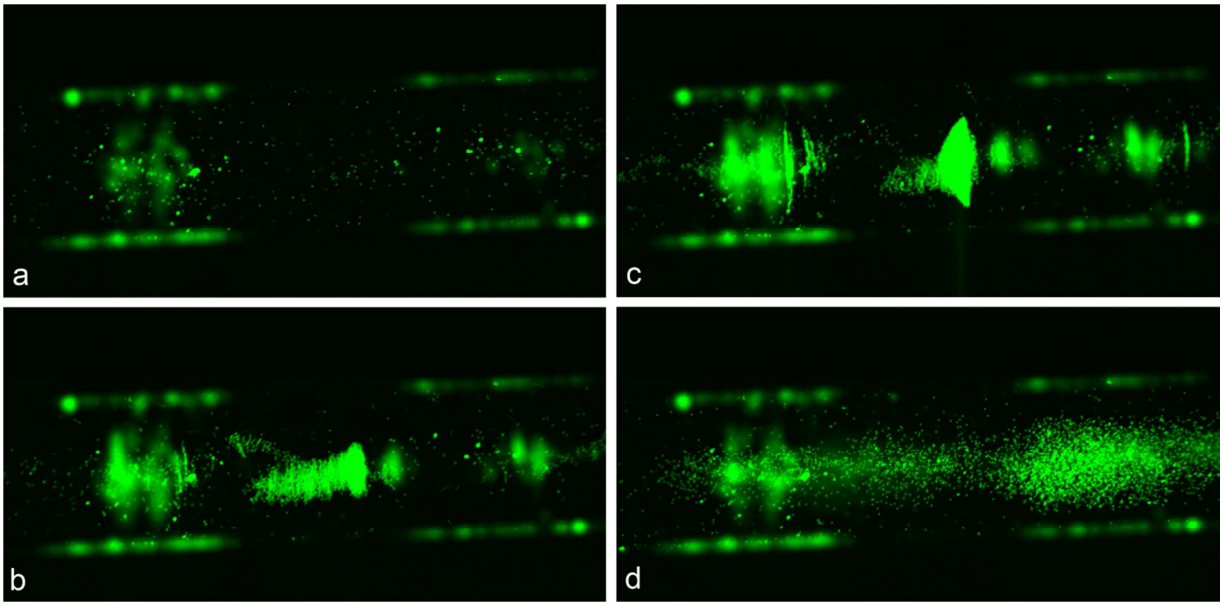

Fig. 7.6. Experimental results: Trapping 2μm beads suspended in DI water ($V_1 = V_2 = 190\ V_{rms}$ at 300 kHz and $V_3 = V_4$ = Ground) (a) t = 0 (b) t = 30 Seconds (c) t = 50 Seconds (d) t = 1 min, Release. For side channel numbers see Fig. 6.1a. Reprinted from Journal of the Association and Laboratory Automation, Volume 15 Issue 3, Hadi Shafiee, John L. Caldwell, and Rafael V. Davalos, A Microfluidic System for Biological Particle Enrichment Using Contactless Dielectrophoresis, p224-232, Copyright (2010), with permission from Elsevier.

7.4. Discussion

The use of a straight channel in this design has several advantages over more complicated configurations. The trajectory of a particle, without DEP influence, is easily predicted and the lack of detailed features simplifies production and replication of the devices. This same lack of complicated features in the channel helps to mitigate fouling effects caused by cell trapping. However, it should be noted that the DEP effect may be reduced significantly at the middle of the channel for wider channels. One method of addressing this negative effect is to use insulating structures inside the main channel. These structures distort the electric field and provide a sufficient gradient for DEP manipulation of cells passing through the center of the channel.

These types of designs may help increase the throughput and trapping efficiency of cDEP devices.

The device presented in this paper exhibited the concentration of microparticles at specific trapping regions within the device during the application of an electric field. The removal of this electric field allows the trapped cells to flow from the device at an increased concentration and these cells may be diverted to a separate reservoir off chip. This “trap and release” concentration strategy can also be incorporated with on-chip analysis systems by diverting the concentrated group of cells into a side channel as has been illustrated with iDEP[57].

Forthcoming generations of cDEP devices may also utilize a “chip and manifold” configuration relying upon disposable, injection molded “chips” inserted into a reusable manifold containing the necessary fluidic and electrical connections. This arrangement would allow metal electrodes in the manifold to be re-used for thousands of experiments while shifting the manufacturing burden to the replication of inexpensive fluidic chips. This use of polymer chips manufactured through injection molding has been demonstrated previously for iDEP [57].

7.5. Conclusion

A microfluidic system was presented that illustrates the great potential for DEP-based concentration of biological particles without negative effects on the sample, extensive sample preparation, or complicated fabrication procedures. Numerical modeling revealed the flexibility of this system’s multiple electrode configurations to divert the particles into a desired trajectory and the device showed the ability to concentrate micro-particles through both positive and negative DEP. By relying upon the particle’s electrical properties to accommodate enrichment, cDEP should be able to achieve a high degree of specificity without extensive sample preparation.

The potential for batch fabrication illustrated in this work, combined with the high performance of the resulting devices makes cDEP an attractive candidate for pre-concentration processes in areas where both rapid and highly accurate results of analyses are required.

Chapter 8
cDEP to Isolate Prostate Tumor Initiating Cells (TICs) from Prostate Cancer Cells

Tumor initiating cells (TICs) are cells within a tumor possessing the ability to generate a new tumor from an existing one that exhibits a similar histopathology as the tumor from which it was derived [76]. Identification of the specific gene expression patterns and genetic alterations in TICs will likely lead to an increased understanding of the most appropriate therapeutic strategies to ablate this cell population. Development of animal models of carcinogenesis and understanding key biological processes, such as metastasis, are some of the crucial biological applications for the TIC hypothesis [168]. One of the critical issues in the current cancer treatment methods is that malignant cells survive chemotherapy and radation. There are evidences that TICs are most likely responsible for therapy resistence [168]. There has been evidences from a variety of tumor types including blood, breast, central nervous system, pancreas, skin, head and neck, colon, and prostate [77, 169-176], that not all cells within the tumor have TIC properties. Some people refer to TICs as tumor or cancer stem cells.

Detection and isolation of TICs in solid tumor has been a technical challenge due to their less accessibility. However, recently CD44+ CD24-/low cells isolated from breast tumor have shown capacity for tumor re-growth through serial transplantation in mice. These cells developed tumors in animal models due to transplantation of as few as one hundred cells, however tumor re-growth failed for breast cancer cells.

Previous work in human prostate cancer cell lines and in primary human prostate samples has identified several markers of TICs or putative stem cells. These markers include increased expression of cell surface proteins such as CD133, CD44, and $\alpha 2\beta$ integrin [177, 178]. Additionally, recent data suggest that increased expression of ATP-dependent membrane pumps (ABCB1/2), which can be measured by flow cytometry and dye exclusion (so-called side population) can be used to isolate cells with increased TIC properties. Data from other tissue types also support the use of aldehyde dehydrogense (ALDH), which can be measured by a

fluorescent substrate, as a marker for putative TICs. To our knowledge, ALDH activity has not been investigated in prostate cancer TICs. To our knowledge the expression of ALDH in primary prostate cancer cells has not been reported. Cramer's studies indicate that approximately 2.5% of cells specifically express ALDH. Additionally, the ALDH positive population had 98% overlap with the CD133 population. Interestingly, in a patient matched sample of benign prostate cells (WFU274PZ), we found lonely 0.05% ALDH positive cells. These data indicate that ALDH positive cells may be increased in tumor derived samples, consistent with its expression being associated with TICs.

Current efforts to isolate and enrich TICs from non-TICs are hampered by the lack of a suitable high throughput and rapid method to isolate these cells. Most methods currently rely on time-consuming labeling of surface marker expression followed by cell sorting via flow cytometry [78-80]. This delay may compromise gene expression. The use of non-invasive methods to detect and enrich cancer cells independent of their genotype is critical for diagnostic and treatment purposes.

In this chapter we investigated the dielectric response of Prostate Tumor Initiating Cells (TIC) and Prostate tumor cells in a microfluidic context utilizing contactless dielectrophoresis (cDEP). The voltages and frequencies at which 10% to 90% of the cells were trapped in the cDEP microfluidic device were investigated experimentally. We observed a distinctive DEP response for the prostate TICs compared to prostate tumor cells. These preliminary results indicate that cDEP could be a promising fast and free-marker method with minimum sample preparation to isolate and enrich TICs vs. non-TICs using their electrical signatures. This will utilize cDEP sorted TICs and non-TICs to assess genetic and epigenetic differences that may be associated with tumorigenesis.

8.1. Dielectrophoresis to Detect CTCs

The motion of the neutral micro-particles exposed in non-uniform electric field, known as dielectrophoresis (DEP), is a promising alternative technique to detect CTCs in biological fluids. Dielectrophoresis uses the electrical signatures of cells exposed in non-uniform electric field to induce translational and rotational motion. The cell response in ac electric fields are different in

different frequencies, therefore DEP devices can be easily reconfigured for different cell types. A DEP device can be used for a range of different cells types by just changing the applied frequency and without changing the device design. For small samples with few target cells, the target cells may be trapped at the trapping zone of the device and the background non-target cells are collected in an outlet reservoir. For larger samples with high number of target cells, cells usually are manipulated in the fluid streams without getting trapped and then isolated and collected in a reservoir. Isolation of 50000 cancer cells in a 10μL of blood has been achieved in less than 5 min [36, 130]. A sensitivity of isolation 20 target cells from one million cells has also been achieved [179]. DEP separation of cells with close electrical signatures will be challenging and may not be effective. Howevr, DEP response of rare target cells can be modulated by labeling cells with microparticles using markers. DEP-activated cell sorting (DACS) has shown the ability of achieving more than 200-fold purity isolation and enrichment of rare bacteria expressing a specific surface marker in one round at a single channel throughput of 10,000 cells per second [180].

Current DEP devices are typically designed around an array of thin-film interdigitated electrodes patterned onto the surface of a substrate within the sample channel. These electrodes generate a non-uniform electric field that interacts with the particles near the surface of the electrode array[181]. An important advantage of DEP to distinguish abnormal cells is that no assumptions regarding their genetic make-up are necessary for the method to be successful. Furthermore, the search strategy relies upon the cells' biophysical properties which are closely aligned with the propensity of the abnormal cell to migrate from its natural environment, an early step in metastatic disease [182]. As opposed to techniques such as fluorescence activated cell sorting (FACS) [183] or pillar-based microfluidic chips [137], no antibody is used in this method for rare cancer cell trapping and identification. Many microchip architectures and configurations have been developed to efficiently sort biological particles by DEP.

The application of DEP to separate target cells from a solution has been studied extensively in the last two decades. Several DEP applications to isolate target cells have been effectively demonstrated including the separation of leukemia, breast cancer and other targeted cells from blood [184-186], cancer cells from CD34+ hematopoietic stem cells [187], neuroblastoma cells from HTB glioma cells [184], cervical carcinoma cells [188], K562 human CML cells [189], mammalian cells based on their cell-cycle phase [190, 191], and the separation

of cells of the same type based on their activation state [192, 193]. In 1992 Gascoyne et al. produced dielectrophoretic characteristics of normal, leukaemic, and differentiation induced leukaemic erythrocytes from mice as a function of frequency through traditional DEP[194]. Experiments were conducted on an interdigitated gold electrode array of 80μm. Murine erythroleukaemia (MEL) cells were suspended in media and concentrated to 10^5 cells/ml. Mouse erythrocytes were harvested from 0.5ml of blood and resuspended with the MEL cells at a concentration of 10^7cells/ml. The conductivity was adjusted using NaCl to be 2mS/m. A root mean square (rms) voltage of 3V was applied while varying frequency from $5x10^2$ to 10^5 Hz. It was shown that HMBA-treated leukaemic cells had negative collection while untreated leukaemic cells showed positive collection at 22kHz. It was deduced from this that these two cells would separate at that frequency. The same deduction was made for leukaemic cells and healthy cells at 30kHz.

In 1994 this same group published results for separation of both leukemia cells and breast cancer cells from human blood using various DEP methods [195, 196]. HL-60 leukaemia cells were suspended with healthy blood cells with a ratio of 2:3. Cells were re-suspended in the same media with $2x10^7$ leukaemia cells and $3x10^7$ normal blood cells. The cell solution had a conductivity of 10mS/m. An interdigiated microelectrode array of 80μm was used once again with glass walls and epoxy cement completing the chamber. Voltage was applied at 5V varying frequency up to 500Hz. MDA231 breast cancer cells were harvested from a pleural effusion and suspended in solution with peripheral blood and T-lymphocytes with a final concentration of $5x10^4$cells/ml. Cells were subjected to a rotating electric field (ROT) and the ROT spectra was measured by timing cell rotation rates (Figure 2). A rotating field from 10kHz to 100MHz was applied by sinusoidal waves in phase quadrature to the electrode array. In this study, the cross over frequencies for HL-60 leukaemic cells, T-lymphocytes, and red blood cells were determined. This frequency was found when (at what frequency) DEP force changed direction. This is an important measurement when determining dielectrophoretic difference amidst different cell types. The crossover frequencies were 180kHz, 320kHz, and 490kHz respectively. From these frequencies, membrane specific capacitance values of 15,11, and $9mF/m^2$ were calculated respectively. Since membrane capacitance is the dominating force in DEP under the given frequencies, this value ultimately determined dielectrophoretic differences in the various cells. The ROT spectra for MDA231 cells, lymphocytes, and erythrocytes along with DEP

responses at various frequencies were also determined by this group in 1994 [196]. Frequencies of 3, 5.5, and 7MHz caused counter rotation in the respective cells. Crossover frequencies were also found for these cells and were 80, 320, and 450kHz respectively. These measurements showed significant differences in these cells' dielectric properties.

In [197] cell sorting conditions were optimized as well as extended to other forms breast cancer to include: MDA-231, MDA-435, and MDA-468. Both ROT and DEP techniques were used for this experiment. Concentrations and conductivities of $5x10^4$ cells/ml, 56mS/m and 10^5-10^6 cells/ml, 10mS/m were used, respectively. Field frequency for the DEP experiment began at 500kHz at $2V_{rms}$ to trap all cells and lowered to the frequency predicted by the ROT analysis for optimal trapping of the breast cancer cells.

Various new methods employing interdigitated electrodes for DEP have recently evolved including DEP field flow fractionation (fff). Gacoyne et al. used this method for cell separation in 2000 [198] as well in later studies including stem cell isolation from adipose tissue in 2008 [199].In the 2008 study MDA-435 cells were suspended with hematopoietic CD34+ stem cells, leukocytes, and buffer for a concentration of $5x10^6$ cells/ml. The DEP signal of 4V p-p at 10kHz was applied for 10 minutes to equilibrate cell height. Flow velocity was applied and DEP was then changed to 40kHz releasing T-leukocytes. DEP was then reduced to 5kHz releasing the MDA-435 cells from the electrodes. Their results suggested that breast cancer cells MDA-433 would separate from T-lymphocytes between the frequencies of 20 and 50kHz. Purging breast cancer cells from CD34+ stem cells occurred at ~40kHz. This study extended its application to separation of the major leukocytes from one another (T and B). This separation occurred between 25 and 45kHz.

The main drawbacks of the microelectrode-based devices, however, are that they are susceptible to electrode fouling and require expensive, complicated fabrication procedures [22]. In addition since the patterned electrodes at the bottom of the sample channel only create an electric field gradient near their surface, only cells close to the electrodes experience a DEP response thus making these devices unsuitable for high-throughput applications. Typical sample volumes that are processed within these devices are on the order of nano- to microliters, far below that of typical clinical diagnostic sample volumes (mL).

8.2. Dielectrophoresis to Detect TICs

Tumor initiating cells (TICs) are cells within a tumor possessing the ability to generate a new tumor from an existing one that exhibits a similar histopathology as the tumor from which it was derived [76]. Identification of the specific gene expression patterns and genetic alterations in TICs will likely lead to an increased understanding of the most appropriate therapeutic strategies to ablate this cell population. Development of animal models of carcinogenesis and understanding key biological processes, such as metastasis are some of the crucial biological applications for the TIC hypothesis [168]. One of the critical issues in the current cancer treatment methods is that malignant cells survive chemotherapy and radiation. There are evidences that TICs are most likely responsible for therapy resistance [168]. There has been evidences from a variety of tumor types including blood, breast, central nervous system, pancreas, skin, head and neck, colon, brain, and prostate [77, 169-176], that not all cells within the tumor have TIC properties. Some people refer to TICs as tumor or cancer stem cells (CSCs).

Detection and isolation of TICs in solid tumor has been a technical challenge due to their less accessibility [200]. However, recently CD44+ CD24-/low cells isolated from breast tumor have shown capacity for tumor re-growth through serial transplantation in mice [170]. These cells developed tumors in animal models due to transplantation of as few as one hundred cells, however tumor re-growth failed for breast cancer cells with different cell marker. A similar investigation hase also been done for brain tumors [201]. In this study CD133+ marker was used to identify brain tumor stem cells and it was shown that 100 CD133+ cells isolated from human brain tumors had the self-renewal capacity to initiate new tumors in the brain of immunocompromised mice [200, 201].

Previous work in human prostate cancer cell lines and in primary human prostate samples has identified several markers of TICs or putative stem cells. These markers include increased expression of cell surface proteins such as CD133, CD44, and $\alpha 2\beta$ integrin [177, 178, 202, 203]. Additionally, recent data suggest that increased expression of ATP-dependent membrane pumps (ABCB1/2), which can be measured by flow cytometry and dye exclusion (so-called side population) can be used to isolate cells with increased TIC properties. Data from other tissue types also support the use of aldehyde dehydrogense (ALDH), which can be measured by a fluorescent substrate, as a marker for putative TICs. To our knowledge ALDH activity has not

been investigated in prostate cancer TICs. Cramer's studies indicate that approximately 2.5% of cells specifically express ALDH. Additionally, the ALDH positive population had 98% overlap with the CD133 population. Interestingly, in a patient matched sample of benign prostate cells (WFU274PZ) we found lonely 0.05% ALDH positive cells. These data indicate that ALDH positive cells may be increased in tumor derived samples, consistent with its expression being associated with TICs [202, 203].

Current efforts to isolate and enrich TICs from non-TICs are hampered by the lack of a suitable high throughput and rapid method to isolate these cells. Most methods currently rely on time-consuming labeling of surface marker expression followed by cell sorting via flow cytometry [78-80]. This delay may compromise gene expression.

Here in this study, we investigated the ability of our recently developed method, contactless dielectrophoresis (cDEP)[69], to characterize and identify prostate tumor initiating cells utilizing their electrical signatures without using established markers of prostate cancer stem cells such as ALDH, CD133, CD44, CD117, and β1-integrin, etc.

8.3. Experimental Results

The voltages and frequencies of the applied signal for the onset of trapping and complete trapping of both prostate cancer cells and negative TICs are reported in Figure 3. Intrestingly, the trapping voltage bandwidth for PC3 is much narrower than negative TIC in our optimized cDEP device. On the other hand, at a certain amount of frequency, the required voltage to trap negative TICs is much higher than the required voltage to trap PC3s. As the frequency increases, the difference between the onset of PC3 and negative TIC trapping decreases. This indicates that the maximum and optimum difference between these cells occures at lower frequencies. At such frequencies, we would expect complete trapping of PC3s and the onset of trapping of negative TICs in the cDEP device.

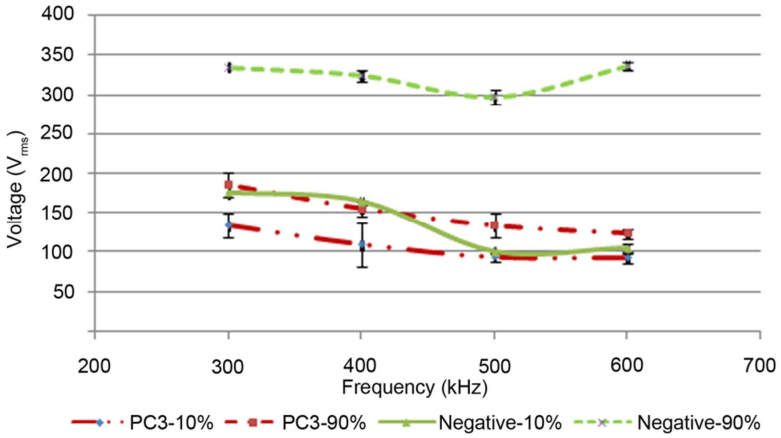

Fig. 8.2.1. The signal parameters required for onset of trapping and complete trapping of prostate cancer cells and TICs (negative ALDH)

The same required signal parameters for onset of trapping and complete trapping of negative and positive TICs are also reported in Figure 4. The DEP response of these cells for complete cell trapping obeys a similar path for the range of the frequencies we tested in the experiments. The cell trap beginning voltage is almost close for both TICs. However, these results indicate that the negative TICs are harder to trap in the cDEP device and requires higher voltage.

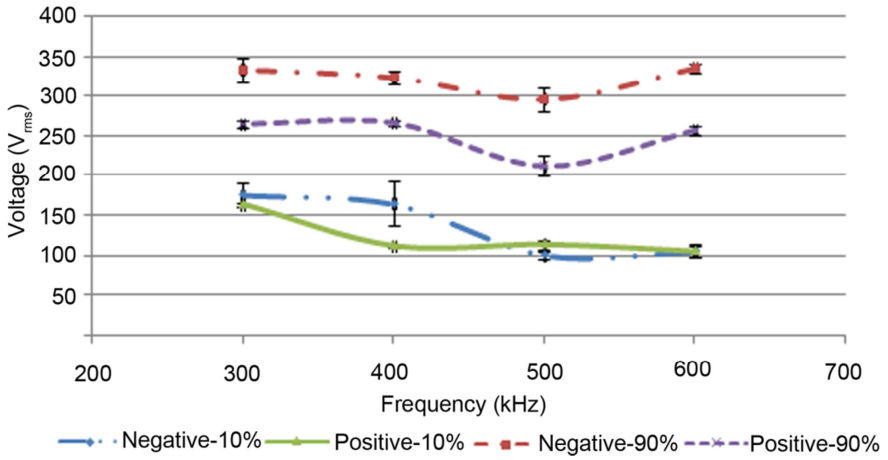

Fig. 8.2.2. The signal parameters required for onset of trapping and complete trapping of negative and positive ALDH.

The voltage bandwidth to trap PC3, positive, and negative TIC at 600 kHz applied frequency is shown in Figure 5. As we discussed earlier in Figure 3, these results show that PC3s are much easier to trap in our cDEP device and they show strong DEP responses at very lower

applied voltages compared to TICs. On the other hand the electrical signature of PC3 and TIC are significantly different which promises their cDEP separation with high selectivity and purity.

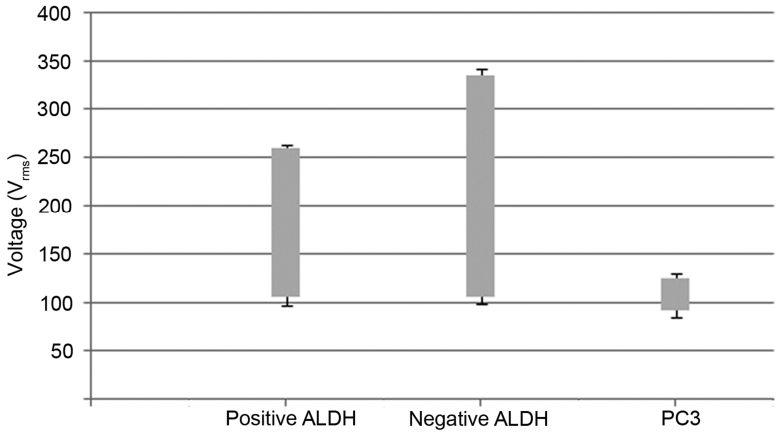

Fig. 8.2.3. Voltage bandwidth for trapping PC3, positive and negative TIC at 600 kHz

8.3. Conclusion

A microfluidic device was designed numerically and fabricated using photolitography techniques to investigate the electrical response of prostate TICs compared to non-TICs. Thrhough our numerical studies we demonstrated that the insulating structures inside the main channel of the cDEP microfluidic devices have a noticable effect on creating non-uniform electric field for DEP cell manipulation. The dimension and the position of these structures can be altered to provide uniform gradient of the electric field across the main channel of the device which consequently increase the selectivity of the device to separate two different cell types. Furthermore, these insulating structures are great tools to increase the throughput of the device by providing high gradient of the electric field in devices with wider channels.

We observed significant differences between the electrical responses of prostate TICs and non-TICs through trapping of these cells in our cDEP device. When an ac signal with a certain amount of frequency (300kHz, 400kHz, 500kHz, and 600kHz) was applied, prostate non-TICs were trapped between the posts at lower voltages compared to TICs. The voltages and frequencies reported in above figures can be used to separate TICs vs. non-TICs in our cDEP device with high selectivity. The TICs can be collected at a reservoir connected to the outlet of the device, while the non-TICs are trapped at the trapping area due to positive DEP. The cDEP

separated and enriched TICs can be used for further interrogations to study their genetics and pathways for target therapies and treatments.

Chapter 9
Future Work

9.1. High throughput cDEP Device

The ability to successfully isolate CTCs or TICs from biological samples which normally are on the order of mLs requires a high throughput microfluidic system. We believe there are applicable and operational strategies to overcome this issue. We believe that we can address throughput challenge by increasing the width, height, and length of the channels and at the same time optimize the insulating post geometries and numbers inside and outside of the main channel to generate strong and uniform gradient of the electric field inside the main channel. We have recently designed a new cDEP device (Fig. 9.1) using Comsol with 5mm width and 8mm length at the trapping area with 3000 circular posts with diameter of 100μm. The gradient of the electric field intensity in this optimized device is comparable to the gradient of the electric field in our current devices represented in the previous chapters. We believe that once we have an engineered platform, we will have little difficulty delivering an enriched sample for animal studies. We have tremendous experience operating microfluidic devices with raw samples and developing such platforms to deliver samples for downstream analysis. We anticipate that minimal sample pre-processing will be necessary for these experiments other than gentle mechanical filtration.

The surface plot of the numerical results for such a wide channel device is reported in Figure 9.2. The voltage and frequency of the applied ac signal through the electrodes in the side channels are 100Vrms at 200kHz, which is a common signal parameters in cDEP technology. We believe that this is the remarkable benefit of cDEP to be able to customize the microfluidic devices by optimizing the geometry of the insulating structures in the device.

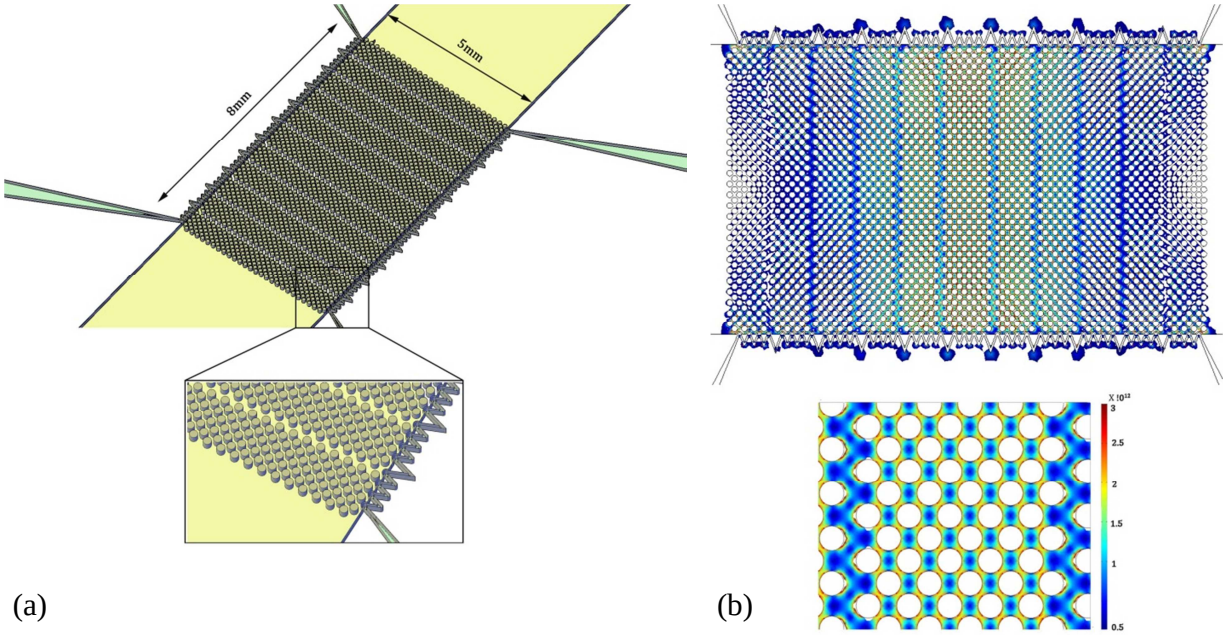

(a) (b)

Fig. 9.1. (a) A cDEP design with 5mm X 8mm dimensions at the trapping area and 3000 pillars with 100um diameter. **(b)** The surface plot of the gradient of the electric field for a 100Vrms at 200kHz ac signal.

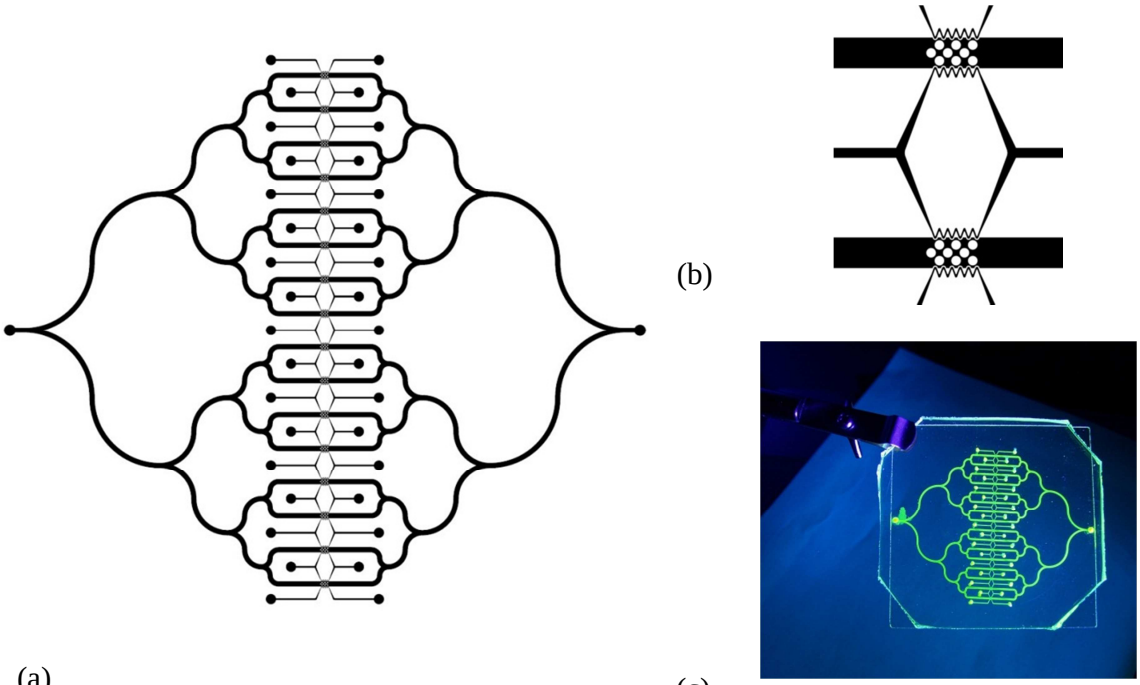

(a) (b) (c)

Fig. 9.2. (a) 2D schematic of a cDEP design with 16 devices in parallel. **(b)** The close view of the trapping area in one of the cDEP devices. **(c)** A fabricated microfluidic device with 16 cDEP devices in parallel.

Furthermore, we can run multiple channels in parallel (Fig. 9.2). We have been able to design and fabricate a cDEP device that includes 16 devices in parallel to each other which can provide us at least 0.5mL/hr. In such device each the length of each branch is the same in order to have equal fluid resistance. This will be crucial to distribute the input sample into even subsamples and use the maximum capacity of a parallel design.

9.2. Isolation of TICs vs. non-TICs Using cDEP

9.2.1. Determine Conditions to Detect and Enrich prostate TICs from Mixture of TICs and non-TICs.

New cDEP devices and platforms are designed through numerical modeling, experimental knowledge of cDEP, and oncology to separate TICs. The proposed use of the cDEP system is to detect/isolate/concentrate TICs from prepared solutions. The following operating conditions are optimized for the separation and enrichment of viable TICs and non-TICs added to experimental buffer or prepared physiologically relevant fluid samples: frequency and amplitude of applied field, solution conductivity, pH and temperature, device geometry and material.

Design: The sorting and isolation of TICs will occur in three steps (Fig 9.3). Step 1: A bulk cell suspension is pumped into channel (syringe pump with sample solution) (Fig 9.3), Step 2: An electric field is applied trapping TICs while pressure driven flow removes the non-trapped suspension from channel, and Step 3: The electric field is removed and pressure driven flow pumps DEP buffer medium (syringe pump with DEP buffer) (Fig 9.3) into channel and removes TIC cell suspension from channel. These TICs will be collected in a different reservoir (reservoir 2) (Fig 9.3). Isolated cells will be evaluated for their TIC properties. Based upon results from DEP characterization we will also develop the next generation of microdevices and a more autonomous platform.

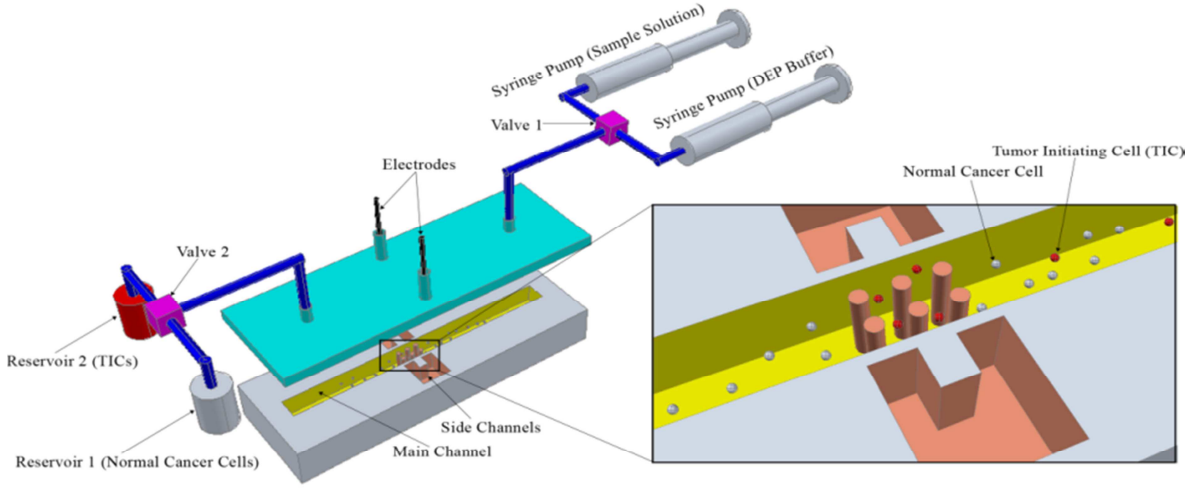

Fig. 9.3. 3D schematic of a cDEP experimental set up.

This will involve designing and fabricating new contactless DEP microfeatures with an appropriate sensitivity to isolate TIC from cancer cells based on their different electrical properties found in the previous experiments and multiphysics numerical modeling software. We will then observe the behavior of TICs in current devices manufactured based on the contactless DEP. After evaluation of device performance (concentration factors, throughput, trapping voltage threshold, and removal efficiencies), the device architecture will be adapted as needed.

9.2.2. TIC Isolation and Validation.

Prostate TICs and non-TICs are isolated using FACS with published and putative markers. Tumor initiation will be validated by in vivo tumorigenesis. TICs isolated by cDEP will be validated for the original cell surface markers and for TIC properties by methods outlined in this aim. The approach is to start with a relatively simple population of tumor cells and move to gradually more complex systems.

Design: The approach here will be starting with prostate cancer cell lines, move to primary cultures, and then move to primary tissue samples. Cell lines to be used will be DU145, PC3, LNCaP. Primary prostate will be acquired by a rapid acquisition method that has been developed by Dr. Scott Cramer at Wake Forest Comprehensive Cancer Center. This institution has an ample urological practice to provide the requisite samples. The method of acquisition allows for prospective identification of tumor vs. benign tissue, which is collected using a sterile biopsy punch. The sample will be processed into single cell suspension with proteolytic enzymes by routine methods. Transition from OR to a single cell suspension can be achieved in under two

hours. For the initial characterization of DEP properties of TIC cell sorting against established or putative markers of prostate cancer stem cells such as CD133, CD44, CD117, ALDH, and β1-integrin, etc. will be used. Positive and negative populations will be validated for tumor initiating capabilities by tissue recombination (mixture of fetal urogential mesenchyme with the epithelium) and grafting under the renal capsules of NOD/SCID/ILR2γnull mice. Histopathology will be assessed to determine tumor formation, which will be compared to the histopathology of the original sample. Validated TICs will be assessed for DEP properties. We will perform similar studies with DEP sorted cells to assess markers such as ALDH/CD133, CD44, etc. The DEP sorted cells will be evaluated for tumorigenic properties by tissue recombination. Pathways that are identified to be enriched or depleted in TIC will be evaluated here for their functional role in tumorigenesis.

9.3. High throughput cDEP-CTC Chip Utilizing Markers

The developed high throughput cDEP devices can be utilized to enhance CTC detection and isolation using markers such as anti-epithelial-cell-adhesion-molecule (EpCAM). We will first need to investigate the effect of low electric field intensity in our cDEP devices on the biological function of EpCAM coated on the surface of the micro-structures. The micro-structures inside the main channel of cDEP devices are functionalized with EpCAM antibody which is frequently observed to be overexpressed in different types of cancer cells. The induced DEP inside the main channel will be utilized to improve the cell micro-structure's surface contact due to positive DEP force applied on CTCs to enhance CTC capture by EpCAM. Flow velocity and shear force are two fundamental parameters in the CTC trapping efficiency. This study will be conducted analytically, numerically and experimentally utilizing the aspects of fluid dynamics, dielectrophoresis, and thermal transport.

9.4. CTC-cDEP Activated Cell Sorting (CTC-cDEP-ACS)

The feasibility of utilizing polymeric microspheres to label the CTCs in order to more significantly differentiate the DEP mobility of these rare cells from their counterparts can be investigated. Functionalized polymer beads with EpCAM antibody will be utilized in order to tag

CTCs. The positive and negative DEP response of the labeled-CTCs at different frequencies, voltages, and medium conductivities will be studied. The interaction between the beads and cells in non-uniform electric field is another crucial subject that will be studied in control devices. The range of frequencies and voltages of the applied signal at which the beads and cells experience positive and negative DEP will be analytically and experimentally explored. These preliminary results will enable me to design a new generation of cDEP devices that are appropriate for CTC tagged with beads. The ability of this technology with the new designed cDEP devices to isolate DEP-labeled rare cells in more complex samples (whole blood) will be explored. An important benefit of this technology is the possibility to label any type of CTC that overexpresses a specific antibody on its surface with functionalized polymeric beads such that their electrical signature will be significantly different from non-target cells in the mixture. This will allow us to isolate different types of CTC with a dominated narrow range of frequency and voltage of the applied signal in the microfluidic device. The method would isolate and enrich transformed cells from blood samples by capitalizing on the selectivity of dielectrophoresis to distinguish minute and induced DEP mobility variations among target and non-target cells.

References

1. Morgan, H. and N.G. Green, *AC Electrokinetics: Colloids and Nanoparticles*. 2003, Hertfordshire, England: Research Studies Press LTD. 324.
2. Lapizco-Encinas, B.H., et al., *Dielectrophoretic concentration and separation of live and dead bacteria in an array of insulators.* Anal Chem, 2004. **76**(6): p. 1571-9.
3. Armstrong, D., et al., *Rapid CE microbial assays for consumer products that contain active bacteria.* FEMS Microbiology Letters, 2001. **194**(1): p. 33-37.
4. Armstrong, D., et al., *Separating microbes in the manner of molecules. 1. Capillary electrokinetic approaches.* Analytical Chemistry, 1999. **71**(24): p. 5465-5469.
5. Girod, M. and D.W. Armstrong, *Monitoring the migration behavior of living microorganisms in capillary electrophoresis using laser-induced fluorescence detection with a charge-coupled device imaging system.* Electrophoresis, 2002. **23**(13): p. 2048-56.
6. Cabrera, C.R. and P. Yager, *Continuous concentration of bacteria in a microfluidic flow cell using electrokinetic techniques.* Electrophoresis, 2001. **22**(2): p. 355-62.
7. Becker, F.F., et al., *The removal of human leukaemia cells from blood using interdigitated microelectrodes.* J. Phys. D: Appl. Phys., 1994. **27**: p. 2659-2662.
8. Gascoyne, P.R.C., et al., *Dielectrophoretic Separation of Cancer Cells from Blood.* IEEE Trans. Industry Applications, 1997. **33**(3): p. 670-678.
9. Huang, Y., et al., *Dielectrophoretic cell separation and gene expression profiling on microelectronic chip arrays.* Anal Chem, 2002. **74**(14): p. 3362-71.
10. Cheng, J., et al., *Isolation of cultured cervical carcinoma cells mixed with peripheral blood cells on a bioelectronic chip.* Anal Chem, 1998. **70**(11): p. 2321-6.
11. Sabounchi, P., et al., *Sample concentration and impedance detection on a microfluidic polymer chip.* Biomed Microdevices, 2008. **10**(5): p. 661-70.
12. Markx, G.H., M.S. Talary, and R. Pethig, *Separation of viable and nonviable yeast using dielectrophoresis.* Journal of Biotechnology, 1994. **32**(1): p. 29-37.
13. Das, C.M., et al., *Dielectrophoretic segregation of different human cell types on microscope slides.* Anal Chem, 2005. **77**(9): p. 2708-19.
14. Gascoyne, P.R., et al., *Isolation of rare cells from cell mixtures by dielectrophoresis.* Electrophoresis, 2009. **30**(8): p. 1388-98.
15. Apostolaki, S., et al., *Circulating HER2 mRNA-positive cells in the peripheral blood of patients with stage I and II breast cancer after the administration of adjuvant chemotherapy: evaluation of their clinical relevance.* Ann Oncol, 2007. **18**(5): p. 851-8.
16. Cristofanilli, M., *The "microscopic" revolution in breast carcinoma.* Cancer, 2005. **103**(5): p. 877-80.
17. Fizazi, K., et al., *High detection rate of circulating tumor cells in blood of patients with prostate cancer using telomerase activity.* Ann Oncol, 2007. **18**(3): p. 518-21.
18. Hayes, D.F., et al., *Circulating tumor cells at each follow-up time point during therapy of metastatic breast cancer patients predict progression-free and overall survival.* Clin Cancer Res, 2006. **12**(14 Pt 1): p. 4218-24.
19. Naoe, M., et al., *Detection of circulating urothelial cancer cells in the blood using the CellSearch System.* Cancer, 2007. **109**(7): p. 1439-45.

20. Wong, P.K., *Electrokinetics in Micro Devices for Biotechnology Applications.* IEEE/ASME Transactions on Mechatronics, 2004. **9**(2): p. 366-376.
21. Dussaud, A.D., *Particle segregation in suspensions subject to high-gradient ac electric fields.* J. Appl. Phys., 2000. **88**(5463): p. 5463-5473.
22. Hughes, M.P., *Strategies for dielectrophoretic separation in laboratory-on-a-chip systems.* Electrophoresis, 2002. **23**(16): p. 2569-82.
23. Fabisiewicz, A., et al. *Detection of circulating cancer cells in peripheral blood as a prognostic factor in early breast cancer*. in *3rd International Symposium on the Molecular Biology of Breast Cancer*. 2005. Molde, NORWAY.
24. Smerage, J.B. and D.F. Hayes, *The measurement and therapeutic implications of circulating tumour cells in breast cancer.* Br J Cancer, 2006. **94**(1): p. 8-12.
25. Budd, G.T., et al., *Circulating Tumor Cells versus Imaging--Predicting Overall Survival in Metastatic Breast Cancer.* Clinical Cancer Research, 2006. **12**(21): p. 6403-6409.
26. Osman, I., et al., *Detection of circulating cancer cells expressing uroplakins and epidermal growth factor receptor in bladder cancer patients.* International Journal of Cancer, 2004. **111**(6): p. 934-939.
27. Galan, M., et al., *Detection of occult breast cancer cells by amplification of CK19 mRNA by reverse transcriptase-polymerase chain reaction: Role of surgical manipulation.* Anticancer Research, 2002. **22**(5): p. 2877-2884.
28. Dingemans, A.M.C., et al., *Detection of cytokeratin-19 transcripts by reverse transcriptase-polymerase chain reaction in lung cancer cell lines and blood of lung cancer patients.* Laboratory Investigation, 1997. **77**(3): p. 213-220.
29. Berteau, P., et al., *Molecular detection of circulating prostate cells in cancer II: Comparison of prostate epithelial cells isolation procedures.* Clinical Chemistry, 1998. **44**(8): p. 1750-1753.
30. Berteau, P., et al., *Influence of blood storage and sample processing on molecular detection of circulating prostate cells in cancer.* Clinical Chemistry, 1998. **44**(3): p. 677-679.
31. Koike, E., et al., *Endoscopic ultrasonography in patients with thyroid cancer: Its usefulness and limitations for evaluating esophagopharyngeal invasion.* Endoscopy, 2002. **34**(6): p. 457-460.
32. Schroder, C.P., et al., *Detection of micrometastatic breast cancer by means of real time quantitative RT-PCR and immunostaining in perioperative blood samples and sentinel nodes.* International Journal of Cancer, 2003. **106**(4): p. 611-618.
33. Traweek, S.T., J. Liu, and H. Battifora, *KERATIN GENE-EXPRESSION IN NONEPITHELIAL TISSUES - DETECTION WITH POLYMERASE CHAIN-REACTION.* American Journal of Pathology, 1993. **142**(4): p. 1111-1118.
34. Pohl, H.A., *The Motion and Precipitation of Suspensoids in Divergent Electric Fields.* J. Appl. Phys., 1951. **22**: p. 869.
35. Pohl, H.A., *Some Effects of Nonuniform Fields on Dielectrics.* J. Appl. Phys. , 1958. **29**: p. 1182-1188.
36. Yang, J., et al., *Cell separation on microfabricated electrodes using dielectrophoretic/gravitational field-flow fractionation.* Anal Chem, 1999. **71**(5): p. 911-8.

37. Gascoyne, P.R.C. and J.V. Vykoukal, *Dielectrophoretic-based sample handling in general purpose programmable diagnostic instruments.* Proceedings of the IEEE, 2004. **92**(1): p. 22-41.
38. Steffen Hardt, F.S., *Microfluidic Technologies for Miniaturized Analysis Systems*. Book, ed. S.D. Senturia. 2007: Springer.
39. Cheng, J., et al., *Preparation and hybridization analysis of DNA/RNA from E. coli on microfabricated bioelectronic chips.* Nat Biotechnol, 1998. **16**(6): p. 541-6.
40. Davalos, R.V. and B. Rubinsky, *Electrical impedance tomography of cell viability in tissue with application to cryosurgery.* Journal of Biomechanical Engineering, 2004. **126**(2): p. 305-309.
41. Jen, C.P. and T.W. Chen, *Selective trapping of live and dead mammalian cells using insulator-based dielectrophoresis within open-top microstructures.* Biomed Microdevices, 2009. **11**(3): p. 597-607.
42. Suehiro, J., et al., *Selective detection of viable bacteria using dielectrophoretic impedance measurement method.* Journal of Electrostatics, 2003. **57**(2): p. 157-168.
43. Li, H. and R. Bashir, *Dielectrophoretic separation and manipulation of live and heat-treated cells of Listeria on microfabricated devices with interdigitated electrodes.* Sensors and Actuators B-Chemical, 2002. **86**(2-3): p. 215-221.
44. Huang, Y., et al., *Differences in the AC electrodynamics of viable and non-viable yeast cells determined through combined dielectrophoresis and electrorotation studies.* Phys Med Biol, 1992. **37**(7): p. 1499-517.
45. Docoslis, A., et al., *A novel dielectrophoresis-based device for the selective retention of viable cells in cell culture media.* Biotechnol Bioeng, 1997. **54**(3): p. 239-50.
46. Masuda, S., T. Itagaki, and M. Kosakada, *Detection of extremely small particles in the nanometer and ionic size range.* IEEE Trans. on Industry Applications, 1988. **24**: p. 740-744.
47. Chou, C., et al., *Electrodeless dielectrophoresis of single- and double-stranded DNA.* Biophysical Journal, 2002. **83**(4): p. 2170-2179.
48. Cummings, E.B. and A. Singh, *Dielectrophoresis in Microchips Containing Arrays of Insulating Posts: Theoretical and Experimental Results.* Analytical Chemistry, 2003. **75**: p. 4724-4731.
49. Lapizco-Encinas, B.H., et al., *Insulator-based dielectrophoresis for the selective concentration and separation of live bacteria in water.* Electrophoresis, 2004. **25**(10-11): p. 1695-704.
50. Lapizco-Encinas, B.H., et al., *An insulator-based (electrodeless) dielectrophoretic concentrator for microbes in water.* J Microbiol Methods, 2005. **62**(3): p. 317-26.
51. Davalos, R.V., et al., *Performance impact of dynamic surface coatings on polymeric insulator-based dielectrophoretic particle separators.* Anal Bioanal Chem, 2008. **390**(3): p. 847-855.
52. Simmons, B.A., et al., *The development of polymeric devices as dielectrophoretic separators and concentrators.* MRS Bulletin, 2006. **31**(2): p. 120-124.
53. Kang, Y., et al., *DC-Dielectrophoretic separation of biological cells by size.* Biomed Microdevices, 2008. **10**(2): p. 243-9.
54. Lapizco-Encinas, B.H., S. Ozuna-Chacon, and M. Rito-Palomares, *Protein manipulation with insulator-based dielectrophoresis and direct current electric fields.* J Chromatogr A, 2008. **1206**(1): p. 45-51.

55. Davalos, R.V., et al., *Performance impact of dynamic surface coatings on polymeric insulator-based dielectrophoretic particle separators.* Analytical and bioanalytical chemistry, 2008. **390**(3): p. 847-855.
56. Lapizco-Encinas, B.H., et al., *An insulator-based (electrodeless) dielectrophoretic concentrator for microbes in water.* Journal of Microbiological Methods, 2005. **62**(3): p. 317-326.
57. Sabounchi, P., et al., *Sample concentration and impedance detection on a microfluidic polymer chip.* Biomedical Microdevices, 2008. **10**(5): p. 661-670.
58. Lapizco-Encinas, B.H., et al., *Dielectrophoretic concentration and separation of live and dead bacteria in an array of insulators.* Analytical Chemistry, 2004. **76**(6): p. 1571-1579.
59. Simmons, B., et al., *Polymeric insulator-based (electrodeless) dielectrophoresis (iDEP) for the monitoring of water-borne pathogens.* Micro Total Analysis Systems 2004, Vol 2, 2005(297): p. 171-173
604.
60. Cummings, E.B., et al., *Fast and selective concentration of pathogens by insulator-based dielectrophoresis.* Abstracts of Papers of the American Chemical Society, 2005. **230**: p. U404-U405.
61. McGraw, G.J., et al., *A Comparison of Insulator-Based Dielectrophoretic Devices for the Monitoring and Separation of Waterborne Pathogens as a Function of Microfabrication Technique.* Antiterrorism and Homeland Defense: Polymers and Materials, 2007. **980**: p. 133-157
273.
62. Ozuna-Chacon, S., et al., *Insulator-based dielectrophoresis.* Revista Mexicana De Ingenieria Quimica, 2007. **6**(3): p. 329-335.
63. Lapizco-Encinas, B.H., S. Ozuna-Chacon, and M. Rito-Palomares, *Protein manipulation with insulator-based dielectrophoresis and direct current electric fields.* Journal of Chromatography A, 2008. **1206**(1): p. 45-51.
64. Jen, C.P. and T.W. Chen, *Trapping of cells by insulator-based dielectrophoresis using open-top microstructures.* Microsystem Technologies-Micro-and Nanosystems-Information Storage and Processing Systems, 2009. **15**(8): p. 1141-1148.
65. Jen, C.P., C.T. Huang, and H.Y. Shih, *Hydrodynamic Separation of Cells Utilizing Insulator-based Dielectrophoresis.* Dtip 2009: Symposium on Design, Test, Integration and Packaging of Mems/Moems, 2009: p. 55-59
429.
66. Jen, C.P. and T.W. Chen, *Selective trapping of live and dead mammalian cells using insulator-based dielectrophoresis within open-top microstructures.* Biomedical Microdevices, 2009. **11**(3): p. 597-607.
67. Stephens, M., et al., *The dielectrophoresis enrichment of CD34+ cells from peripheral blood stem cell harvests.* Bone Marrow Transplant, 1996. **18**(4): p. 777-82.
68. Sabounchi, P., et al. *Joule Heating Effects on Insulator-based Dielectrophoresis.* in *Twelfth International Conference on Miniaturized Systems for Chemistry and Life Sciences*. 2008. San Diego, California, USA.
69. Shafiee, H., et al., *Contactless dielectrophoresis: a new technique for cell manipulation.* Biomed Microdevices, 2009. **11**: p. 997-1006.

70. Borgatti, M., et al., *Antibody-antigen interactions in dielectrophoresis buffers for cell manipulation on dielectrophoresis-based Lab-on-a-chip devices.* Minerva Biotecnologica, 2007. **19**(2): p. 71-74.
71. Del Bene, F., et al., *A model-based approach to the in vitro evaluation of anticancer activity.* Cancer Chemotherapy and Pharmacology, 2009. **63**(5): p. 827-836.
72. Ntouroupi, T.G., et al., *Detection of circulating tumour cells in peripheral blood with an automated scanning fluorescence microscope.* British Journal of Cancer, 2008. **99**(5): p. 789-795.
73. Sarantseva, S.V. and A.L. Schwarzman, *Modern genetic approaches to searching for targets for medicinal preparations.* Russian Journal of Genetics, 2009. **45**(7): p. 761-770.
74. Tatosian, D.A. and M.L. Shuler, *A Novel System for Evaluation of Drug Mixtures for Potential Efficacy in Treating Multidrug Resistant Cancers.* Biotechnology and Bioengineering, 2009. **103**(1): p. 187-198.
75. Leary, J.F., et al. *High-throughput cell analysis and sorting technologies for clinical diagnostics and therapeutics*. in *Conference on Clinical Diagnostic Systems*. 2001. San Jose, Ca: Spie-Int Soc Optical Engineering.
76. Reya, T., et al., *Stem cells, cancer, and cancer stem cells.* Nature, 2001. **414**: p. 105-111.
77. Tang, D.G., et al., *Prostate cancer stem/progenitor cells: identification, characterization, and implications.* Mol Carcinog, 2007. **46**(1): p. 1-14.
78. Collins, A., et al., *Prospective identification of tumorigenic prostate cancer stem cells.* Cancer Res, 2005. **65**: p. 10946-10951.
79. Patrawala, L., et al., *Highly purified CD44+ prostate cancer cells from xenograft human tumors are enriched in tumorigenic and metastatic progenitor cells.* Oncogene, 2006. **25**(12): p. 1696-708.
80. Patrawala, L., et al., *Hierarchical organization of prostate cancer cells in xenograft tumors: the CD44+alpha2beta1+ cell population is enriched in tumor-initiating cells.* Cancer Res, 2007. **67**(14): p. 6796-805.
81. Pohl, H.A., *Dielectrophoresis: The Behavior of Neutral Matter in Nonuniform Electric Fields.* Cambridge University Press, Cambridge, U.K., 1978.
82. Holmes, D., *Electrical Cell Manipulation In Microfluidic Systems*, in *Institut de microélectronique et microsystèmes*. 2006, ÉCOLE POLYTECHNIQUE FÉDÉRALE DE LAUSANNE (EPFL): Lausanne.
83. Jones, T.B., *Electromechanics of Particles*. 1995, USA: Cambridge University Press. 265.
84. Kaler, K. and T.B. Jones, *Dielectrophoretic Spectra of Single Cells Determined by Feedback-Controlled Levitation.* Biophysical Journal, 1990. **57**(2): p. 173-182.
85. Jones, T.B., *Basic theory of dielectrophoresis and electrorotation.* IEEE Eng Med Biol Mag, 2003. **22**(6): p. 33-42.
86. Morgan, H., T. Sun, and D. Holmes, *Single Cell Dielectric Spectroscopy.* Journal of Physics D: Applied Physics, 2007. **40**(1).
87. Arnold, W.M.K.J.G.m.b.H., Juelich (Germany, F.R.). Inst. fuer Medizin); Zimmermann, U., *Rotating-field-induced rotation and measurement of the membrane capacitance of single mesophyll cells of Avena sativa* Plant physiology and biochemistry, 1982. **v. 37**(10): p. 908-915.
88. Kurschner, M., et al., *Effect of fluorine substitution on the interaction of lipophilic ions with the plasma membrane of mammalian cells.* Biophys J, 2000. **79**(3): p. 1490-7.

89. Jayjock, M.A., et al., *Formulation effect on the dermal bioavailability of isothiazolone biocide.* Food Chem Toxicol, 1996. **34**(3): p. 277-82.
90. Goater, A.D., J.P.H. Burt, and R. Pethig, *A combined travelling wave dielectrophoresis and electrorotation device: applied to the concentration and viability determination of Cryptosporidium.* Journal of Physics D-Applied Physics, 1997. **30**(18): p. L65-L69.
91. Freitag, R., et al., *THE EFFECT OF OSMOTIC AND MECHANICAL STRESSES AND ENZYMATIC DIGESTION ON THE ELECTRO-ROTATION OF INSECT CELLS (SPODOPTERA-FRUGIPERDA).* Journal of Biotechnology, 1989. **11**(4): p. 325-336.
92. Asami, K. and T. Yonezawa, *Dielectric behavior of wild-type yeast and vacuole-deficient mutant over a frequency range of 10 kHz to 10 GHz.* Biophysical Journal, 1996. **71**(4): p. 2192-2200.
93. Gimsa, J., C. Pritzen, and E. Donath, *CHARACTERIZATION OF VIRUS-RED-CELL INTERACTION BY ELECTROROTATION.* Studia Biophysica, 1989. **130**(1-3): p. 123-131.
94. Zhou, X.F., G.H. Markx, and R. Pethig, *Effect of biocide concentration on electrorotation spectra of yeast cells.* Biochim Biophys Acta, 1996. **1281**(1): p. 60-4.
95. Ziervogel, H., et al., *ELECTROROTATION OF LYMPHOCYTES - THE INFLUENCE OF MEMBRANE EVENTS AND NUCLEUS.* Bioscience Reports, 1986. **6**(11): p. 973-982.
96. Gascoyne, P.R.C., et al., *Dielectrophoretic separation of cancer cells from blood.* IEEE Transactions on Industry Applications Annual Meeting of the Industry-Applications-Society, 1997. **33**(3): p. 670-678.
97. Kang, K.H., et al., *Effects of dc-dielectrophoretic force on particle trajectories in microchannels.* Journal of Applied Physics, 2006. **99**(6).
98. Zimmermann, U., Pilwat, G., Beckers, F., Riemann, F.,. . , Vol. 3, pp. 58-83., *Effects of external electrical fields on cell membranes.* BIoelectrochem Bioenerg, 1976. **3**: p. 58-83.
99. Sale, A.J. and W.A. Hamilton, *Effects of high electric fields on micro-organisms. 1. Killing of bacteria and yeasts.* Biochimica et Biophysica Acta, 1967. **148**: p. 781-788.
100. Lee, R.C., D. Zhang, and J. Hannig, *Biophysical Injury Mechanisms in Electrical Shock Trauma*, in *Ann. Rev.Biomed. Eng.*, M.L. Yarmish, K.R. Diller, and M. Toner, Editors. 2000, Annual Review Press: Palo Alto. p. 477-509.
101. Weaver, J.C., *Electroporation of cells and tissues.* IEEE Transactions on Plasma Science, 2000. **28**(1): p. 24-33.
102. Davalos, R.V., L.M. Mir, and B. Rubinsky, *Tissue ablation with irreversible electroporation.* Annals of Biomedical Engineering, 2005. **33**(2): p. 223-231.
103. Edd, J., et al., *In vivo results of a new focal tissue ablation technique: irreversible electroporation.* IEEE Transactions on Biomedical Engineering, 2006. **53**(7): p. 1409-1415.
104. Rubinsky, B., G. Onik, and P. Mikus, *Irreversible electroporation: A new ablation modality – clinical implications.* Technology in Cancer Research and Treatment, 2007. **6**(1): p. 37-48.
105. Rubinsky, B., *Irreversible Electroporation in Medicine.* Technology in Cancer Research and Treatement, 2007. **6**(4): p. 255-260.
106. Onik, G., P. Mikus, and B. Rubinsky, *Irreversible electroporation: implications for prostate ablation.* Technol Cancer Res Treat, 2007. **6**(4): p. 295-300.

107. Al-Sakere, B., et al., *A study of the immunological response to tumor ablation with irreversible electroporation.* Technology in Cancer Research and Treatement, 2007. **6**: p. 301-306.
108. Al-Sakere, B., et al., *Tumor ablation with irreversible electroporation.* PLoS ONE, 2007. **2**(11): p. e1135.
109. Lavee, J., et al., *A novel nonthermal energy source for surgical epicardial atrial ablation: irreversible electroporation.* Heart Surgery Forum, 2007. **10**(2): p. E162-7.
110. Hoffman, G.A., *Cells in electric field. Physical and practical electronic aspects of electro cell fusion and electroporation*, in *Electroporation and Electrofusion in Cell Biology*, E. Neumann, A.E. Sowers, and C.A. Jordan, Editors. 1989, Plenum Press: New York, NY. p. 389-407.
111. Kekez, M.M., P. Savic, and B.F. Johnson, *Contribution to the biophysics of the lethal effects of electric field on microorganisms.* Biochim Biophys Acta, 1996. **1278**(1): p. 79-88.
112. Krassowska, W., et al., *Viability of cancer cells exposed to pulsed electric fields: the role of pulse charge.* Ann Biomed Eng, 2003. **31**(1): p. 80-90.
113. Okino, M., et al., *Optimal electric conditions in electrical impulse chemotherapy.* Jpn J Cancer Res, 1992. **83**(10): p. 1095-101.
114. Shoenbach, K.H., et al., *The effect of pulsed fields on biological cells: Experiments and applications.* IEEE Transactions Biomed Eng, 1997. **25**(284-292).
115. Vernhes, M.C., P.A. Cabanes, and J. Teissie, *Chinese hamster ovary cells sensitivity to localized electrical stresses.* BIoelectrochem Bioenerg, 1999. **48**(1): p. 17-25.
116. Schoenbach, K.H., et al., *The effect of pulsed fields on biological cells: Experiments and applications.* IEEE Trans Biomed Eng, 1997. **25**: p. 284-292.
117. Martin, G.T., U.F. Pliquett, and J.C. Weaver, *Theoretical analysis of localized heating in human skin subjected to high voltage pulses.* Bioelectrochemistry, 2002. **57**(1): p. 55-64.
118. Tropea, B.I. and R.C. Lee, *Thermal injury kinetics in electrical trauma.* J Biomech Eng, 1992. **114**(2): p. 241-50.
119. Edd, J.F. and R.V. Davalos, *Mathematical modeling of irreversible electroporation for treatment planning.* Technology in Cancer Research and Treatment, 2007. **6**: p. 275-286.
120. Davalos, R.V. and B. Rubinsky, *Temperature considerations during irreversible electroporation.* International Journal of Heat and Mass Transfer, 2008. **51**(23-24): p. 5617-5622.
121. Ivorra, A. and B. Rubinsky, *Electric field modulation in tissue electroporation with electrolytic and non-electrolytic additives.* Bioelectrochemistry, 2007. **70**(2): p. 551-60.
122. Ivorra, A. and B. Rubinsky, *In vivo electrical impedance measurements during and after electroporation of rat liver.* Bioelectrochemistry, 2007. **70**(2): p. 287-95.
123. Pohl, H., *The Motion and Precipitation of Suspensoids in Divergent Electric Fields.* Applied Physics, 1951. **22**: p. 869-871.
124. Pohl, H., *Some Effects of Nonuniform Fields on Dielectrics.* Applied Physics, 1958. **29**: p. 1182-1188.
125. Crane, J. and H. Pohl, *A study of living and dead yeast cells using dielectrophoresis.* Journal of the Electrochemical Society, 1968. **115**(6): p. 584-586.
126. Toner, M. and D. Irimia, *BLOOD-ON-A-CHIP.* Annual Review of Biomedical Engineering, 2005. **7**(1): p. 77-103.

127. Yang, J., et al., *Cell separation on microfabricated electrodes using dielectrophoretic/gravitational field flow fractionation.* Analytical Chemistry, 1999. **71**(5): p. 911-918.
128. Das, C.M., et al., *Dielectrophoretic Segregation of Different Human Cell Types on Microscope Slides.* Analytical Chemistry, 2005. **77**(9): p. 2708-2719.
129. Griffith, A.W. and J.M. Cooper, *Single-cell measurements of human neutrophil activation using electrorotation.* Analytical Chemistry, 1998. **70**(13): p. 2607-12.
130. Toner, M. and D. Irimia, *Blood-on-a-chip.* Annu Rev Biomed Eng, 2005. **7**: p. 77-103.
131. EG Richard Lee, J.F., J Lukens, F Paraskevas, JP Greer, GM Rodgers, MM Wintrobe, *Wintrobe Clinical Hemotology*, ed. 10. 1999, Philadelphia: Lippincott Williams & Wilkins.
132. Fukuda, S. and G.W. Schmid-Schonbein, *Centrifugation attenuates the fluid shear response of circulating leukocytes.* J Leukoc Biol, 2002. **72**(1): p. 133-9.
133. Lundahl, J., et al., *Altered expression of CD11b/CD18 and CD62L on human monocytes after cell preparation procedures.* J Immunol Methods, 1995. **180**(1): p. 93-100.
134. Sritharan, D., *Size-based cell sorting by deterministic lateral displacement*, in *Chemical Engineering*. 2009, Northeastern University: Boston.
135. Stone, H.A. and S. Kim, *Microfluidics: Basic Issues, Applications, and Challenges.* AIChE Journal, 2001. **47**(6): p. 1250-1254.
136. Iakovlev, V., et al., *Quantitative detection of circulating epithelial cells by Q-RT-PCR.* Breast Cancer Research and Treatment, 2007.
137. Nagrath, S., et al., *Isolation of rare circulating tumour cells in cancer patients by microchip technology.* Nature, 2007. **450**(7173): p. 1235-9.
138. Paterlini-Brechot, P. and N.L. Benali, *Circulating tumor cells (CTC) detection: Clinical impact and future directions.* Cancer Letters. **In Press, Corrected Proof**.
139. Wong, N.S., et al., *Prognostic significance of circulating tumour cells enumerated after filtration enrichment in early and metastatic breast cancer patients.* Breast Cancer Research and Treatment, 2006. **99**(1): p. 63-69.
140. Beckman, M., *New technologies aim to find cancer in the blood.* Journal of the National Cancer Institute, 2006. **98**(17): p. 1180-1181.
141. Racila, E., et al., *Detection and characterization of carcinoma cells in the blood.* Proc Natl Acad Sci U S A, 1998. **95**(8): p. 4589-94.
142. Gomella, L.G., G.V. Raj, and J.G. Moreno, *Reverse transcriptase polymerase chain reaction for prostate specific antigen in the management of prostate cancer.* J Urol, 1997. **158**(2): p. 326-37.
143. Ghossein, R.A., S. Bhattacharya, and J. Rosai, *Molecular detection of micrometastases and circulating tumor cells in solid tumors.* Clin Cancer Res, 1999. **5**(8): p. 1950-60.
144. Stathopoulou, A., et al., *Molecular detection of cancer cells in the peripheral blood of patients with breast cancer: comparison of CK-19, CEA and maspin as detection markers.* Anticancer Res, 2003. **23**(2C): p. 1883-90.
145. Molnar, B., et al., *Circulating tumor cell clusters in the peripheral blood of colorectal cancer patients.* Clin Cancer Res, 2001. **7**(12): p. 4080-5.
146. Fetsch, P.A., et al., *Detection of circulating tumor cells and micrometastases in stage II, III, and IV breast cancer patients utilizing cytology and immunocytochemistry.* Diagn Cytopathol, 2000. **22**(5): p. 323-8.

147. Witzig, T.E., et al., *Detection of circulating cytokeratin-positive cells in the blood of breast cancer patients using immunomagnetic enrichment and digital microscopy.* Clin Cancer Res, 2002. **8**(5): p. 1085-91.
148. Wang, Z.P., et al., *Identification and characterization of circulating prostate carcinoma cells.* Cancer, 2000. **88**(12): p. 2787-95.
149. Mehes, G., et al., *Circulating breast cancer cells are frequently apoptotic.* Am J Pathol, 2001. **159**(1): p. 17-20.
150. Allard, W.J., et al., *Tumor cells circulate in the peripheral blood of all major carcinomas but not in healthy subjects or patients with nonmalignant diseases.* Clin Cancer Res, 2004. **10**(20): p. 6897-904.
151. Fehm, T., et al., *Cytogenetic evidence that circulating epithelial cells in patients with carcinoma are malignant.* Clinical Cancer Research, 2002. **8**(7): p. 2073-2084.
152. Hayes, D.F., et al., *Monitoring expression of HER-2 on circulating epithelial cells in patients with advanced breast cancer.* International Journal of Oncology, 2002. **21**(5): p. 1111-1117.
153. Cristofanilli, M., et al., *Circulating tumor cells, disease progression, and survival in metastatic breast cancer.* New England Journal of Medicine, 2004. **351**(8): p. 781-791.
154. Kurusu, Y., J. Yamashita, and M. Ogawa, *Detection of circulating tumor cells by reverse transcriptase-polymerase chain reaction in patients with resectable non-small-cell lung cancer.* Surgery, 1999. **126**(5): p. 820-826.
155. Burchill, S.A., et al., *Comparison of the RNA-amplification based methods RT-PCR and NASBA for the detection of circulating tumour cells.* British Journal of Cancer, 2002. **86**(1): p. 102-109.
156. Flanagan, L.A., et al., *Unique dielectric properties distinguish stem cells and their differentiated progeny.* Stem Cells, 2008. **26**(3): p. 656-65.
157. Davalos, R.V., I.L. Mir, and B. Rubinsky, *Tissue ablation with irreversible electroporation.* Ann Biomed Eng, 2005. **33**(2): p. 223-31.
158. Edd, J.F. and R.V. Davalos, *Mathematical modeling of irreversible electroporation for treatment planning.* Technol Cancer Res Treat, 2007. **6**(4): p. 275-86.
159. Gascoyne, P.R.C., et al., *Isolation of rare cells from cell mixtures by dielectrophoresis.* Electrophoresis, 2009. **30**(8): p. 1388-1398.
160. Docoslis, A., et al., *A novel dielectrophoresis-based device for the selective retention of viable cells in cell culture media.* Biotechnology and Bioengineering, 1997. **54**(3): p. 239-250.
161. Li, H.B. and R. Bashir, *Dielectrophoretic orientation, manipulation and separation of live and heat-treated cells of Listeria on microfabricated devices with interdigitated electrodes*, in *Biomems and Bionanotechnology*, R.P. Manginell, et al., Editors. 2002. p. 167-172.
162. Asbury, C.L., A.H. Diercks, and G. van den Engh, *Trapping of DNA by dielectrophoresis.* Electrophoresis, 2002. **23**(16): p. 2658-2666.
163. Weaver, J.C., *Electroporation theory: Concepts and mechanisms*, in *Methods in Molecular Biology*. 1995, Humana Press, Inc.: Totowa, NJ. p. 3-28.
164. Marszalek, P., D.S. Liu, and T.Y. Tsong, *Schwan equation and transmembrane potential induced by alternating electric field.* Biophys J, 1990. **58**(4): p. 1053-8.

165. Davalos, R., B. Rubinsky, and Y. Huang, *Electroporation: bio-electrochemical mass transfer at the nano Scale.* Microscale Thermophysical Engineering, 2000. **4**(3): p. 147-159.
166. Lee, E.S., et al., *Microfluidic electroporation of robust 10-microm vesicles for manipulation of picoliter volumes.* Bioelectrochemistry, 2006. **69**(1): p. 117-25.
167. Shafiee, H., P.A. Garcia, and R.V. Davalos, *A preliminary study to delineate irreversible electroporation from thermal damage using the arrhenius equation.* J Biomech Eng, 2009. **131**(7): p. 074509.
168. Wicha, M.S., S. Liu, and G. Dontu, *Cancer stem cells: an old idea--a paradigm shift.* Cancer Res, 2006. **66**(4): p. 1883-90; discussion 1895-6.
169. Tang, C., B.T. Ang, and S. Pervaiz, *Cancer stem cell: target for anti-cancer therapy.* FASEB J, 2007. **21**(14): p. 3777-85.
170. Al-Hajj, M., et al., *Prospective identification of tumorigenic breast cancer cells.* Proc Natl Acad Sci U S A, 2003. **100**(7): p. 3983-8.
171. Collins, A.T., et al., *Prospective identification of tumorigenic prostate cancer stem cells.* Cancer Res, 2005. **65**(23): p. 10946-51.
172. Li, C., C.J. Lee, and D.M. Simeone, *Identification of human pancreatic cancer stem cells.* Methods Mol Biol, 2009. **568**: p. 161-73.
173. Li, C., et al., *Identification of pancreatic cancer stem cells.* Cancer Res, 2007. **67**(3): p. 1030-7.
174. Prince, M.E., et al., *Identification of a subpopulation of cells with cancer stem cell properties in head and neck squamous cell carcinoma.* Proceedings of the National Academy of Sciences of the United States of America, 2007. **104**(3): p. 973-978.
175. Ricci-Vitiani, L., et al., *Identification and expansion of human colon-cancer-initiating cells.* Nature, 2007. **445**(7123): p. 111-5.
176. Singh, S.K., et al., *Identification of human brain tumour initiating cells.* Nature, 2004. **432**(7015): p. 396-401.
177. Rupesh I. Bhatt, M.D.B., Claire A. Hart, Paul Gilmore, Vijay A.C. Ramani, Nicholas J. George, Noel W. Clarke, *Novel methods for the isolation and characterization of the putative prostatic stem cell.* Cytometry, 2003. **54A**: p. 89-99.
178. Patrawala, L., et al., *Side population is enriched in tumorigenic, stem-like cancer cells, whereas ABCG2(+) and ABCG2(-) cancer cells are similarly tumorigenic.* Cancer Research, 2005. **65**(14): p. 6207-6219.
179. Gascoyne, P., et al., *Microsample preparation by dielectrophoresis: isolation of malaria.* Lab Chip, 2002. **2**(2): p. 70-5.
180. Hu, X.Y., et al., *Marker-specific sorting of rare cells using dielectrophoresis.* Proceedings of the National Academy of Sciences of the United States of America, 2005. **102**(44): p. 15757-15761.
181. Yang, J., et al., *Cell separation on microfabricated electrodes using dielectrophoretic/gravitational field flow fractionation.* Analytical Chemistry, 1999. **71**(5): p. 911-918.
182. Lambrechts, A., M. Van Troys, and C. Ampe, *The actin cytoskeleton in normal and pathological cell motility.* International Journal of Biochemistry & Cell Biology, 2004. **36**(10): p. 1890-1909.
183. Lostumbo, A., et al., *Flow cytometry: A new approach for the molecular profiling of breast cancer.* Experimental and Molecular Pathology, 2006. **80**(1): p. 46-53.

184. Huang, Y., et al., *Dielectrophoretic cell separation and gene expression profiling on microelectronic chip arrays.* Anal Chem, 2002. **74**: p. 3362-3371.
185. Gascoyne, P., et al., *Dielectrophoretic Separation of Cancer Cells from Blood.* IEEE Trans. Industry Applications, 1997. **33**: p. 670-678.
186. Cheng, J., et al., *Preparation and hybridization analysis of DNA/RNA from E. coli on microfabricated bioelectronic chips.* Nat Biotechnol, 1998. **16**: p. 541-546.
187. Stephens, M., et al., *The dielectrophoresis enrichment of CD34+ cells from peripheral blood stem cell harvests.* Bone Marrow TRansplant, 1996. **18**: p. 777-782.
188. Cheng, J., et al., *Isolation of cultured cervical carcinoma cells mixed with peripheral blood cells on a bioelectronic chip.* Anal Chem, 1998. **70**: p. 2321-2326.
189. Altomare, L., et al., *Levitation and movement of human tumor cells using a printed circuit board device based on software-controlled dielectrophoresis.* Biotechnol Bioeng, 2003. **82**: p. 474.
190. Huang, Y., et al., *Introducing dielectrophoresis as a new force field for field-flow fractionation.* Biophys J, 1997. **73**: p. 1118-1129.
191. Kim, U.-J., et al., *Selection of mammalian cells based on their cell-cycle phase using dielectrophoresis.* Proc Natl Acad Sci, 2007. **104**: p. 20708-20712.
192. Griffith, A. and J. Cooper, *Single-cell measurements of human neutrophil activation using electrorotation.* Anal Chem, 1998. **70**: p. 2607-2612.
193. Toner, M. and D. Irimia, *Bone-on-a-chip.* Ann Rev Biomed Eng, 2005. **7**: p. 77-103.
194. Gascoyne, P.R.C., et al., *Dielectrophoretic Separation of Mammalian-Cells Studied by Computerized Image-Analysis.* Measurement Science & Technology, 1992. **3**(5): p. 439-445.
195. Becker, F.F., et al., *The Removal of Human Leukemia-Cells from Blood Using Interdigitated Microelectrodes.* Journal of Physics D-Applied Physics, 1994. **27**(12): p. 2659-2662.
196. Becker, F.F., et al., *Separation of Human Breast-Cancer Cells from Blood by Differential Dielectric Affinity.* Proceedings of the National Academy of Sciences of the United States of America, 1995. **92**(3): p. 860-864.
197. Gascoyne, P.R.C., et al., *Dielectrophoretic separation of cancer cells from blood.* Ieee Transactions on Industry Applications, 1997. **33**(3): p. 670-678.
198. Wang, X.B., et al., *Cell separation by dielectrophoretic field-flow-fractionation.* Analytical Chemistry, 2000. **72**(4): p. 832-839.
199. Vykoukal, J., et al., *Enrichment of putative stem cells from adipose tissue using dielectrophoretic field-flow fractionation.* Lab on a Chip, 2008. **8**(8): p. 1386-1393.
200. Ailles, L.E. and I.L. Weissman, *Cancer stem cells in solid tumors.* Current Opinion in Biotechnology, 2007. **18**(5): p. 460-466.
201. Uchida, N., et al., *Direct isolation of human central nervous system stem cells.* Proc Natl Acad Sci U S A, 2000. **97**(26): p. 14720-5.
202. Barclay, W.W., et al., *Characterization of adult prostatic progenitor/stem cells exhibiting self-renewal and multilineage differentiation.* Stem Cells, 2008. **26**(3): p. 600-10.
203. Barclay, W.W. and S.D. Cramer, *Culture of mouse prostatic epithelial cells from genetically engineered mice.* Prostate, 2005. **63**(3): p. 291-8.